Scuola Internazionale Superiore di Studi Avanzati - Trieste

International School for Advanced Studies

SISSA

Neurobiology Sector

The voltage-dependence of TMEM16B/Anoctamin2:

the calcium-activated chloride channel in olfactory transduction

Thesis submitted for the degree of

"Doctor Philosophiae"

CANDIDATE:

Valentina Cenedese

SUPERVISOR:

Prof. Anna Menini

SISSA - Via Bonomea 265 - 34136 TRIESTE - ITALY

Elogio del cambiamento

or "Nothing is certain except change"

"Avevo scoperto che uscire dalla mia testa era impossibile come fuggire da una cassaforte. Impossibile cedere alla carne la supremazia della mia identità. Decisi allora di percorrere il cammino opposto: visto che non potevo scendere, avrei fatto risalire tutte le mie sensazioni! Puro intelletto, iniziai ad assorbire la mia forma fisica, poi presi a incorporare i bisogni, i desideri, le emozioni. Esaminavo tutto ciò che sentivo e poi come mi sentivo a sentirlo. Capii che la cosiddetta "realtà" era una costruzione mentale. Illusione completa? Non ci è dato saperlo. Ma con ogni evidenza non avrei mai percepito nella sua interezza quello che in me c'era di reale. L'intelletto mi avrebbe sempre fornito un fantasma incompleto. "Vivo male all'interno di un pazzo! La mia barca razionale naviga nella demenza!" Quello che all'inizio mi pareva un incubo, piano piano si trasformò in speranza. Tutto ciò che avvertivo come "la mia essenza" erano immagini illusorie, per nulla diverse da quelle di un sogno, pertanto avevo la possibilità di cambiare la percezione di me stesso" Alejandro Jodorowsky, La danza della realtà

"Make a radical change in your lifestyle and begin to boldly do things which you may previously never have thought of doing, or been too hesitant to attempt. So many people live within unhappy circumstances and yet will not take the initiative to change their situation because they are conditioned to a life of security, conformity, and conservatism, all of which may appear to give one peace of mind, but in reality nothing is more dangerous to the adventurous spirit within a man than a secure future. The very basic core of a man's living spirit is his passion for adventure. The joy of life comes from our encounters with new experiences, and hence there is no greater joy than to have an endlessly changing horizon, for each day to have a new and different sun." Jon Krakauer, Into the wild

"Un coniglio bianco viene estratto da un cilindro vuoto. Dal momento che l'animale è molto grosso, ci vogliono milioni di anni per fare questo gioco di prestigio. Sulla punta dei suoi peli nascono i bambini. In questo modo hanno la possibilità di stupirsi di questa incredibile magia. Tuttavia, a mano a mano che diventando adulti, scivolano sempre più giù nella pelliccia del coniglio. E lì rimangono. Molti stanno così bene che non osano più arrampicarsi nuovamente sui peli sottili. Alcuni si imbarcano in questo viaggio pericoloso

alla ricerca dei confini ultimi della lingua e dell'esistenza. Alcuni di loro cadono, altri però si aggrappano con tutte le loro forze ai peli del coniglio e gridano agli uomini che, comodamente sistemati nella morbida pelliccia dell'animale, mangiano e bevono in assoluta tranquillità. "Signori e signore!" dicono "siamo sospesi nel vuoto!"
Ma agli esseri umani che vivono di sotto non importa nulla. Anzi, prima commentano "Uffa, che scocciatori" poi continuano a ripetere le stesse cose di prima "Mi passi il sale?" J.Gaarder, Il mondo di Sofia

"For what it's worth it's never too late to be whoever you want to be. There's no time limit, stop whenever you want. You can change or stay the same, there are no rules to this thing. We can make the best or the worst of it. I hope you make the best of it. And I hope you see things that startle you. I hope you feel things you never felt before. I hope you meet people with a different point of view. I hope you live a life you're proud of. If you find that you're not, I hope you have the strength to start all over again." Benjamin Button

"Quando si prova a scalare una montagna per dimostrare la propria bravura, è raro che si arrivi alla vetta. E se ci si arriva è una vittoria ben meschina. Per consolidarla bisogna continuare a misurarsi, incessantemente, condannati ad aderire per sempre ad una falsa immagine di sè, ossessionati dalla paura che l'immagine non sia vera e che qualcuno lo scopra." R. Pirsig, Lo zen e l'arte della manutenzione della motocicletta

Awakening is not a thing. It is not a goal, not a concept. It is not something to be attained. It is a metamorphosis. If the caterpillar thinks about the butterfly it is to become, saying 'And then I shall have wings and antennae,' there will never be a butterfly. The caterpillar must accept its own disappearance in its transformation. When the marvellous butterfly takes wing, nothing of the caterpillar remains." Alejandro Jodorowsky, The spiritual journey of Alejandro Jodorowsky: the creator of El topo

Declaration

The work described in this Thesis was carried out at the International School for Advanced Studies, Trieste, between November 2007 and November 2011.

The work described in this Thesis is included in:

Simone Pifferi, Valentina Cenedese and Anna Menini

Anoctamin2/TMEM16B: a calcium-activated chloride channel in olfactory transduction

Exp Physiol February 2012 97 (2) 193-199

I collaborated with Simone Pifferi and Anna Menini in writing the manuscript.

Valentina Cenedese, Giulia Betto, Fulvio Celsi, O. Lijo Cherian, Simone Pifferi, and Anna Menini

The voltage-dependence of the TMEM16B/anoctamin2 calcium-activated chloride channel is modified by mutations in the first putative intracellular loop

J Gen Physiol. 2012 Mar 12. [Epub ahead of print]

Data reported in this article arise from my own experiments and some experiments in collaboration with Giulia Betto and Lijo O. Cherian. I also performed the data analysis and wrote the first draft of the manuscript.

Abstract

Ca^{2+}-activated Cl^- channels are involved in several physiological processes. In vertebrate olfactory transduction a Ca^{2+}-dependent Cl^- efflux greatly amplifies the odorant response. The binding of odorants to receptors in the cilia of olfactory sensory neurons activates a transduction cascade that involves the opening of cyclic nucleotide-gated channels and the entry of Ca^{2+} in the cilia. Ca^{2+} activates a Cl^- current that, in the presence of a maintained elevated intracellular Cl^- concentration, produces an efflux of Cl^- ions and amplifies the depolarization. TMEM16A/anoctamin1 and TMEM16B/anoctamin2 have been shown to function as CaCCs. TMEM16B is expressed in the cilia of olfactory sensory neurons, microvilli of vomeronasal sensory neurons, and in the synaptic terminals of retinal photoreceptors, but very little information is available on the structure-function relation. Here we have performed the first site-directed mutagenesis study on TMEM16B to understand the molecular mechanisms of voltage- and Ca^{2+}-dependence. We have mutated amino acids in the first putative intracellular loop and measured the properties of the wild type and mutant TMEM16B channels expressed in HEK 293T cells using the whole-cell voltage-clamp technique in the presence of various intracellular Ca^{2+} concentrations. Mutation of E367 into glutamine or deletion of five consecutive glutamates $_{386}$EEEEE$_{390}$ did not greatly affect the apparent Ca^{2+} affinity, but modified the voltage-dependence shifting the conductance-voltage relations toward more positive voltages. These findings indicate that glutamates E367 and $_{386}$EEEEE$_{390}$ in the first intracellular putative loop play an important role in the voltage-dependence of TMEM16B, thus providing an initial structure-function study for this channel.

Contents

Abbreviations

A9C	Anthracene-9-carboxylic acid
AC	Adenylyl cyclase
Anoctamin	ANion selective and have eight (OCT) transmembrane segments
ASL	Airway surface liquid
ATP	Adenosine TriPhosphate
BK	Big Potassium (channel)
CaCC	Ca^{2+}-activated Cl^- channel
CaM	Calmodulin (for Calcium-Modulated protein)
CaMK	Calcium calmodulin Kinase
cAMP	Cyclic Adenosine MonoPhosphate
CF	Cystic fibrosis
CFTR	Cystic fibrosis transmembrane regulator
CNG	Cyclic nucleotide-gated (channel)
DIDS	4,4'diisothiocyanostilbene-2,2'-disulphonic acid
DOG1	Discovered On GIST-1 tumor
DRG	Dorsal root ganglia
E_{Cl}	Cl^- equilibrium potential
FFA	Flufenamic Acid
GPCR	G protein coupled receptor
IMCD	Intramedullary collecting duct
IP_3	Inositol trisphosphate
KO	Knock out
MFA	Mefenamic Acid
MPP4	Seven membrane palmitoylated protein 4
n	Hill coefficient
NFA	Niflumic acid

NKCC1	Na-K-Cl cotransporter
NPPB	5-nitro-2-(3-phenylpropylamino)benzoic acid
OR	Odorant receptor
ORAOV2	Oral cancer Overexpressed
OSN	Olfactory sensory neuron
P2Y	Purinergic receptor
PCR	Polymerase chain reaction
PDZ	Post synaptic density protein (PSD95), Drosophila disc large tumor suppressor (Dlg1), and Zonula occludens-1 protein (zo-1)
PLC	Phospholipase C
PSD95	Postsynaptic density protein 95
RPE	Retinal pigment epithelium
RTP	Replication Telomere Protein
SCN	Isothiocyanate
SITS	4-acetamido-4'-isothiocyanostilbene- 2.2'-disulphonic acid
TAOS-2	Tumor Amplified and Overexpressed
TM	Transmembrane domain
TMEM	Transmembrane proteins with unknown function
TRP	Transient Receptor Protein

1 Introduction

1.1 Chemosensation

Chemosensation, the detection of chemicals in the external environment, is essential for the survival of the individuals and of the species. It provides information on food, mates, danger, predators and pathogens. The olfactory system detects and discriminates myriad chemical structures across a wide range of concentrations. This task of broad chemical recognition requires a massive repertoire of receptors to match the diversity in chemical structures, different signalling pathways and anatomically segregated subsystems to sample their environment (reviewed by Kaupp, 2010).

1.1.1 The main olfactory system

In the nose of vertebrates, odorants are detected by the main olfactory epithelium located in the nasal cavity, where it lines a series of cartilaginous outcroppings, called turbinates (Fig. 1 A). The main olfactory epithelium (MOE) is a columnar pseudo-stratified epithelium and is composed of several types of cells: olfactory sensory neurons (OSNs), supporting cells (sustentacular cells) and basal cells (stem cells) (Fig. 1 B). Moreover the olfactory epithelium of all vertebrates contains Bowmann's glands, which produce a layer of mucus that covers the epithelial surface. The supporting cells are columnar epithelial cells and they extend vertically from the epithelial surface, where they end with microvilli and they contact the basal lamina with branched digitiform processes from the opposite projection (Breer *et al.*, 2006; Munger *et al.*, 2009).

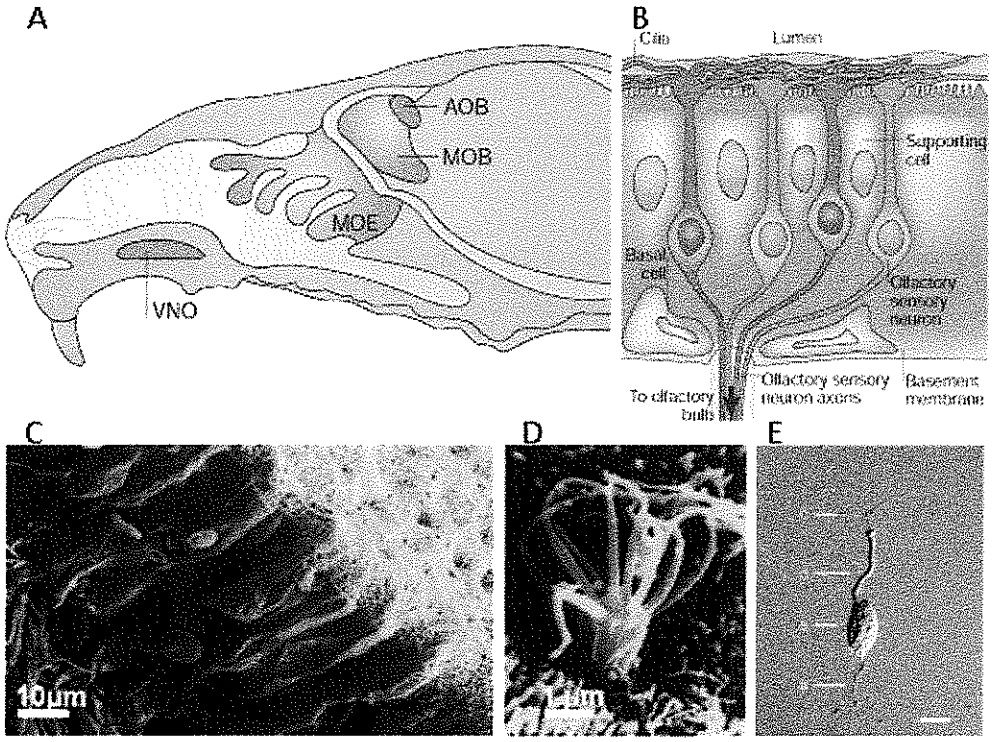

Figure 1: **Organization of the olfactory epithelium**: A . Schematic diagram of half a mouse head. Axons of sensory neurons in the main olfactory epithelium (MOE) project to the main olfactory bulb (MOB), and axons of sensory neurons in the vomeronasal organ (VNO) project to the accessory olfactory bulb (AOB). B. Cross-section of the main olfactory epithelium (Mombaerts, 2004). C. Microphotograph of human olfactory epithelium and D. olfactory sensory neurons knob/cilia obtained with scanning electron microscopy (Morrison & Costanzo, 1990). E. Photograph of an isolated frog olfactory sensory neuron under differential interference optic, c: cilia; d: dendrite; s: soma; a: axon (Kleene & Gesteland, 1981)

The OSNs are generated *in situ* from stem cells (basal cells) (Caggiano *et al.*, 1994). Like in other epithelia, cell renewal persists throughout adult life to replace OSNs, which have a lifespan of weeks to months (Graziadei *et al.*, 1978).

OSNs are bipolar neurons (Fig. 1 E) with a single dendrite that reaches up to the surface of the tissue and ends in a knob-like swelling from which some 20–30 very fine cilia project (Menco, 1980). These cilia, which lie in the thin layer of mucus covering the tissue (Fig. 1 C and D), are the site of the sensory transduction apparatus, where the odor binds the receptor and triggers the olfactory response. A thin axon from the proximal pole of the cell projects directly to higher brain regions, passing through the

cribiform plate into a region of the forebrain known as the olfactory bulb (MOB, Fig. 1 A) (Mombaerts, 2004).

In the bulb the odorant information is further processed by the activity of inhibitory interneurons, periglomerular cells, and granule cells (Lowe, 2003; Schoppa & Urban, 2003). The axons of mitral and tufted cells (the output neurons of the olfactory bulb) project through the lateral olfactory tract to the olfactory cortex. The olfactory cortex consists of all brain regions that receive direct input from the mitral and tufted cell axons of the olfactory bulb (Allison, 1954; Carmichael *et al.*, 1994). This comprises distinct areas: the piriform cortex, olfactory tubercle, anterior olfactory nucleus, and specific parts of the amygdala and the entorhinal cortex. Further projections from the olfactory cortex reach, through the thalamus, the orbitofrontal cortex, that is thought to be responsible for perception and discrimination of odors. Instead, the pathways leading to the amygdala and hypothalamus are thought to be involved in the emotional and motivational aspects of smell as well as the behavioral and physiological effects of odors (Buck, 2000; Menini *et al.*, 2004).

1.2 Odorant receptors

The molecular era of research into the chemical senses came of age in 1991 with the discovery of odorant receptor genes (Buck & Axel, 1991; Buck, 2004). Odorant receptors (ORs) belong to the superfamily of G protein coupled receptors (GPCRs) with seven hydrophobic membrane-spanning regions (7TM) structure (Fig. 2 A). ORs have an unusually long second extracellular loop and an extra pair of conserved cysteines in this loop (Mombaerts, 1999), they differ in their amino acid sequence in the third, fourth, and fifth transmembrane regions, which may form the ligand-binding pocket for odorant molecules.

By application of degenerate polymerase chain reaction (PCR), a diverse superfamily of ~1,000 genes was identified in the rat where RNA transcripts were localized to the olfactory mucosa (Buck & Axel, 1991). In the same work Buck & Axel found that ORs coding region has an

intronless structure. Humans have a similar number of odorant receptor genes, although a large fraction of them appear to be pseudogenes and only between 300 and 400 are functional genes (Mombaerts, 1999). Mouse ORs sequence repertoire instead shows only the 20% of pseudogenes (Zhao & Firestein, 1999; Young & Trask, 2002; Young *et al.*, 2003; Godfrey *et al.*, 2004).

The intact mouse OR genes can be grouped into families, defined by an amino-acid identity of >40% (Zhang & Firestein, 2002), and containing between 1 and 50 member genes. Class I genes (~10% of the mouse repertoire) resemble the OR genes of fish, but class II genes are, so far, unique to terrestrial vertebrates. OR genes are spread over ~50 clusters localized on nearly all chromosomes.

ORs are located in the cilia of olfactory sensory neurons where odorants bind and activate the transduction cascade. Each OSN expresses only one type of OR (Chess *et al.*, 1994; Malnic *et al.*, 1999; Serizawa *et al.*, 2003; Shykind, 2005). Each OR could be activated by different odorant molecules (Fig 2 B), and each odorant molecule could activate different ORs. Moreover, based on the spatial distribution of OR genes, the olfactory epithelium can be divided in four zones along the antero-posterior axis. Each OR gene is expressed only in one zone but, inside it, the OSNs expressing that OR gene are randomly scattered (Ressler *et al.*, 1993; Sullivan *et al.*, 1994; Vassar & Holcroft, 1994). All the neurons expressing a particular receptor, no matter where they are found on the epithelial sheet, converge to a single 'target' in the olfactory bulb. These targets are the glomeruli, which are globose neural structures, constituted of the incoming axons of OSNs and the dendrites of the the mitral cell, the main projection cell in the bulb (Mombaerts *et al.*, 1996).

Up to now the identification of the ligands for ORs is still very limited (Mombaerts, 2004). This is due to the difficulty to express ORs in heterologous systems. The main difficulty seems to be the OR protein trafficking to the plasma membrane. This issue will be likely resolved by the discovery of accessory proteins that are involved in processing and trafficking of OR proteins. Indeed, it has been found that members of the RTP protein family were able to interact both in vivo and in vitro with OR

proteins and induced their functional expression in heterologous systems (Saito *et al.*, 2004; Zhuang & Matsunami, 2007). Moreover Von Dannecker et al. (Von Dannecker *et al.*, 2005, 2006) reported that also Ric-8B, a putative guanine nucleotide exchange factor interacts with Gαolf and is able to promote the expression in heterologous systems.

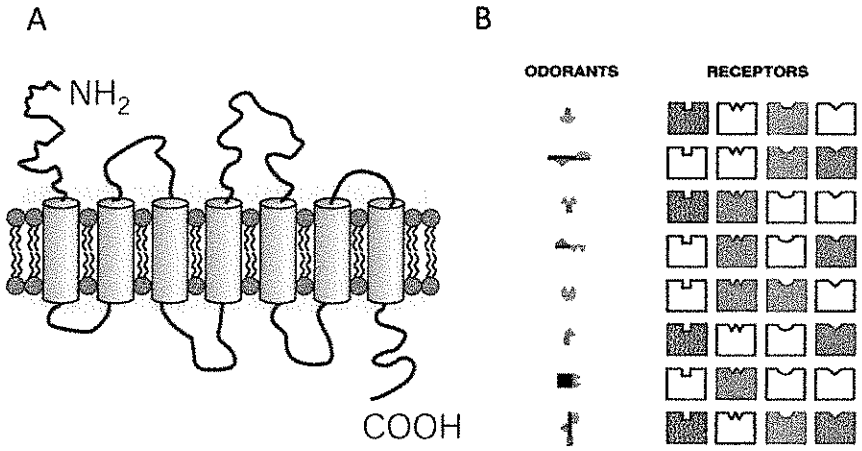

Figure 2: **Odorant receptors, one neuron-one receptor:** A. Schematic topology of ORs with the typical 7 transmembrane domains of G-protein coupled receptor (Mombaerts, 2004). B. Combinatory code betwen odorants and receptors (Malnic *et al.*, 1999).

1.3 Olfactory transduction

The origin of odorant perception is the chemical interaction of odorant molecules with OSNs that converts the chemical information into electrical signals carrying information about the external world to the brain. Transduction of odorants takes place in the cilia of OSNs. The binding of an odor activates the G protein coupled to the OR (Menco *et al.*, 1992; Belluscio *et al.*, 1998), which stimulates the adenylyl cyclase III (ACIII) triggering the synthesis of cAMP (Lowe *et al.*, 1989; Bakalyar & Reed, 1990; Wong *et al.*, 2000). Therefore cAMP opens cyclic nucleotide-gated (CNG) channels (Nakamura & Gold, 1987; Frings *et al.*, 1995) allowing Na^+ and Ca^{2+} flow from outside to inside the cilium generating an inward depolarizing current and the increase in the ciliary intracellular Ca^{2+} concentration ($[Ca^{2+}]_i$) (Restrepo *et al.*, 1990; Kleene & Gesteland, 1991; Kleene, 1993; Leinders-Zufall *et al.*, 1997). In turn, Ca^{2+} -activated Cl^-

channels (CaCCs) (Kleene & Gesteland, 1991; Kurahashi & Yau, 1993; Lowe & Gold, 1993*a*), which mediate a flux of Cl^- from inside to outside the cilium, further amplifies the depolarization due to CNG mediated-current. OSNs accumulate Cl^- ions thanks to different mechanisms. Among these the $Na^+/K^+/2Cl^-$ cotransporter NKCC1 has been shown to have an important role (Kaneko *et al.*, 2004; Reisert *et al.*, 2005; Nickell *et al.*, 2006, 2007; Hengl *et al.*, 2010). Moreover $Cl^-/HCO3^-$ exchanger SLC4A1 has been shown to localize to the olfactory cilia (Hengl et al., 2010) where it works as an additional mechanism for ciliary Cl^- uptake. (Fig. 3)

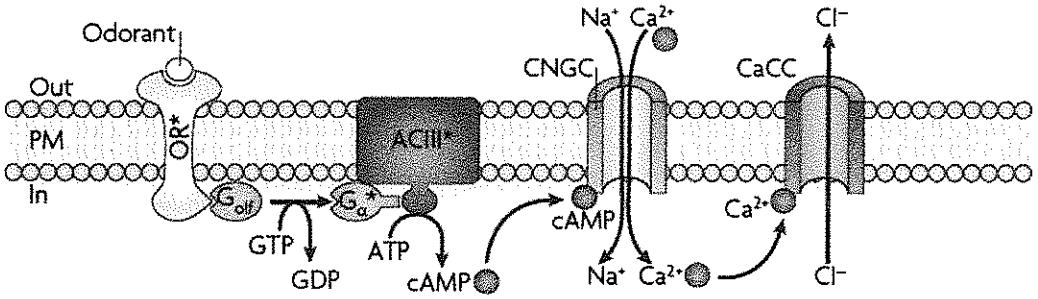

Figure 3: **Signal transduction in OSNs.** The binding of an odorant to the odorant receptor (OR) successively activates the trimeric, olfaction-specific G protein (Golf),adenylyl cyclase type III (ACIII), the olfactory cyclic nucleotide-gated channel (CNGC;composed of one B1b, one A4 and two A2 subunits) and a Ca^{2+}-activated Cl^- channel (CaCC). Activation of both channel types finally leads to depolarization (Kaupp, 2010).

Therefore, the odor-induced current, generated by the conversion of the binding of the chemical stimulus into an electrical signal, is composed by two components: the CNG-mediated current and the Ca^{2+} -activated Cl^- current. In isolated OSNs, the response to odor stimuli has been well characterized. Most often, the response has been measured under voltage-clamp upon presentation of a brief pulse of odor. The response typically lasts 1 s or more. In amphibians, the range of latency between arrival of the stimulus and the onset of the current goes from 150 to 600 ms (Firestein & Werblin, 1987; Kurahashi, 1989; Firestein *et al.*, 1990; Takeuchi *et al.*, 2003). In mouse and rat, the value of latency is shorter, almost 160 ms (Reisert & Matthews, 2001; Grosmaitre *et al.*, 2006). For a strong stimulus, the amplitude of peak current reaches several hundred

pA: 700 pA in amphibians (Kurahashi, 1989; Firestein *et al.*, 1990; Lowe & Gold, 1991; Takeuchi *et al.*, 2003) to 1.5 nA in rat (Ma *et al.*, 1999). The odor response creates a transient increase in cytoplasmic Ca^{2+} with a time course of the same range of the odor induced current. The dose response relationship between the odor and the peak current is generally well fitted by the Hill equation:

$$I = I_{max} [C]_i^{nH} / ([C]_i^{nH} + K_{1/2}^{nH}) \qquad [eq.1]$$

where I_{max} is the maximum macroscopic current, C is the concentration of odorant, $K_{1/2}$ is the half-maximally effective concentration, and *n*H is the Hill coefficient. In isolated salamander OSNs under whole-cell recording conditions, $K_{1/2}$ for the 3 odors isoamylacetate, cineole and acetophenone ranged from 3 to 90 µM (Firestein *et al.*, 1993). (Fig. 4)

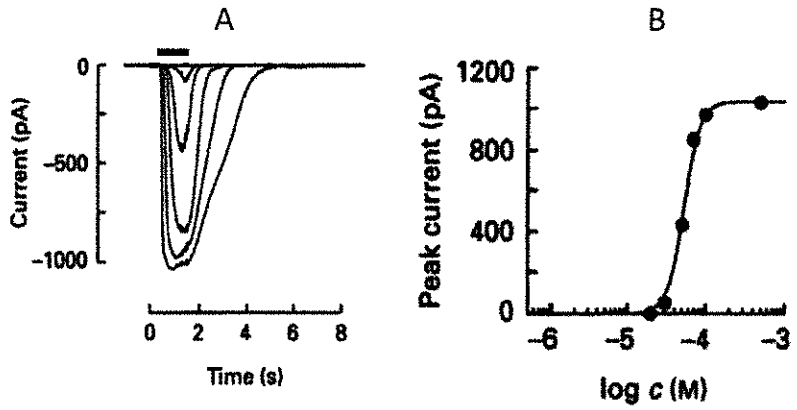

Figure 4: **Odor response relationship of OSNs under voltage clamp**: A. Responses of isolated salamander OSNs to odorant stimulation (various concentration of isoamyl acetate presented for 1.2 s) measured with the voltage-clamp whole-cell configuration at -55 mV holding potential. B. Plot of the odorant induced current versus the odor concentration. The solid line is the best fit of the Hill equation to the data with $K_{1/2}$ = 53 µM and n= 4.2 (Firestein et al., 1993).

1.4 The molecular identity of channels involved in olfactory transduction

1.4.1 CNG channels

The finding that the stimulation of OSNs causes an increase in intracellular cAMP levels was soon followed by the description of how cAMP leads to a change in membrane conductance and how the primary electrical signal is generated. Nakamura and Gold reported currents activated by cAMP and cGMP from patches excised from toad olfactory cilia (Nakamura & Gold, 1987) as previously described for photoreceptors (Fesenko *et al.*, 1985; Haynes & Yau, 1985). The CNG channel has been described for a number of different species (including salamander, frog, newt, rat and mouse (Firestein & Shepherd, 1991; Frings *et al.*, 1992; Kleene, 1994; Munger *et al.*, 2001)).

The relation between concentration of cAMP and CNG current is well fitted with a Hill equation (see [eq.1]). $K_{1/2}$ values for half-activation by cAMP are in the micromolar range, but vary considerably between species: about 3 µM in mouse (Pifferi *et al.*, 2006*a*; Michalakis *et al.*, 2006) 4.1 µM in rat (Bönigk *et al.*, 1999), 2 µM in frog (Kleene, 1999), 19 µM in toad (Kurahashi & Kaneko, 1993). The Hill coefficient ranges from 1.3 and 2.3 suggesting that at least 2 molecules of cAMP must bind before channel opening.

Kaupp and collaborators (Kaupp *et al.*, 1989) first cloned the CNG channel in retinal rods. CNG channels are composed of four subunits forming a tetramer with a central pore. The topology of each subunit shows six transmembrane-spanning domains, a pore-loop domain between the fifth and sixth transmembrane domain, and intracellular N- and C-terminal regions (Fig. 5 A). CNG channels are activated by the direct binding of cyclic nucleotides to a large C-terminal cyclic nucleotide-binding domain and are only weakly sensitive to membrane voltage (Kaupp & Seifert, 2002). The olfactory CNG channels are composed of three types of subunits: CNGA2, CNGA4 and CNGB1b with a stoichiometry of two

CNGA2, one CNGA4 and one CNGB1b (Dhallan *et al.*, 1990; Ludwig *et al.*, 1990; Liman & Buck, 1994; Zheng & Zagotta, 2004) (Fig 5 B).

The channel is mainly present in the ciliary membrane (Kurahashi & Kaneko, 1991; Lowe & Gold, 1993*b*) but it is also expressed in the soma and dendrite at much lower densities. The channel density in the cilium has been estimated by electrophysiological methods with widely differing results: 1750 channels/μm^2 in toad (Kurahashi & Kaneko, 1993), 67–202 channels/μm^2 in frog (Kleene, 1994; Larsson *et al.*, 1997), and 8 channels/μm^2 at the dendritic knob/cilia in rat (Reisert *et al.*, 2003). CNG channels are permeable to all monovalent cations Na^+, K^+, Li^+, Rb^+ and Cs^+ with similar permeability ratios in rat (Frings *et al.*, 1992) and in newt (Kurahashi, 1990) and are modulated by divalent cations on both sides of the ciliary membrane. Ca^{2+} and Mg^{2+} have many effects on the olfactory CNG channel through both intracellular and extracellular mechanisms. They permeate and at the same time block the current carried by Na^+ (Zufall & Firestein, 1993; Kleene, 1995; Frings *et al.*, 1995; Seifert *et al.*, 1999) with a higher effect at negative potentials, resulting in a single channel conductance from 0.56 to 1.5 pS.

CNG channels are desensitized by Ca^{2+}–CaM-mediated feedback inhibition, which lowers the cAMP sensitivity. Although all three olfactory CNG channel subunits have CaM binding sites, only a so-called 'IQ motif' in the B1b subunit renders the channel sensitive to CaM (Fig. 5 B). CaM is pre-associated with the channel, allowing for rapid negative feedback (Kaupp, 2010).

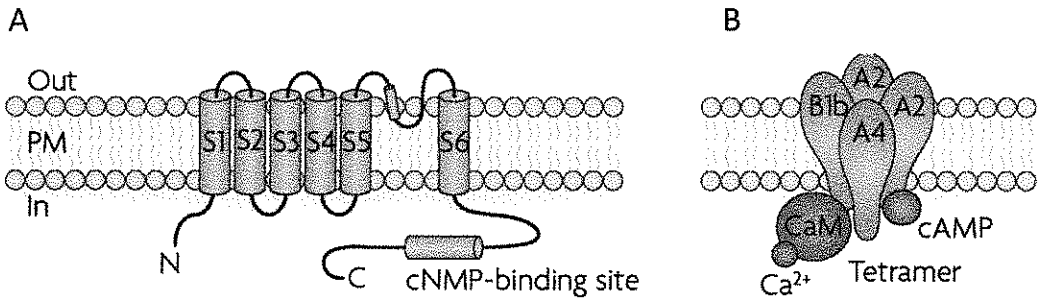

Figure 5: **The topology and oligomeric state of CNG channel**: A. Topology: each TM domain is indicated by a number, the pore loop is located between 5 and 6. The cyclic nucleotide binding site is located in the C-terminal domain. B. Tetrameric organization: cAMP binding domain located in A2 subunit and CaM binding site located in the B1b subunit (Kaupp, 2010).

1.4.2 Ca^{2+} -activated Cl^- channel

In 1991 Kleene and Gesteland reported the presence of a Ca^{2+} -activated Cl^- current in frog olfactory cilia (Kleene & Gesteland, 1991). After this report CaCCs have been described in OSNs of amphibians (Kurahashi & Yau, 1994) and mammals (Lowe & Gold, 1993*b*; Reisert *et al.*, 2003; Reisert & Bradley, 2005). This conductance is of significant importance for olfactory transduction, indeed under voltage clamp conditions a large fraction of the odour-induced inward current is carried by this channel, ranging from 36%-65% amphibians (Kurahashi & Yau, 1993; Zhainazarov & Ache, 1995; Lowe & Gold, 1993*a*;) and 85%-90% in rat (Reisert *et al.*, 2003) and mouse (Nickell *et al.*, 2006; Boccaccio & Menini, 2007).

The excitatory nature of this Cl^- current depends on the reversal potential for the Cl^- channel which is positive with respect to the resting potential. The reversal potential has in fact been measured to be about 0 mV in Xenopus leavis (Zhainazarov & Ache, 1995). For the newt, an intracellular Cl^- concentration of 40 mM was measured with fluorescent probe (Nakamura *et al.*, 1997; Kaneko *et al.*, 2001).

In frog the channels are present in virtually all the olfactory cilia (Kleene, 1994). In rat the channel density in the cilium is estimated to be four functional Cl^- channels per CNG channel (Reisert *et al.*, 2003).

The conductance is half-activated at 4.7 μM Ca^{2+} with a Hill coefficient of 2 (Kleene & Gesteland, 1991; Reisert *et al.*, 2003, 2005; Pifferi *et al.*, 2006*b*).

The single channel conductance has been extimated to be only 0.8 pS in frog (Larsson *et al.*, 1997) and 1.5 pS in rat (Reisert *et al.*, 2003), 1.6 pS for mouse (Pifferi *et al.*, 2006*b*) and the maximum open probability of this channel is 0.97. The very small conductance with high maximum open probability allows a high amplification without an increase of noise, giving OSNs the ability to improve their signal to noise ratio (Kleene, 1997). Rodent (mouse and rat) Ca^{2+}-activated Cl^- currents, recorded in inside-out excised patches from the dendritic knob/cilia, show a Ca^{2+} -dependent reduction of the amplitude of the current (inactivation) which is reversible

after removal of Ca^{2+} (Reisert *et al.*, 2003, 2005; Pifferi *et al.*, 2006*b*). In amphibian OSNs excised intact cilium the current does not show spontaneous inactivation after exposure to Ca^{2+} (Kleene & Gesteland, 1991; Kleene, 1993). Moreover, the channel shows a rundown in activity after patch excision (Reisert *et al.*, 2003, 2005).

Very recently the group of Jentsch showed that Ca^{2+}-activated Cl^- currents were undetectable in mice lacking the CaCC TMEM16B (see later) and these mice seem to have no deficits in odour sensitivity (Billig *et al.*, 2011), supporting previous findings on a KO mouse for NKCC1 (Smith *et al.*, 2008).

1.4.2.1 Properties of CaCCs

CaCCs perform many important functions in cell physiology including secretion of fluids from acinar cells of secretory glands, regulation of cardiac and neuronal excitability, mediation of the fast block of polyspermy in amphibian oocytes and regulation of vascular tone.

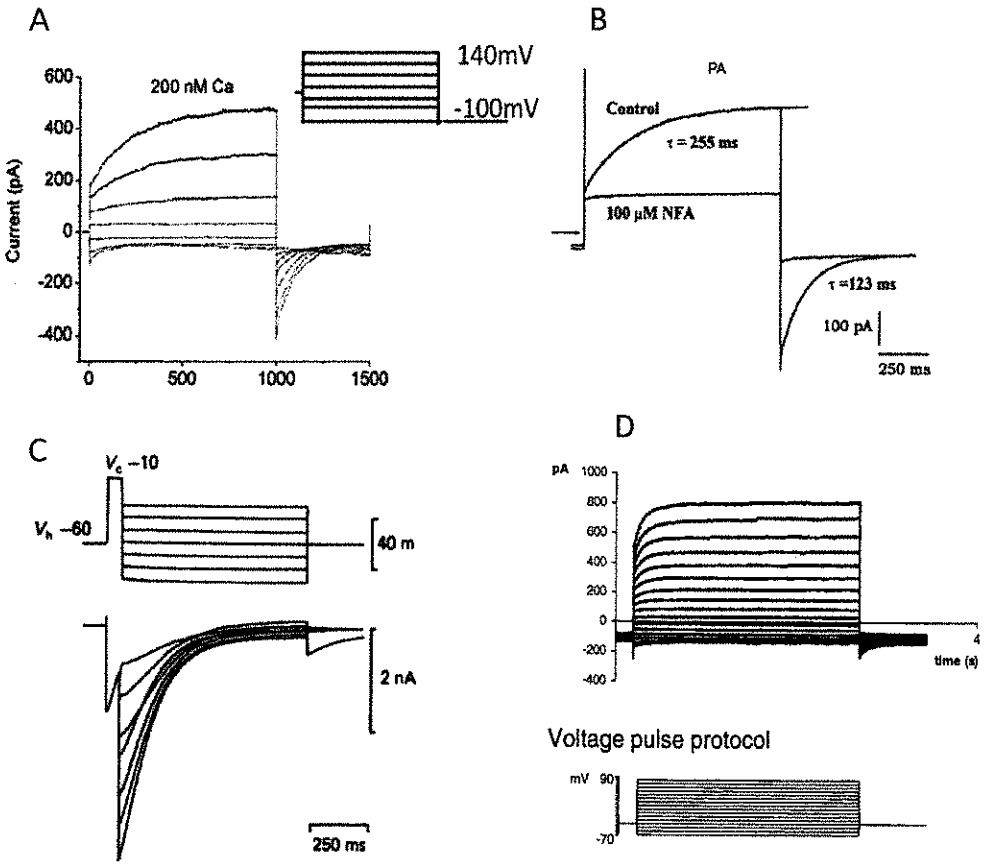

Figure 6. **Examples of classic CaCCs recorded in *X. laevis* oocytes and mammalian cells.** A. CaCC in *X. laevis* oocyte. The patches were clamped from a holding potential of 0 mV to potentials between 140 and -100 mV for 1 s, followed by a 500-ms pulse to -100 mV (Qu and Hartzell, 2000). B. CaCC recorded in rat pulmonary artery (PA) smooth muscle cells, representative current tracings recorded in the absence (Control) and presence of 100 μM NFA, voltage-dependent currents were evoked by 1-s step depolarization from a holding potential of -50 mV to +70 mV, followed by 1-s return steps to -80 mV (Greenwood *et al.*, 2001). C. CaCC recorded in cultured rat dorsal root ganglia neurons activated by a depolarizing prepulse (Mayer, 1985). D. Whole-cell Cl(Ca) currents recorded from a single isolated mouse pancreatic acinar cell. Currents were elicited using the voltage pulse protocol shown (Kidd & Thorn, 2000*a*).

The activation of CaCCs requires cytosolic Ca^{2+} which can be induced through different approaches: application of constant amounts of Ca^{2+}; photorelease of Ca^{2+}; induction of Ca^{2+} release by IP_3 or enhancing Ca^{2+} entry by application of Ca^{2+} ionophores (Hartzell *et al.*, 2005).

CaCCs are activated by cytosolic Ca^{2+} with half-maximal concentrations in the submicromolar range. Several studies reported comparable $K_{1/2}$ values (283 nM at +100 mV in pulmonary artery endothelial cells (Nilius *et al.*, 1997), 0.9 μM at +120 mV in *Xenopus* oocytes (Kuruma & Hartzell 1999), 63 nM at +97 mV (Arreola *et al.*, 1996) and Hill coefficients higher than 1, suggesting that more than one Ca^{2+} ion is required to activate the channel. Ca^{2+} binding is voltage sensitive with higher level of affinity at positive membrane potentials than negative membrane potentials (Arreola *et al.*, 1996; Kuruma & Hartzell, 2000; Reisert *et al.*, 2003). Some results indicate that when $[Ca^{2+}]_i$ is lower than 1 μM the Ca^{2+} -activated Cl^- current is both voltage (showing an outward rectification in the current-voltage relationship) and time dependent (slowly reaching a steady-state level of the current), whereas at higher concentrations both voltage and time dependence disappears (Fig. 7) (Arreola *et al.*, 1996; Kuruma & Hartzell, 1999). The outward rectification at low Ca^{2+} concentrations might be explained by a voltage dependence of the apparent affinity of CaCCs for Ca^{2+} (Arreola *et al.*, 1996; Nilius *et al.*, 1997; Kuruma & Hartzell, 1999).

Permeant anions could influence the activation of CaCCs (Greenwood & Large, 1999). It has been found that anions with higher permeability, such as SCN^-, NO_3^- and I^-, generate a faster activation and slower deactivation, effects which seem to be independent of the channel affinity for Ca^{2+}. These data suggest that in some systems the process of CaCCs gating could be coupled to the permeation mechanism. CaCCs are relatively nonselective, indeed some authors prefer to define them as anion channels rather than Cl^- channels (Jentsch, 2002). The selectivity sequence for CaCCs of Xenopus oocytes, rat parotid gland and lachrymal glands is $SCN^->NO_3^->I^->Br^->Cl^->F^-$ (Evans & Marty, 1986; Large & Wang, 1996; Nilius *et al.*, 1997; Kidd & Thorn, 2000; Qu & Hartzell, 2000; Perez-Cornejo & Arreola, 2004) and the Na^+ permeability is about 10 % that of

Cl^- (PNa/PCl=0.1). The understanding of the precise mechanisms of anion permeation in CaCCs requires the molecular identification of these channels coupled with mutagenesis and structural studies.

Specific channel blockers with high binding affinity are powerful tools for investigating ion channels, but unfortunately no specific CaCCs' blockers exist (Verkman & Galietta, 2009). The most common blockers for native CaCCs are NFA (niflumic acid) and flufenamic acid (White & Aylwin, 1990), that block CaCCs in *Xenopus* oocytes at concentrations of about 10 µM (Qu & Hartzell, 2001). Other commonly used chloride channel blockers are tamoxifen, DIDS, SITS, NPPB, A9C although they are less effective on CaCCs (Frings *et al.*, 2000).

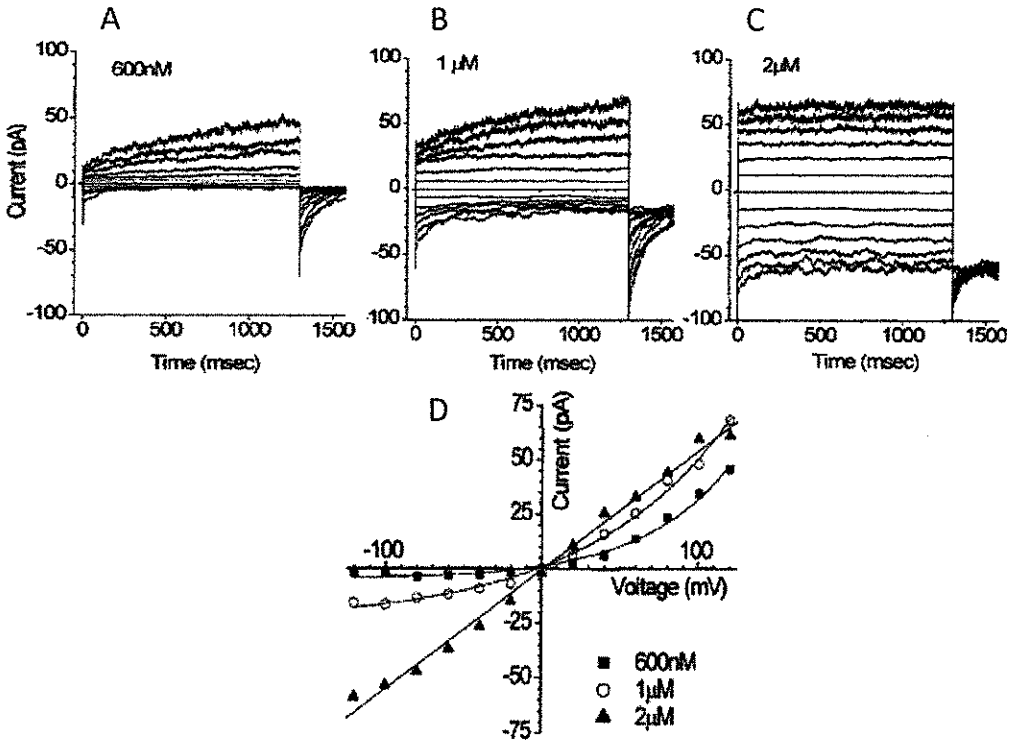

Figure 7: **Ca^{2+} dependence of Cl^- current in excised patches from *Xenopus* oocyte**: A, B and C. The cytosolic face of an excised patch was exposed to solutions with different free [Ca^{2+}] as indicated. The patch was voltage clamped by stepping to various potentials between -120 and +120 mV for 1.3 s from the holding potential of 0 mV, followed by a step to -120 mV for 0.3 s. D. Steady state current–voltage relationships of currents in A, B and C. (Kuruma & Hartzell, 2000).

The activation of CaCCs by Ca^{2+}, as well as the degree of cooperativity, depends on the membrane voltage in many systems (Arreola *et al.*, 1996; Frings *et al.*, 2000).

The activation of CaCCs in *Xenopus oocytes* and in rat parotid gland (Arreola *et al.*, 1996; Kuruma & Hartzell, 2000) has been modelled assuming that 2 or 3 Ca^{2+} ions interact with closed states of the channel in a linear sequence. Arreola and colleagues' model proposes 3 closed states and 1 open state with 2 Ca^{2+} ions bound (Fig 8, Scheme 1) (Arreola *et al.*, 1996). Kuruma and Hartzell instead, suggested that 3 Ca^{2+} ions bind and their model has 4 closed and 3 open states (Fig. 8, Scheme 2) (Kuruma & Hartzell, 2000).

Both models assumed that the Ca^{2+} binding sites are independent but have the same affinity. At low Ca^{2+} concentrations, both models describe quite well the opening of the channels, but not at high concentrations. The discrepancy between the two models is at the level of voltage dependence: Arreola's model defines the voltage dependence both in the Ca^{2+} binding and in the open to closed state; Kuruma and Hartzell's model, in contrast, assumes that the voltage dependence is only in the open to closed transition. Piper and Large in 2003 (Piper & Large, 2003), analysing single channel events from smooth muscle cells, agreed with Kuruma and Hartzell's model about the number of closed and open states but they defined the voltage dependence at the level of the transition between C1 and C2. Furthermore, because at higher Ca^{2+} concentrations the conductance decreased from 3.8 to 1.2 pS, it was proposed that channel conductance depends on the occupancy of the Ca^{2+}-binding sites.

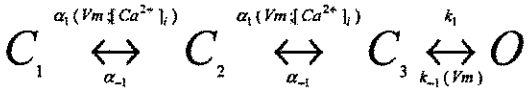

Scheme 1

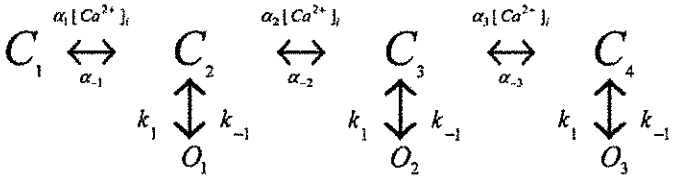

Scheme 2

Figure 8: **Gating schemes for CaCCs**: CaCCs are proposed to have several closed (C) and open (O) states. Rate constants are shown to be voltage (Vm) and/or Ca2+ sensitive. Scheme 1 was proposed by Arreola et al. (Arreola *et al.*, 1996) and Scheme 2 by Kuruma & Hartzell (Kuruma & Hartzell, 2000).(Hartzell *et al.*, 2005)

1.5 Molecular identity

The identification of the CaCCs' molecular identity is an important goal in understanding their role in physiology and in disease, but it has remained elusive for a long time. This difficulty arised from two crucial point: the favorite expression system for expression cloning of ion channels has been the *Xenopus* oocyte, but this cell expresses huge edogenous Ca^{2+}activated Cl^- current, moreover specific blockers for these channels were not available (Verkman & Galietta, 2009). Various protein families, such as CLCA and Bestrophins, have been proposed as candidates for the CaCC, but they did not recapitulate all the characteristic features of endogenous CaCCs.

1.5.1 CLCA

The Ca^{2+} -activated Cl^- channel (CLCA) family was purified from bovine trachea (Cunningham *et al.*, 1995), but CLCA is unlikely to function as native CaCC. CLCA generates indeed Ca^{2+}-activated Cl^- currents with the same ionic selectivity than CaCCs, but the I-V relationship obtained in whole-cell experiments were linear, currents were not blocked by NFA, were activated by depolarization in the absence of Ca^{2+} and were sensitive to the reducing agent dithiothreitol while native currents are not (Cunningham *et al.*, 1995).

Structure–function analysis has not provided any clear evidence that CLCAs are actually channels, they have, indeed, very high homology to known cell adhesion proteins and some are soluble, secreted proteins (Loewen & Forsyth, 2005).

From analysis of the CLCA protein sequences a metallohydrolase structural domain was predicted, which raises the possibility that CLCA can perform catalytic functions similar to those of metalloproteases (Pawłowski *et al.*, 2006). It it seems therefore reasonable to conclude that CLCA is not a valid candidate for CaCC.

1.5.2 Bestrophins

The first gene of the Bestrophin family (hBest-1) was cloned in 1998 and was the one responsible for the Best vitelliform macular desease (Petrukhin *et al.*, 1998).

Bestrophin 1 is assumed to form the basolateral CaCC in the retinal pigment epithelium (RPE) of the eye. Bestrophin 1 is expressed at high levels in or close to the basolateral membrane of retinal pigment epithelial (RPE) cells (Marmorstein *et al.*, 2000).

The so-called light peak in the electrooculogram of the eyes is presumably generated by Ca^{2+}-dependent activation of Cl^- channels in the basolateral membrane of the retinal pigment epithelium (Hartzell *et al.*, 2008). The light peak is reduced in patients with autosomal dominant vitelliform macular dystrophy (Best disease) who carry mutations in bestrophin 1: it was assumed that bestrophins is the CaCC in the basolateral membrane of RPE cells (Qu & Hartzell, 2004). However, its role in RPE is still matter of debate (Kunzelmann *et al.*, 2009).

It was shown that bestrophins function as CaCCs (Qu *et al.*, 2004; Tsunenari *et al.*, 2003; Sun *et al.*, 2002) with many features that resemble those of native CaCCs. Although both expressed bestrophin channels and native CaCCs are gated directly by Ca^{2+} and both exhibit the same anion selectivity sequence, there were, tough, some important discrepancies: expressed hBest1 and mBest2 have an apparent affinity for Ca^{2+} that is 10 times higher than that of CaCCs (Pifferi *et al.*, 2006*b*); bestrophins mediated currents with no outward rectification neither time-dependent activation (Tsunenari *et al.*, 2003, 2006; Qu *et al.*, 2004; Pifferi *et al.*, 2006*b*; Hartzell *et al.*, 2008); in olfactory sensory neurons and submandibolar gland acinar cells of knock-out mice Ca^{2+} -activated Cl^- currents were unaffected (Pifferi *et al.*, 2009*b*; Romanenko *et al.*, 2010); mice knock-in for the mutation W93C in hBest1, responsible for the Best vitelliform macular dystrophy, exhibited unaltered Ca^{2+} -activated Cl^- current (Zhang *et al.*, 2010) and when Best3 was downregulated, Ca^{2+} -activated Cl^- current was not affected (Matchkov *et al.*, 2008).

1.5.3 Anoctamins/TMEM16

In 2008 the molecular identity of CaCCs has been understood thanks to the discoveries of three different laboratories working in different fields. Using different approaches these groups found that TMEM16A, also known as Anoctamin1 (Ano1), functions as a CaCCs (Caputo *et al.*, 2008; Schroeder *et al.*, 2008; Yang *et al.*, 2008). In 2009, another member of the family, TMEM16B/Anoctamin2 (Ano2) was shown to function as CaCC (Stöhr *et al.*, 2009; Stephan *et al.*, 2009; Pifferi *et al.*, 2009*a*).

The term 'TMEM16' comes from 'Transmembrane proteins with unknown function 16', while 'Anoctamin' was coined because these channels are ANion selective and hydropathy analysis indicated that they have eight (OCT) transmembrane segments (Yang *et al.*, 2008). However, it is still not clear if all the members of the family function as CaCCs.

The TMEM16 family consists in 10 members. They are found throughout the eukaryotes, including mammals (Fig. 9), flies, worms, plants, protozoa and yeast, but they seems to be best represented in the higher vertebrates.

In vertebrates the TMEM16 family was first described in a bioinformatic study (Katoh & Katoh, 2003, 2005). Before this recent discovery, TMEM16 proteins were already known, with various names, as proteins involved in some different tumors (West *et al.*, 2004; Huang *et al.*, 2006; Espinosa *et al.*, 2008; Kashyap *et al.*, 2009).

Current data suggest that members of the TMEM16 protein family are involved in both normal vertebrate development and disease; the existence of multiple TMEM16 paralogs in mice and humans might have evolved to allow tissue-specific expression of proteins with similar functions (Galindo & Vacquier, 2005; Rock & Harfe, 2008; Duran & Hartzell, 2011).

Almaça and colleagues in 2009 have shown that TMEM16F/Ano6, TMEM16H/Ano8 and TMEM16J/Ano9 work as Cl^- channels implicated in the control of cell volume (Almaça *et al.*, 2009), whereas Galietta's group found that transfection of TMEM16C, TMEM16F, TMEM16G, TMEM16H, TMEM16J and TMEM16K in HEK 293 cells did not result in increased anion

transport or membrane currents (reviewed by Scudieri *et al.*, 2012). Schreiber and colleagues in 2010 showed that TMEM16H/Ano8 inhibit TMEM16A/Ano1 current (Schreiber *et al.*, 2010). Thus, it is likely that these proteins of the family are not CaCCs but have different functions. In this respect it has been recently found that TMEM16F (anoctamin 6) is involved in phospholipid scramblase activity (Suzuki *et al.*, 2010).

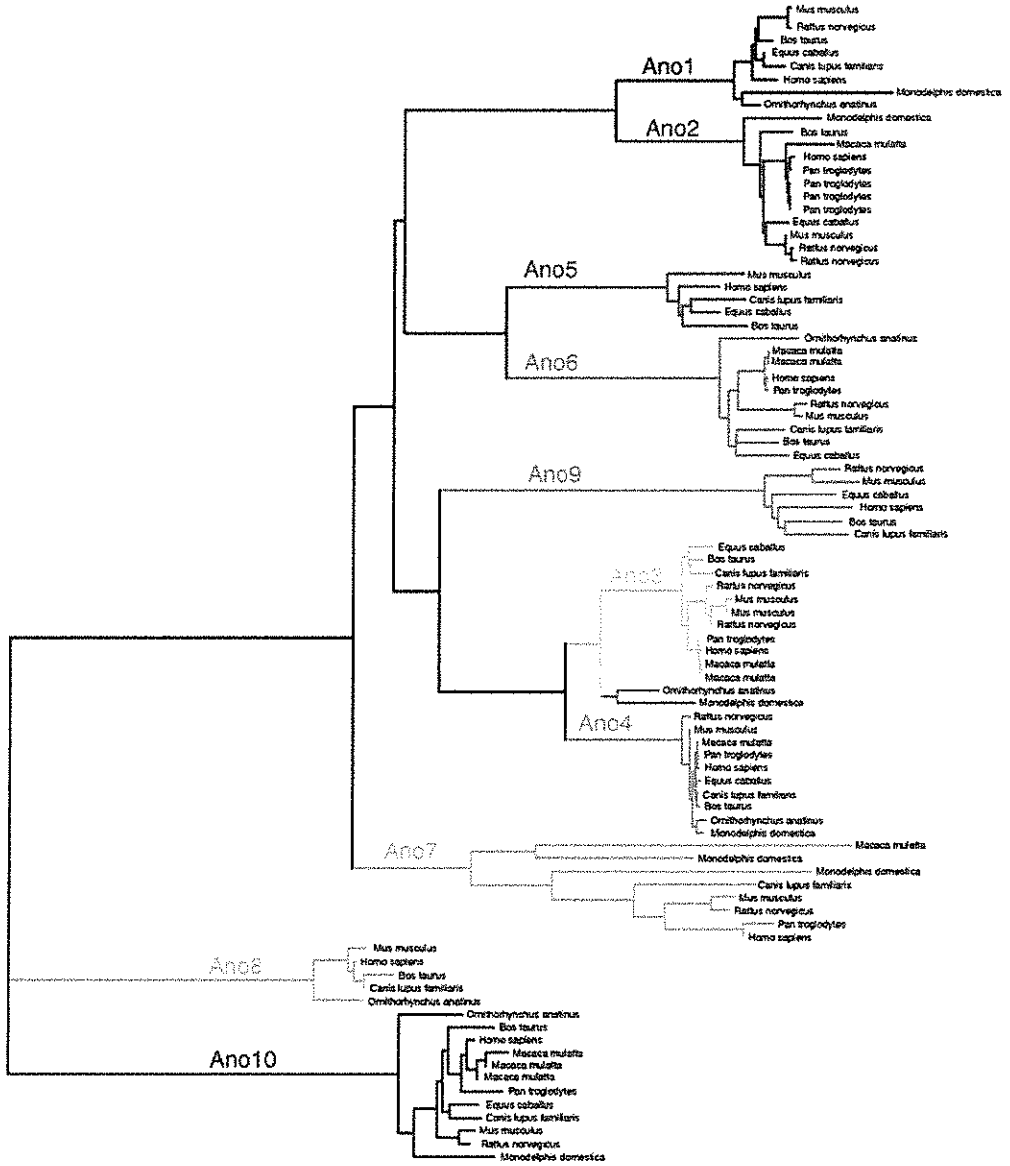

Figure 9: **Phylogeny of the ANO/TMEM16 family:** Human ANO1 was subjected at NCBI to position-specific iterated BLAST (2.2.18+) (http://www.ncbi.nlm.nih.gov/blast) (Altschul *et al.*, 1990) threshold of 0.005 against all mammalian sequences in the reference proteins database (ref_seq_protein) through 6 iterations to find all of the mammalian members of the family. The tree was constructed using the fast minimal evolution method (Desper & Gascuel, 2004) using distances computed according to (Grishin, 1995). (Hartzell *et al.*, 2009).

1.5.3.1 Cellular expression

In order to understand if TMEM16 proteins are the proteins responsible for the endogenous CaCCs many studies on their expression, their structure-function relationship and their involvement in the physiological processes on different systems, were performed.

Huang et al. (Huang *et al.*, 2009) generated an antibody against mouse TMEM16A and they found it is expressed in the airway epithelial cells and smooth muscle cells, in the apical membranes of epithelial cells in exocrine glands, trachea and in the interstitial cells of Cajal.

Reduction of TMEM16A expression with siRNAs in pulmonary artery smooth muscle cells led to an almost total loss of whole-cell CaCC currents (Manoury *et al.*, 2010).

TMEM16A mRNA is also detected in smooth muscle cells isolated from mouse portal vein, thoracic aorta, and carotid artery with varied abundance (Davis *et al.*, 2010).

Immunostaining signals for TMEM16A have been detected in most DRG sensory neurons (Yang *et al.*, 2008) and in presynaptic terminal of photoreceptors (Mercer *et al.*, 2011). TMEM16B was found in OSNs, VNOs and in presynaptic terminal of photoreceptors (Stöhr *et al.*, 2009; Mercer *et al.*, 2011; Billig *et al.*, 2011; Stephan *et al.*, 2009; Rasche *et al.*, 2010; Hengl *et al.*, 2010; Sagheddu *et al.*, 2010). TMEM16C is expressed in the nervous system, TMEM16E is known for its involvement, when mutated, in a genetic disorder called ganthodiaphyseal dysplasia. TMEM16F and TMEM16K are expressed ubiquitously and TMEM16G is specifically expressed in prostate (Galietta, 2009).

1.5.3.2 Topology

All TMEM16 proteins have a similar putative topology, indeed bioinformatic hydropathy analysis showed eight transmembrane segments and intracellular N- and C-termini, a conserved C-terminal domain of unknown function (DUF590) and a N-linked glycosylation site in the last extracellular loop (except in TMEM16K) (Hartzell *et al.*, 2009; Kunzelmann *et al.*, 2009; Flores *et al.*, 2009; Galietta, 2009). Interestingly, the transmembrane segments are the regions of TMEM16 proteins showing maximal conservation (Fig. 10).

The pore is predicted between the 5th and 6th transmembrane helices (TM5 and TM6) together with a P-loop dipping back into the membrane (except in TMEM16H and K) (Katoh & Katoh, 2003, 2005; Galindo & Vacquier, 2005; Yang *et al.*, 2008).

The primary sequence identity between TMEM16A and TMEM16B is relatively high (~60%) but decreases progressively with the other TMEM16 proteins, so that TMEM16F, G, H, J, and K are only 20–30% identical (Galietta, 2009).

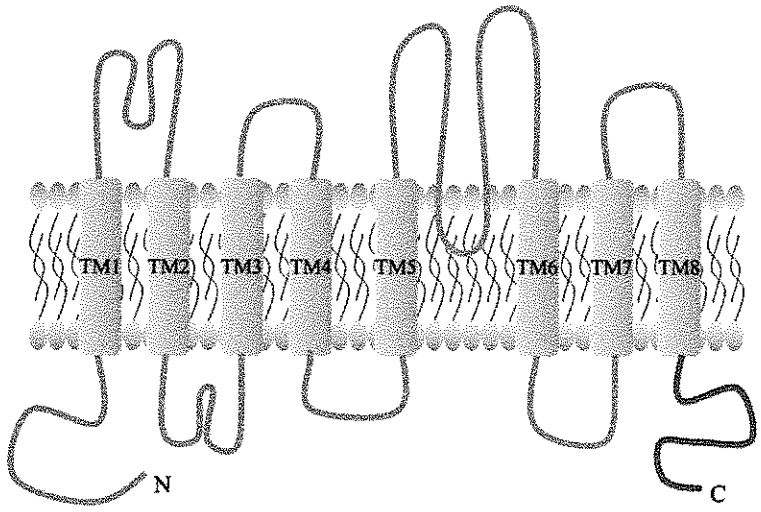

Figure 10: **Predicted topology of TMEM16 proteins:** topology of TMEM16A/ANO1. The cytosolic C-terminal domain of mANO1 is coloured red. (Park *et al.*, 2011)

TMEM16 channels exhibit multiple alternatively spliced forms: Caputo et al. (Caputo *et al.*, 2008) reported the existence of different TMEM16A isoforms generated by alternative splicing. Some samples showed the co-existence of more than one isoform, whereas others revealed the preferential inclusion or skipping of one segment (*b* or *d*). In contrast, segment *c* was almost always included in most samples. They called the minimal isoform TMEM16A (0) and it consists of 840 aminoacids with a significantly shortened amino-terminus. Four alternative regions could be inserted to this minimal isoform: segment a (116 residues) at the N-term; segment b (22 residues) before the first transmembrane domain; segment c (4 residues) and segment d (26 residues) in the first intracellular loop. All isoforms, including TMEM16A (0), are functional, their biophysical characterization will be described later (Caputo *et al.*, 2008; Ferrera *et al.*, 2009, 2011).

TMEM16G has two splice variants: a 933-amino-acid plasma membrane protein and a shorter 179-amino-acid cytosolic protein (Bera *et al.*, 2004) and other members of the family have also short splice variant transcripts suggesting the possibility that they could have additional non-channel functions or could fulfill tasks in intracellular compartments.

TMEM16B exists in two different splice variant, the retinal and the olfactory isoforms (Pifferi *et al.*, 2009*a*; Stephan *et al.*, 2009; Stöhr *et al.*, 2009). Preliminary data also indicated the existence of more splice variants for TMEM16B (Saidu S.P., Stephan A.B., Caraballo S.M., Zhao H. and Reisert J., Association for Chemoreception Sciences Meeting 2010, abstract P68).

Interesting structural aspects of TMEM16A came to light recently from the work of two different groups (Fallah *et al.*, 2011; Sheridan *et al.*, 2011). TMEM16A exists as a homodimer and the multimerization seems to occur intracellularly before the channel is trafficked to the membrane (Sheridan *et al.*, 2011), the domains involved are still not known and the similarity to ClC family channels about the presence of two pores in the channel remains to be determined. The possibility of a hetero-oligomerization with other family members has not been investigated yet.

1.5.3.3 TMEM16A

1.5.3.3.1 Ca^{2+} sensitivity

The relation between current and Ca^{2+} concentration is well described with the Hill equation. Yang et al. in 2008 found, in excised patches, that the half-maximal activation of TMEM16A is 2.6 μM at -60 mV and 0.3 μM at +60 mV displaying a voltage-dependence of the apparent affinity for Ca^{2+}. Moreover, TMEM16A was inhibited by Ca^{2+} concentrations higher than 10 μM. The single channel conductance was determined to be 8.6 pS in HEK293 cells (Yang *et al.*, 2008; Huang *et al.*, 2012).

Affinity for Ca^{2+} is dependent on the splice variant expressed: a minimal isoform of TMEM16A lacking all four alternatively spliced exons gives rise to robust current activated by Ca^{2+}, showing that calcium-sensing elements are still present (Ferrera *et al.*, 2011). Inclusion of segment *b* (26 aminoacids in the N- terminal) reduces the apparent affinity for Ca^{2+} by nearly fourfold (Ferrera *et al.*, 2009). Xiao et al. (Xiao *et al.*, 2011) found that deleting segment c (EAVK) dramatically decreases apparent Ca^{2+} affinity.

From the primary protein sequence of TMEM16A typical high-affinity calcium binding sites such as EF hands and C2 domains cannot be identified, only a reminescence of the Ca^{2+} bowl of BK channels is present in the first intracellular loop as a stretch of 5 consecutive conserved glutamic acid residues (Schreiber & Salkoff, 1997; Ferrera *et al.*, 2010). In contrast with this hypotesis, Xiao et al. in 2011 mutating these amino acids (EEEE) found no alteration of the apparent Ca^{2+}affinity (Xiao *et al.*, 2011).

A *bona fide* calcium binding site remains to be conclusively identified and might be formed from disparate regions on the channel.

It is also possible that an auxiliary protein binds to and mediates TMEM16A activation upon an increase in intracellular calcium levels. Calmodulin has been proposed to carry out such a function. Tian et al. (2011) reported that calmodulin can be coimmunoprecipitated with

TMEM16A and that calmodulin inhibitors decreased whole-cell currents of TMEM16A (Tian *et al.*, 2011).

1.5.3.3.2 Voltage-dependence

TMEM16A-mediated current shows outwardly rectifying behavior of the steady-state current-voltage relationship at low Ca^{2+} concentrations. However, elevation of intracellular Ca^{2+} to micromolar concentrations produces a current-voltage relationship close to linearity (Fig. 11) (Schroeder *et al.*, 2008; Caputo *et al.*, 2008; Yang *et al.*, 2008; Hartzell *et al.*, 2009).

The voltage-dependence changes in different splice variants: the minimal TMEM16A isoform, that has shorter intracellular domains, gives rise to a channel that mediate currents that are Ca^2 dependent but are unaffected by membrane potential, with the absence of the time-dependent relaxation upon depolarizing step (Caputo *et al.*, 2008; Ferrera *et al.*, 2009, 2011); the absence of the four amino acids (E-A-V-K) corresponding to segment *c* in the first intracellular loop, alters the voltage dependence of the channel making the channel less sensitive to membrane voltage and abolishes the time-dependent relaxation in response to a depolarization (Ferrera *et al.*, 2009). Xiao et al. in 2011 tested the same deletion and found a reduced Ca^{2+} sensitivity (as described in the previous paragraph), and a shift of the activation curve to more positive potentials, indicating that the voltage-dependence is affected. In the same work (Xiao *et al.*, 2011) they mutated five consecutive glutamic acid residues in alanine in the first intracellular loop, adjacent to segment c and found that this mutation abolishes intrinsic voltage-dependence of the channel (Xiao *et al.*, 2011).

It remains to be determined how voltage modulates TMEM16A channel function and how calcium and voltage couple to modulate channel gating.

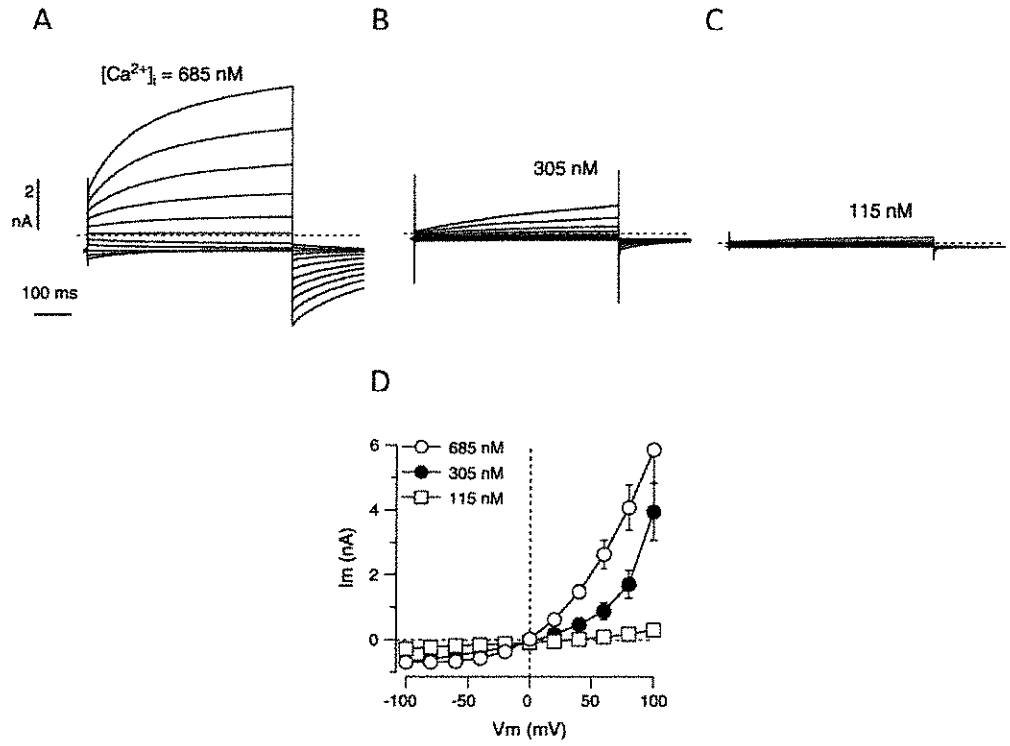

Figure 11: **Membrane current associated with TMEM16A**: A, B and C. Representative traces recorded from HEK-293 tranfected with TMEM16A (abcd). Experiments were perfomed in whole-cell voltage clamp using the intracellular Ca^{2+} concetrations as indicated. Currents were elicited at membrane potentials in the range – 100 to + 100. D. Current-voltage relationship from the traces in A, B and C. (Ferrera *et al.*, 2011)

1.5.3.3.3 Ionic selectivity

Cells expressing TMEM16A show channels with the following permeability sequence to anions: NO_3^- (2.20)> I^- (1.85)> Br^-(1.74) > Cl^- (1.0) > F^- (0.43) (Schroeder *et al.*, 2008; Yang *et al.*, 2008). A report indicated that the ionic selectivity of TMEM16A shifts during channel activation (Schroeder *et al.*, 2008).

The reentrant loop between TM5 and TM6 has been proposed to form the pore of the channel. Mutagenesis of positive amino acids critical for pore formation has revealed indeed that the selectivity has been affected, indicating that this region is involved in the pore formation (Yang *et al.*, 2008). By mutating an arginine and a glutamine in TM3 and TM6,

respectively the ion selectivity and voltage dependence were altered (Caputo *et al.*, 2008).

Xiao and colleagues (Xiao *et al.*, 2011) found that the substitution of Cl^- with other anions changes different features of the current: the time-dependent relaxation due to depolarization is reduced; outward rectification is less pronounced; G-V relationship is shifted to more negative potentials; the reversal potential of the current carried by mixtures of Cl^- and I^- cannot be described by the Goldman–Hodgkin–Katz equation. All together these data supports the idea that channel gating is dependent on ion permeation (Xiao *et al.*, 2011).

1.5.3.3.4 Pharmacology

One of the problems for the identification of the molecular identity of CaCCs has been the absence of specific blockers (Verkman & Galietta, 2009).

Traditionally, endogenous CaCCs have been inhibited by NFA, DIDS and NPPB. NPPB and NFA, strongly inhibit TMEM16A channels in the micromolar range (Caputo *et al.*, 2008).

Yang and colleagues (Yang *et al.*, 2008) reported that Tamoxifen blocked TMEM16A, whereas Schroeder and co-workers (Schroeder *et al.*, 2008) found it to be inactive.

Namkung and colleagues in 2010 reported that tannic acid blocked the TMEM16A current with K_d of 6 μM and at 100% inhibition at higher concentrations (Namkung *et al.*, 2010).

1.5.3.3.5 Post transductional modification

The analysis of the primary sequence of mammalian TMEM16A indicated the presence of putative phosphorylation sites for protein kinases A, C, and G, as well as CaMKII and casein kinase. However, TMEM16A activity in HEK-293 cells is not significantly affected by either staurosporine, a nonspecific kinase inhibitor, or the CaMKII inhibitor KN93 (Tian *et al.*, 2011).

1.5.3.3.6 TMEM16A, role in human disease

TMEM16A has been found overexpressed in human cancers. Oncologists have recognized TMEM16A by several other names including DOG1 (Discovered On GIST-1 tumor), ORAOV2 (Oral cancer Overexpressed), and TAOS-2 (Tumor Amplified and Overexpressed). In both oral and head and neck squamous cell carcinomas, amplification of the TMEM16A locus is correlated with a poor outcome (Carles *et al.*, 2006; Huang *et al.*, 2006). TMEM16A expression is significantly increased in patients with a propensity to develop metastases (Duran & Hartzell, 2011).

The relationship between cancer and a protein with a role in Cl^- transport is not clear. CaCCs may be important in proliferation, migration, and resistance of cancer cells to apoptotic stimuli (Galietta, 2009).

TMEM16A was also found to be one of the candidate genes responsible for autosomal recessive hearing impairment (Kalay *et al.*, 2007).

1.5.3.4 TMEM16B

Along with TMEM16A, TMEM16B has been shown to work as a CaCC. When TMEM16B was expressed in *Axolotl* oocytes (Schroeder *et al.*, 2008) or in HEK cells (Stöhr *et al.*, 2009; Stephan *et al.*, 2009; Pifferi *et al.*, 2009*a*; Sagheddu *et al.*, 2010) it displayed properties resembling those of CaCCs.

Among members of the mouse family, TMEM16B is the most similar to TMEM16A, with 62% amino acid identity (Yang *et al.*, 2008). In the developing mouse nervous system, TMEM16B has been detected in the neural tube and in dorsal root ganglia (Rock & Harfe, 2008).

In humans, TMEM16B (also known as C12orf3; DKFZp434P102; anoctamin-2 or ANO2) has been shown to be involved in two types of diseases. Indeed, large deletions of TMEM16B together with von Willebrand factor genes are involved in some cases of the severe von Willebrand disease type 3, a heritable bleeding disorder that slows the blood-clotting process (Schneppenheim *et al.*, 2007). A recent genome-wide association study in a Japanese population indicated that single nucleotide polymorphisms located in or adjacent to gene TMEM16B were significantly associated with panic disorder (Otowa *et al.*, 2009).

Stöhr et al. in 2009, cloned human and mouse TMEM16B and showed that it is abundantly present in the photoreceptor synaptic terminals in mouse retina (Stöhr *et al.*, 2009). In the same work Stöhr and colleagues found that TMEM16B colocalizes with adaptor proteins PSD95, VELI3, and MPP4 at the ribbon synapses and contains a consensus PDZ class I binding motif capable of interacting with PDZ domains of PSD95.

Before knowing its possible role as a CaCC, Yu et *al.* (Yu *et al.*, 2005) showed, by *in situ* hybridization, that TMEM16B is expressed in mature sensory neurons of the mouse olfactory epithelium. Moreover, from an analysis of the olfactory ciliary proteome (Mayer *et al.*, 2009; Stephan *et al.*, 2009), TMEM16B was found to be a prominent protein and the relative expression level between TMEM16B and CNG channel subunits (Rasche *et*

al., 2010) confirms the electrophysiological results previously obtained (Reisert *et al.*, 2003).

Immunohistochemistry experiments showed that TMEM16B is expressed in the ciliary layer of the olfactory epithelium (Fig. 12) (Rasche *et al.*, 2010; Hengl *et al.*, 2010; Sagheddu *et al.*, 2010; Billig *et al.*, 2011) together with the $Na^+/K^+/2\ Cl^-$ cotransporter NKCC1 (Hengl *et al.*, 2010), that mediates Cl^- accumulation into the cilia (Reisert *et al.*, 2005). Immunohistochemistry experiments showed that TMEM16B (Rasche et al., 2010) and it is expressed also at the apical surface of the vomeronasal epithelium (Billig et al., 2011).

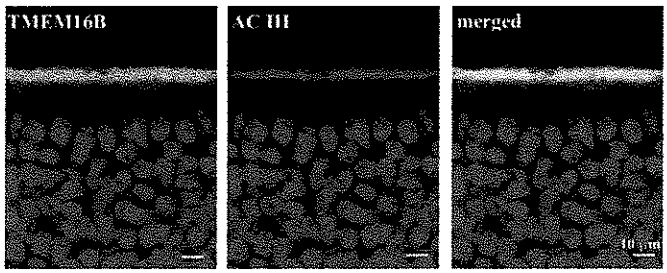

Figure 12: **Localization of TMEM16b/anoctamin2 at the surface of the olfactory epithelium:** Immunostaining of sections of the olfactory epithelium. Confocal micrographs showing TMEM16B and adenylyl cyclase III (AC3) expression at the surface of the olfactory epithelium. Cell nuclei were stained by DAPI. The image on the right was obtained from the merge of the left and center images. (Sagheddu *et al.*, 2010)

Stephan and colleagues (Stephan et al., 2009) characterized the mouse olfactory TMEM16B isoform, composed of 24 exons (909 amino acids), with a predicted molecular weight of ~110 kDa (Fig. 13). Exon 3, which encodes 33 amino acids in the predicted N-terminal cytoplasmic domain, is lacking in a minority of transcripts in both OSNs and retinal cells, where TMEM16B was first studied (Stöhr et al., 2009). The olfactory TMEM16B variant also lacks the exon 13 (4 amino acids of unknown function) in the first intracellular loop in the retinal variant. Preliminary data also indicated the existence of more splice variants for TMEM16B (Saidu S.P., Stephan A.B., Caraballo S.M., Zhao H. and Reisert J., Association for Chemoreception Sciences Meeting 2010, abstract P68).

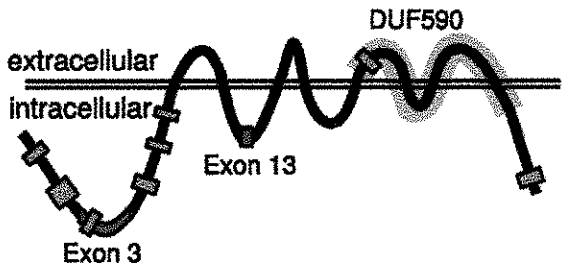

Figure 13: **Schematic of ANO2 predicted transmembrane topology**.Green boxes indicate segments identified by mass spectrometry. Red boxes indicate segments encoded by exon 3 and the retinal exon 13. Gray highlights a conserved domain (DUF590) in all Anoctamin family members.

Recently, Billig *et al.* (2011) succeeded in knocking out TMEM16B in mice and showed that Ca^{2+}-activated Cl^- currents were undetectable in OSNs of knockout mice. This important result, together with previous data from several laboratories, clearly indicates that TMEM16B is the principal subunit of the ciliary CaCC.

1.5.3.5 Biophysical properties

A side-by-side comparison of the functional properties measured in excised inside-out patches and whole-cell from the native olfactory current and the TMEM16B-induced current in HEK cells showed remarkable similarities (Stephan *et al.*, 2009; Pifferi *et al.*, 2009*a*; Sagheddu *et al.*, 2010).

1.5.3.5.1 Ca^{2+} sensitivity

TMEM16B dose-response relations indicate that the half maximal concentration of Ca^{2+} is slightly voltage dependent: $K_{1/2}$ was 4.9 μM at -50 mV and 3.3 μM at +50 mV (Pifferi et al., 2009a) and was 1.8 μM at -40 mV and 1.2 μM at +40 mV (Stephan et al., 2009). In both isoforms the Hill coefficient was ~ 2.

The single channel conductance was estimated to be between 0.8 and 1.2 pS by noise analysis (Stephan et al., 2009; Pifferi et al., 2009a).

In heterologusly expressed TMEM16B, using the whole-cell configuration at low Ca^{2+} concentrations, depolarizing voltage steps elicited an instantaneous outward current followed by a time-dependent outward relaxation. Hyperpolarizing voltage steps induced instantaneous inward currents followed by a relaxation toward less negative values.

At high Ca^{2+} concentrations the time-dependent component was strongly reduced and the instantaneus current became predominant (Fig. 14 A and B) (Pifferi et al., 2009a). In contrast with TMEM16A, TMEM16B was not inhibited by high Ca^{2+} concentrations (Stephan et al., 2009; Pifferi et al., 2009a).

Sr^{2+} efficiently activated TMEM16B while Ba^{2+} only activated a small current and no current was measured in the presence of Mg^{2+} (Stephan *et al.*, 2009; Pifferi *et al.*, 2009*a*). Like TMEM16A, also TMEM16B sequence does not show any canonical Ca^{2+} binding site.

1.5.3.5.2 Voltage-dependence

The current-voltage relationship of the TMEM16B steady-state current, obtained from whole-cell recordings, shows outward rectification at low Ca^{2+} concentrations which becomes linear increasing the Ca^{2+} concentration (Fig. 14 C) (Pifferi *et al.*, 2009*a*).

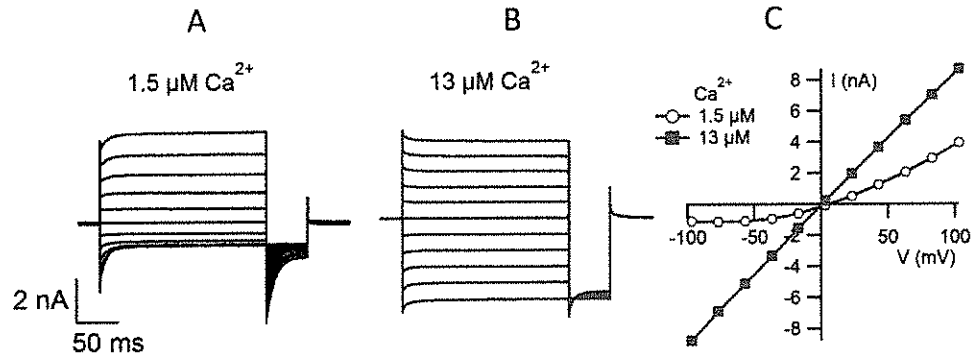

Figure 14: **Whole-cell Ca^{2+}-activated currents induced by mTMEM16B transfection in HEK 293T cells.** A and B. Whole-cell voltage-clamp recordings obtained with a pipette solution containing nominally 1.5 µM free Ca^{2+} (A) or 13 µM free Ca^{2+}(B). Voltage steps of 200 ms duration were given from a holding potential of 0 mV to voltages between −100 and +100 mV in 20 mV steps followed by a step to −100 mV. C. Current–voltage relation activated by 1.5 µM and 13 µM Ca^{2+} measured at the end of the voltage steps from the cell shown in A and B. (Modified from Pifferi *et al.*, 2009*a*)

1.5.3.5.3 Ionic permeability

Halide permeability sequence for TMEM16B is $SCN^- > I^- > NO3^- > Br^- > Cl^- >$ MeS > F^- with permeability ratios (PX/PCl) of 3.85:1.78:1:0.12 (Stephan *et al.*, 2009), similar to SCN > I > NO3 >Br > Cl > MeS 12.8: 4.9 : 3.7 : 2.1: 1.0 : 0.1 (Fig. 15 A)(Pifferi *et al.*, 2009*a*; Sagheddu *et al.*, 2010).

From whole-cell recordings with flash photolysis of caged Ca^{2+}, Sagheddu and colleagues in 2010 showed that the reversal potential for some external large anions changes with time, both in native olfactory CaCCs and in TMEM16B-induced currents in HEK cells (Fig 15 B)(Sagheddu et al., 2010). This behavior was also observed in TMEM16A expressed in *Axolotl* oocytes (Schroeder et al., 2008) and in cation channels such as TRPV1 and P2X (Khakh & Lester, 1999; Chung et al., 2008).

A possible mechanism explaining the dynamic ion selectivity of TMEM16B channel is the presence of at least two open states with different ion selectivity and Ca^{2+}-dependent open probability where the more selective open state is favored by high Ca^{2+} concentrations and the less selective open state by low Ca^{2+} concentrations (Sagheddu et al., 2010).

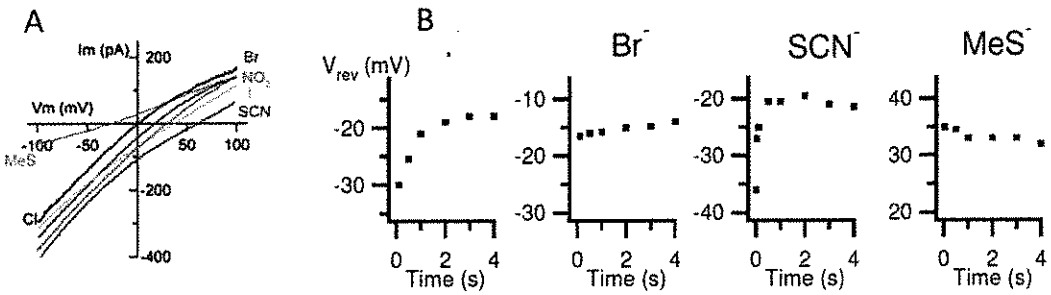

Figure 15: **Ionic permeability of TMEM16B:** A. Current–voltage relations for mTMEM16B currents activated by 100 µM Ca^{2+} in an inside-out membrane patch, obtained from a ramp protocol. Bath solutions contained 140 mM NaCl or the Na salt of other anions, as indicated. Current traces were from the same patch (Pifferi *et al.*, 2009*a*). B. Currents recorded from a HEK 293T cell expressing TMEM16B/anoctamin2. Uncaging techinique for Ca^{2+} release was used in the whole cell configuration. External Cl^- was substituted with the anions indicated. Vrev as a function of time for external I- (from recordings in A), Br-, SCN-, MeS-, each from a different cell (Sagheddu *et al.*, 2010).

1.5.3.5.4 Inactivation and rundown

Inactivation is defined as slow decrease of the current amplitude in the presence of the constant Ca^{2+} concentration.

When TMEM16B was activated by Ca^{2+} it developed a current which inactivated. The inactivation process was reversible, voltage-dependent, and Ca^{2+} -dependent, being more pronounced at hyperpolarized potentials and at high Ca^{2+} concentrations (Fig. 17 A) (Stephan et al., 2009; Pifferi et al., 2009a). This behavior is similar to the one found in the native olfactory current, although the inactivation of the native current is displayed both at positive and negative potentials (Reisert et al., 2003). The reason of this discrepancy is not clear yet. It is possible that TMEM16B constitutes only a part of the native olfactory CaCC (Stephan et al., 2009).

In excised patches TMEM16B displays an irreversible rundown similarly to native olfactory CaCC (Reisert *et al.*, 2003; Stephan *et al.*, 2009; Pifferi *et al.*, 2009*a*) which is not observed in TMEM16A, neither in whole-cell experiment with TMEM16B.

Rundown is a decrease in the current amplitude with time, upon subsequent application of Ca^{2+} and reaches a relatively stationary value afterwards, indicating that some modulatory substrates may be lost after patch excision (Fig. 17 B).

In the attempt to determine the rundown mechanism, Pifferi and colleagues in 2009 added several compounds (such as Na_3VO_4, DTT, calmodulin, cAMP, PIP_3) to the cytoplasmic side of the patch, but none of them was effective in reducing the rundown (Pifferi *et al.*, 2009*a*). The molecular mechanism of rundown is still not known.

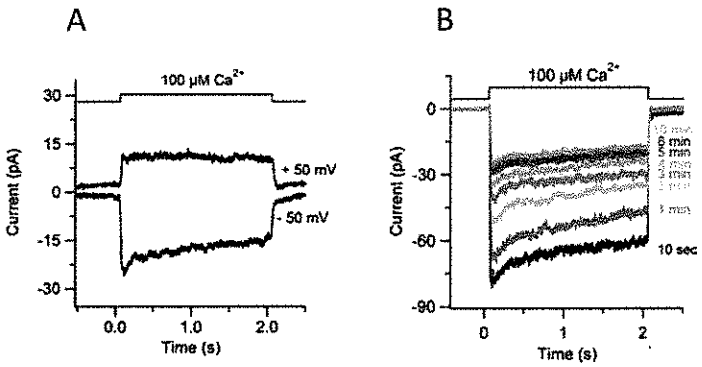

Figure 17: **Inactivation and rundown of the mTMEM16B-mediated current in excised inside-out membrane patches.** An inside-out membrane patch was excised from HEK 293T cells transfected with mTMEM16B and the cytoplasmic side was exposed to 100 µM Ca^{2+} at the time indicated in the upper trace. A. Inactivation was voltage-dependent. Currents activated by 100 µM Ca^{2+} at -50 mV or +50 mV after 3 or 4 min from patch excision respectively. Current traces were from the same patch. B. Rundown: repetitive applications of Ca^{2+} produced a current of decreasing amplitude. The holding potential was -50 mV. The number next to each trace indicates the initial time of Ca^{2+}application after patch excision. (Pifferi *et al.*, 2009*a*)

2 Aims

The molecular mechanisms of TMEM16B channel gating are unknown. Although TMEM16B sequence does not show any apparent canonical Ca^{2+}-binding site, nor voltage sensor, the first intracellular loop contains conserved glutamic acid residues, thought to be involved in channel gating. Therefore, the work Cenedese et al., 2012 aimed at identifying the amino acids involved in TMEM16B channel gating by voltage and Ca^{2+} through a biophysical and mutagenesis study.

3 Materials and methods

3.1 Cell culture and transfection

HEK-293 cells were grown in DMEM (Gibco, Italy) supplemented with 10% fetal bovine serum (Sigma, Italy), 100 IU/ml penicillin and 100 µg/ml streptomycin (Sigma) at 37°C in a humidified CO_2 incubator. Transfection of HEK-293 cells was performed by using FuGENE 6 reagent (Roche Diagnostics, Germany) according to the manufacturer's protocol. HEK293 cells were transfected with mouse TMEM16B cDNA in pCMV-Sport6 mammalian expression plasmid obtained from RZPD (Germany; clone identification: IRAVp968H1167D; accession number BC033409) or with mutants for mTMEM16B. Mutations were made using a PCR-based site-directed mutagenesis kit (Gene Tailor mutagenesis kit, Invitrogen, OR, USA) and confirmed by DNA sequencing. Cotransfection with EFGP in pGFP (Clontech, USA) was used as reporter and only green fluorescent cells were used for experiments. After 36-48 hours after transfection the cells were plated on Petri dishes treated with poly-L-lysine (Sigma, Italy) to improve the adhesion and used for electrophysiological recording in the following 24-48 hours. Mutations were made using a PCR-based site-directed mutagenesis kit (Gene Tailor mutagenesis kit, Invitrogen, OR, USA) and confirmed by DNA sequencing.

3.2 Experimental setup and recordings

The experiments described in this thesis were performed in two different setups using the same experimental procedure.

The preparation was visualized with an Olympus IX70 or IMT2 inverted microscope (Olympus, Japan) placed on an antivibration table (TMC, USA). A homemade Faraday cage provided adequate electrical shielding. Patch pipettes were made of borosilicate glass (WPI, USA) and pulled with a PP-830 puller (Narishige, Japan). Patch pipettes filled with the

intracellular solution had a resistance of about 3-5 MΩ when immersed in the bath solution. Pipettes were mounted in a pipette holder with an Ag/AgCl electrode for electrical recording. The holder movements were controlled by an electronic micromanipulator (Patchstar, Scientifica, UK) or by a mechanical micromanipulator for bigger displacements (MC-35A, Narishige, Japan) and by a hydraulic micromanipulator for smaller movements to approach the cells (MWO-3 Narishige, Japan). Currents were recorded with an Axopatch 1D or Axopatch 200B amplifier controlled by Clampex 9 or 10 via a Digidata 1332A or 1440 (Axon Instruments, or Molecular Devices, Union City, CA, USA). Data were low-pass filtered at 5 kHz and sampled at 10 kHz. The recording chamber was continuously bathed with mammalian Ringer solution while an aspiration tube, placed at the opposite site and connected with a trap bottle, controlled the level of solution in the recording chamber. Experiments were performed at room temperature (20-25°C). Currents recordings from HEK 293T cells expressing TMEM16B or its mutants were performed in the whole-cell voltage-clamp configuration as previously described (Pifferi et al., 2006, 2009). Membrane capacitance and series resistance were compensated with the amplifier during the experiments. In most experiments we applied voltage steps of 200 ms duration from a holding potential of 0 mV ranging from -100 to +100 mV (or from -200 to +200 mV), followed by a step to -100 mV. A single-exponential function was fitted to tail currents to extrapolate the current value at the beginning of the step to -100 mV. In another set of experiments channels were activated by a 200 ms pulse to +100 mV and then rapidly closed by application of hyperpolarizing steps. Single-exponential functions were fitted to tail currents at each voltage step. Membrane current density was calculated dividing the current by the cell capacitance. The conductance, *G*, was calculated as $G = I / (V - V_{rev})$, where is the tail current, V is the membrane voltage, V_{rev} is the current reversal potential. Since in our experimental conditions the calculated equilibrium potential for Cl^- ranged between -1.5 to +1.9 mV and the measured V_{rev} was close to 0 mV, V_{rev} was set to 0 mV in all calculations.

As previously reported (Pifferi et al., 2006), control experiments in non-transfected and only EGFP-transfected cells did not show any significant Ca^{2+} -activated current.

3.3 Solutions

Solutions with different ionic compositions were used for experiments. Mammalian Ringer's solution was applied extracellularly in the bath, while intracellular solutions contained different Ca^{2+} concentrations. The compositions of solutions used for recordings are listed in the following table:

	NaCl (mM)	**CsCl** (mM)	**KCl** (mM)	**$CaCl_2$** (mM)	**$MgCl_2$** (mM)	**HEDTA** (mM)
Ringer	140	-	5	2	1	-
0 µM Ca^{2+}	-	140	-	-	-	10
0.5 µM Ca^{2+}	-	140	-	1.242	-	10
1.5 µM Ca^{2+}	-	140	-	3.209	-	10
3.8 µM Ca^{2+}	-	140	-	5.866	-	10
13 µM Ca^{2+}	-	140	-	8.263	-	10
100 µM Ca^{2+}	-	140	-	9.98	-	10

All solutions contained also 10 mM HEPES as pH buffer and adjusted to pH 7.4 with NaOH for Ringer solution, 7.2 with CsOH for intracellular solutions. The Ringer solution contained also 10 mM glucose. The program WinMAXC (C. Patton, Stanford University, Palo Alto, CA USA) was used to calculate free Ca^{2+} concentrations in buffered solutions. The free Ca^{2+} concentrations in the HEDTA-buffered Ca^{2+} solutions were determined by Fura-4F (Molecular Probes-Invitrogen, Italy) measurements by using an LS-50B luminescence spectrophotometer (PerkinElmer, USA) as previously described (Pifferi et al., 2006). The total Cl^- concentration was 158 mM in the extracellular solution, while in the pipette solution ranged from 140 mM in 0 Ca^{2+} to 160 mM in 100 µM Ca^{2+}, with a calculated equilibrium

potential for Cl^- of -1.5 and +1.9 mV, respectively. All chemicals, unless otherwise stated, were purchased from Sigma (Milano, Italy).

3.4 Data analysis

Data are presented as mean ± SEM, with *n* indicating the number of cells. Statistical significance was determined using paired or unpaired *t*-tests, or ANOVA, as appropriate. When a statistically significant difference was determined with ANOVA, a post hoc Tukey test was done to evaluate which data groups showed significant differences. *P* values <0.05 were considered significant. Data analysis and figures were made with Igor Pro software (Wavemetrics, USA).

4 Results

Simone Pifferi, Valentina Cenedese and Anna Menini

Anoctamin2/TMEM16B: a calcium-activated chloride channel in olfactory transduction

Exp Physiol February 2012 97 (2) 193-199

Symposium Report

Anoctamin 2/TMEM16B: a calcium-activated chloride channel in olfactory transduction

Simone Pifferi, Valentina Cenedese and Anna Menini

SISSA, International School for Advanced Studies, and Italian Institute of Technology, SISSA Unit, Via Bonomea 265, 34136 Trieste, Italy

In vertebrate olfactory transduction, a Ca^{2+}-dependent Cl^- efflux greatly amplifies the odorant response. The binding of odorants to receptors in the cilia of olfactory sensory neurons activates a transduction cascade that involves the opening of cyclic nucleotide-gated channels and the entry of Ca^{2+} into the cilia. The Ca^{2+} activates a Cl^- current that, in the presence of a maintained elevated intracellular Cl^- concentration, produces an efflux of Cl^- ions and amplifies the depolarization. In this review, we summarize evidence supporting the hypothesis that anoctamin 2/TMEM16B is the main, or perhaps the only, constituent of the Ca^{2+}-activated Cl^- channels involved in olfactory transduction. Indeed, studies from several laboratories have shown that anoctamin 2/TMEM16B is expressed in the ciliary layer of the olfactory epithelium, that there are remarkable functional similarities between currents in olfactory sensory neurons and in HEK 293 cells transfected with anoctamin 2/TMEM16B, and that knockout mice for anoctamin 2/TMEM16B did not show any detectable Ca^{2+}-activated Cl^- current. Finally, we discuss the involvement of Ca^{2+}-activated Cl^- channels in the transduction process of vomeronasal sensory neurons and the physiological role of these channels in olfaction.

(Received 26 July 2011; accepted after revision 30 August 2011; first published online 2 September 2011)

Corresponding author A. Menini: SISSA, Via Bonomea 265, 34136 Trieste, Italy. Email: menini@sissa.it

The sense of smell and olfactory transduction

The sense of smell allows the organisms to detect chemicals present in the external environment. Vertebrates mainly detect odorants by the main olfactory epithelium located in the nasal cavity (Fig. 1*A*), but rodents and many other mammals also use additional sensory systems, such as the vomeronasal organ, which is mainly involved in pheromone detection, the septal organ and the Grüneberg ganglion (Munger *et al.* 2009; Tirindelli *et al.* 2009).

In the main olfactory epithelium, primary olfactory sensory neurons (OSNs) are responsible for the detection of odorant molecules and the generation of the neural signal that is transmitted to the brain (Fig. 1*B*). At the apical part of these bipolar neurons, the dendritic tip is slightly enlarged into an olfactory knob, from which tens of cilia protrude into the olfactory mucus that covers the surface of the epithelium (Fig. 1*A–C*). A single axon projects from the basal part of the neuron directly to the olfactory bulb. The cilia are the site of sensory transduction; indeed, at this level odorant molecules bind to odorant receptors, and this interaction triggers an increase in the intraciliary concentration of cAMP through the activation of the receptor-coupled G protein and adenylyl cyclase (Fig. 1*D*). Cyclic nucleotide-gated (CNG) channels located in the ciliary membrane are directly activated by cAMP, inducing a depolarizing influx of Na^+ and Ca^{2+} ions (reviewed by Schild & Restrepo, 1998; Pifferi *et al.* 2006*a*, 2009*c*; Kleene, 2008). The intracellular increase of Ca^{2+} concentration directly gates Ca^{2+}-activated Cl^- channels (CaCCs). The OSNs maintain an unusually high internal concentration of Cl^- (about 50 mM), which is in the same range as the Cl^- concentration present in the mucus at the external side of the ciliary membrane (Reuter *et al.* 1998; Kaneko *et al.* 2001, 2004). Therefore, in physiological conditions, the opening of CaCCs causes an efflux of Cl^- ions from the cilia, corresponding to an inward current that further contributes to the depolarization of OSNs (Kleene & Gesteland, 1991; Kleene, 1993, 1997; Kurahashi & Yau, 1993; Lowe & Gold, 1993; Boccaccio & Menini, 2007; reviewed by Frings *et al.* 2000; Kleene, 2008; Frings, 2009). The depolarization spreads passively to the dendrite and soma of the neuron, triggering action potentials that are

DOI: 10.1113/expphysiol.2011.058230

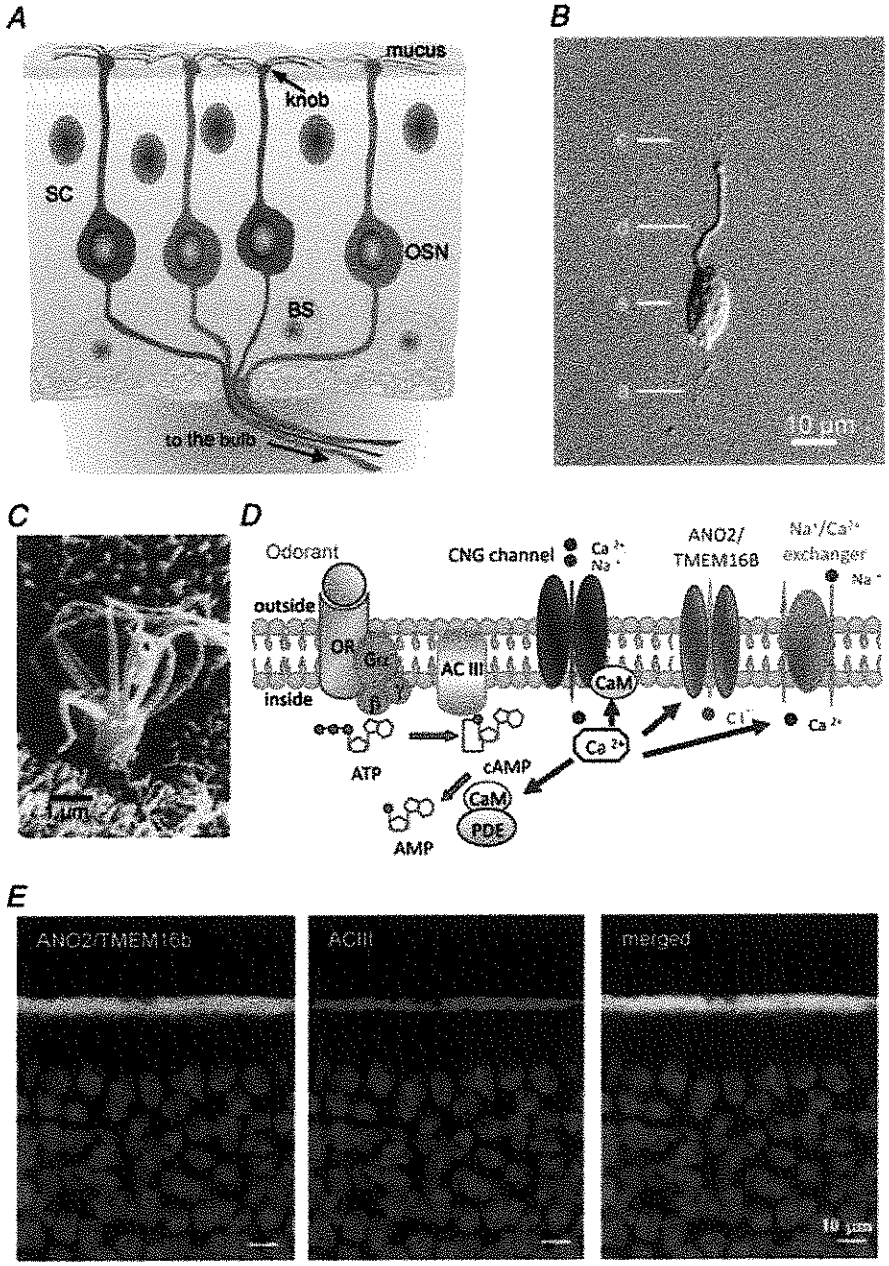

Figure 1. The olfactory epithelium and olfactory transduction
A, schematic diagram showing the various cell types composing the olfactory epithelium: OSN, olfactory sensory neuron; SC, supporting cell; and BS, basal cell. *B*, photograph of an isolated frog OSN under differential interference optics: c, cilia; d, dendrite; s, soma; and a, axon. Reprinted from Kleene & Gesteland (1981), copyright 1981, with permission from Elsevier. *C*, scanning electron micrograph of the knob of a human OSN showing the protrusion of several cilia. Adapted from Morrison & Costanzo (1990), with permission. *D*, schematic representation of the olfactory transduction taking place in the cilia. Abbreviations: ACIII, adenylyl cyclase III; CNG channel, cyclic nucleotide-gated channel; CaM, calmodulin; G, G protein; OR, odorant receptor; and PDE, phosphodiesterase. ANO2/TMEM16B indicates the Ca^{2+}-activated Cl^- channel. Modified from Pifferi *et al.* (2006*a*), with permission. *E*, immunostaining of sections of the mouse olfactory epithelium. Confocal micrographs showing TMEM16B and ACIII expression at the surface of the olfactory epithelium. Cell nuclei were stained by 4′,6-diamidino-2-phenylindole (DAPI). The image on the right was obtained by merging the left and centre images. Reprinted from Sagheddu *et al.* (2010).

conducted along the axon to the olfactory bulb. As OSNs have a high resting membrane resistance (>1 GΩ), a very small depolarizing current is sufficient to trigger action potentials (Lynch & Barry, 1989; Schild & Restrepo, 1998; Pun & Kleene, 2004).

Calcium-activated chloride channels in the cilia of olfactory sensory neurons

The presence of a Ca^{2+}-activated Cl^- current in frog OSNs has been known since the pioneering study of Kleene & Gesteland (1991), which showed that a rise in intraciliary Ca^{2+} concentration directly activates an anion-selective current in the ciliary membrane. Since this first study, the functional properties of olfactory CaCCs have been investigated with several electrophysiological techniques. For example, the field potential recorded at the surface of the olfactory epithelium in response to odorants (the electro-olfactogram) is primarily caused by the depolarizing action of Cl^- current, because more than 80% of the response can be blocked by niflumic acid, a blocker for CaCCs (Nickell *et al.* 2006). The large contribution of the Cl^- conductance to the transduction current was confirmed by experiments in isolated OSNs obtained with the suction pipette or in the whole-cell voltage-clamp configuration (Reisert *et al.* 2005; Boccaccio & Menini, 2007). In a set of experiments, the contribution of CaCCs to the transduction current was estimated by activating CNG channels in the ciliary region by flash photolysis of caged cAMP (Boccaccio & Menini, 2007). Upon flash photolysis, CNG channels are activated by cAMP, allowing the flux of Ca^{2+} ions in the cilia and the subsequent opening of CaCCs (Boccaccio *et al.* 2006; Boccaccio & Menini, 2007). The rising phase of the response at −50 mV in Ringer solution containing 1 mM Ca^{2+} was multiphasic, composed of a primary phase of the response due to Na^+ and Ca^{2+} influx through CNG channels and a secondary phase due to Cl^- efflux through CaCCs. Moreover, the secondary phase of the response was absent with low extracellular Ca^{2+} concentrations or at +50 mV, when the influx of Ca^{2+} through CNG channels is strongly reduced and therefore the contribution of CaCCs is expected to be negligible (Boccaccio & Menini, 2007). These experiments showed that up to 90% of the transduction current is carried by Cl^-.

A more precise characterization of the biophysical properties of olfactory CaCCs was achieved by experiments on excised inside-out membrane patches from the dendritic knob/cilia of mouse OSNs, a technique that allows a control of the concentration of Ca^{2+} at the intracellular side of the channels (Reisert *et al.* 2005; Pifferi *et al.* 2006*b*, 2009*b*). The dose–response relation was well fitted by the Hill equation with half-maximal activation between 2.2 and 4.7 μM Ca^{2+} and Hill coefficient between 2.0 and 2.8. Reisert *et al.* (2003) estimated a CaCC channel density of 62 μm^{-2} compared with only 8 μm^{-2} for CNG channels. Moreover, this conductance showed a Ca^{2+}-dependent inactivation, which was reversible after removal of Ca^{2+} for a few seconds, but also an irreversible run-down, indicating that some modulatory component of the channel may be lost after the excision of the membrane (Reisert *et al.* 2003, 2005). The olfactory CaCC is apparently not affected by Ca^{2+}–calmodulin (Kleene, 1999; Reisert *et al.* 2003) and, at present, no modulators of the channel activity are known.

All these studies clearly showed that CaCCs are present at a high density in the cilia of OSNs and that they contribute to the transduction current. However, it is important to note that, as previously pointed out (Smith *et al.* 2008; Kleene, 2009), it is possible that the secondary Cl^- current may not be required for normal olfactory behaviour. Indeed, given the high resting membrane resistance of OSNs, it is possible that a small primary current through CNG channels is sufficient to trigger action potentials and to allow near-normal olfactory behaviour.

Anoctamin 2/TMEM16B

The molecular identity of the CaCC present in the cilia of OSNs, as well as that of CaCCs in general, has been elusive for a long time. In 2008, three independent studies reported that anoctamin 1/TMEM16A displays many features of native CaCCs (Caputo *et al.* 2008; Schroeder *et al.* 2008; Yang *et al.* 2008). The role of TMEM16A as a CaCC suggested that other members of the family may also act as CaCCs (reviewed by Flores *et al.* 2009; Galietta, 2009; Hartzell *et al.* 2009; Kunzelmann *et al.* 2011). Indeed, when anoctamin 2/TMEM16B (which we will term TMEM16B in this review) was expressed in axolotl oocytes (Schroeder *et al.* 2008) or in HEK 293 cells (Pifferi *et al.* 2009*a*; Sagheddu *et al.* 2010; Stephan *et al.* 2009; Stöhr *et al.* 2009) it also displayed properties resembling those of CaCCs.

In 2005, Yu *et al.* showed by *in situ* hybridization that TMEM16B is expressed in mature sensory neurons of the mouse olfactory epithelium, well before knowing its possible role as a CaCC. Moreover, TMEM16B was found to be a prominent protein in the olfactory ciliary proteome (Mayer *et al.* 2009; Stephan *et al.* 2009), and the relative expression level between TMEM16B and CNG channel subunits (Rasche *et al.* 2010) was in good agreement with the electrophysiological results obtained by Reisert *et al.* (2003). Immunohistochemistry experiments (Fig. 1*E*) showed that TMEM16B is expressed in the ciliary layer of the olfactory epithelium (Hengl *et al.* 2010; Rasche *et al.* 2010; Sagheddu *et al.* 2010; Billig *et al.* 2011) together with the Na^+–K^+–$2Cl^-$ cotransporter NKCC1 (Hengl *et al.*

2010), which mediates Cl^- accumulation into the cilia (Reisert *et al.* 2005).

A side-by-side comparison of the functional properties measured in excised inside-out patches from the native olfactory current and the TMEM16B-induced current in HEK 293 cells showed remarkable similarities (Fig. 2*A* and *B*). Dose–response relations indicate that the half-maximal concentration of Ca^{2+} is very similar: 4.9 μM for TMEM16B and 4.7 μM for native channels at −50 mV (Fig. 2*C*). Moreover, both channels have the same anion selectivity; indeed, they are more permeable to anions larger than Cl^-, and almost impermeable to methanesulfonate (Fig. 2*D*–*F*). TMEM16B and native CaCCs show also a similar sensitivity to Cl^- channel blockers; both are reversibly blocked by niflumic acid but are insensitive to SITS (Fig. 2*G*–*I*). Moreover, TMEM16B

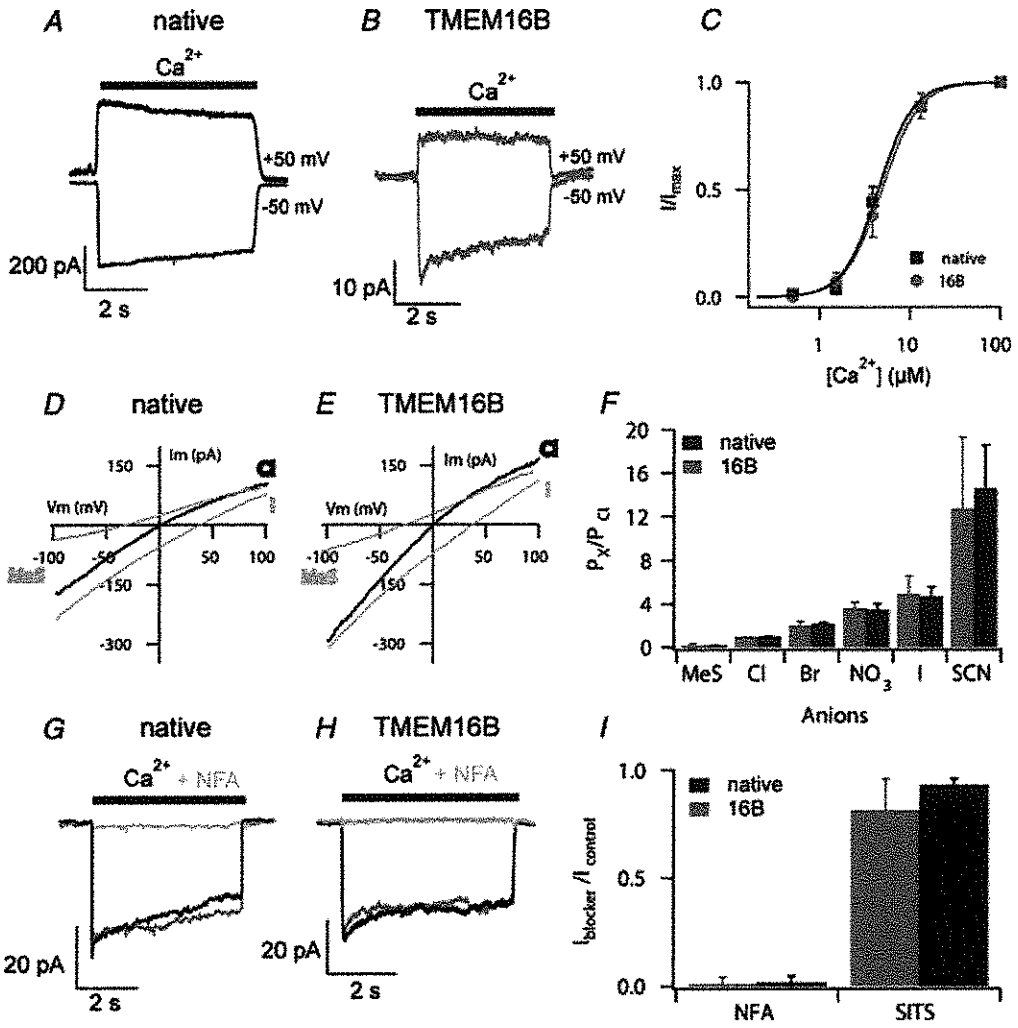

Figure 2. Comparison between the electrophysiological properties of native olfactory Ca^{2+}-activated Cl^- channels and TMEM16B-induced currents in HEK 293 cells
Currents were measured by exposing the cytoplasmic side of membrane patches excised from dendritic knob/cilia of mouse olfactory sensory neurons or from HEK 293 cells expressing TMEM16B. *A* and *B*, currents activated by 100 μM Ca^{2+} at −50 or +50 mV. *C*, normalized currents measured at −50 mV were plotted *versus* Ca^{2+} concentrations and fitted to the Hill equation. The Ca^{2+} concentration producing half-maximal activation was 4.7 μM for olfactory native currents and 4.9 μM for TMEM16B-induced currents. The Hill coefficient was 2.5. *D* and *E*, current–voltage relations from a ramp protocol activated by 100 μM Ca^{2+}. Bath solutions contained 140 mM NaCl, or the sodium salt of iodide (I) or of methanesulfonate (MeS), as indicated. *F*, comparison between the relative permeability ratios (P_X/P_{Cl}) calculated with the Goldman–Hodgkin–Katz relation from measured reversal potentials. *G* and *H*, intracellular blockage by 300 μM niflumic acid (NFA) of the current activated by 100 μM Ca^{2+} at −50 mV. *I*, comparison between the current ratios measured at −50 mV in the presence and in the absence of 300 μM NFA or 5 mM SITS. Modified from Pifferi *et al.* (2006*b*), copyright (2006) National Academy of Sciences, USA, and from Pifferi *et al.* (2009*a*), with permission.

displays a Ca^{2+}-dependent inactivation and an irreversible run-down in a similar manner to native olfactory CaCCs (Reisert *et al.* 2003; Pifferi *et al.* 2009*a*; Stephan *et al.* 2009).

A more recent study also reported a side-by-side comparison obtained in whole-cell recordings with flash photolysis of caged Ca^{2+}, showing that the reversal potential for some external large anions changes with time, both in native olfactory CaCCs and in TMEM16B-induced currents in HEK 293 cells (Sagheddu *et al.* 2010). Further experiments are required to establish the mechanisms of dynamic selectivity. This behaviour was also observed in TMEM16A expressed in axolotl oocytes (Schroeder *et al.* 2008) and in cation channels such as TRPV1 and P2X (Khakh & Lester, 1999; Chung *et al.* 2008).

Recently, Billig *et al.* (2011) succeeded in knocking out TMEM16B in mice and showed that Ca^{2+}-activated Cl^- currents were undetectable in knockout mice. This important result, together with previous data from several laboratories, clearly indicates that TMEM16B is the principal subunit of the ciliary CaCC.

What about the physiological role of TMEM16B in olfaction? Confirming the initial report on *NKCC1* knockout mice (Smith *et al.* 2008), Billig *et al.* (2011) found that disruption of TMEM16B did not reduce mouse performance in some olfactory behavioural tasks, suggesting that CaCC may be dispensable for near-normal olfaction.

Calcium-activated chloride channels in vomeronasal sensory neurons

Some recent results indicated the presence of a Ca^{2+}-activated Cl^- current in vomeronasal sensory neurons also, where it contributes up to 80% of the response to urine (Yang & Delay, 2010; Kim *et al.* 2011). In addition, experiments using flash photolysis of caged Ca^{2+} in the microvilli of isolated mouse vomeronasal sensory neurons showed that a large Cl^- current of more than 300 pA can be activated at −50 mV by Ca^{2+} in symmetrical Cl^- solutions (M. Dibattista & A. Menini, unpublished results). Immunohistochemistry experiments showed that TMEM16B (Rasche *et al.* 2010) and TMEM16A are expressed at the apical surface of the vomeronasal epithelium (Billig *et al.* 2011). Furthermore, Billig *et al.* (2011) measured Ca^{2+}-activated currents in vomeronasal sensory neurons that were not present in knockout mice for TMEM16B.

Conclusions

Current evidence suggests that anoctamin 2/TMEM16B is the major subunit of the Ca^{2+}-activated Cl^- current in the cilia of OSNs, although other subunits may also be expressed. However, the physiological role of this current in olfaction remains unclear, because knockout mice for TMEM16B show near-normal olfactory behaviour. Future experiments will have to establish whether CaCCs are involved in a slight increase of olfactory sensitivity not detected in previous experiments. It is possible that their presence at high density in the olfactory cilia is useful to preserve the detection of odorants also in the presence of modifications that may change extracellular ion concentrations. Furthermore, recent studies indicated that vomeronasal sensory neurons also possess a high density of CaCCs in their microvilli and that both TMEM16A and TMEM16B are expressed at the apical surface of the vomeronasal epithelium. Further experiments will be necessary to clarify the role of CaCCs in the vomeronasal system.

References

Billig GM, Pál B, Fidzinski P & Jentsch TJ (2011). Ca^{2+}-activated Cl^- currents are dispensable for olfaction. *Nat Neurosci* **14**, 763–769.

Boccaccio A, Lagostena L, Hagen V & Menini A (2006). Fast adaptation in mouse olfactory sensory neurons does not require the activity of phosphodiesterase. *J Gen Physiol* **128**, 171–184.

Boccaccio A & Menini A (2007). Temporal development of cyclic nucleotide-gated and Ca^{2+} -activated Cl^- currents in isolated mouse olfactory sensory neurons. *J Neurophysiol* **98**, 153–160.

Caputo A, Caci E, Ferrera L, Pedemonte N, Barsanti C, Sondo E, Pfeffer U, Ravazzolo R, Zegarra-Moran O & Galietta LJV (2008). TMEM16A, a membrane protein associated with calcium-dependent chloride channel activity. *Science* **322**, 590–594.

Chung MK, Güler AD & Caterina MJ (2008). TRPV1 shows dynamic ionic selectivity during agonist stimulation. *Nat Neurosci* **11**, 55–64.

Flores CA, Cid LP, Sepúlveda FV & Niemeyer MI (2009). TMEM16 proteins: the long awaited calcium-activated chloride channels? *Braz J Med Biol Res* **42**, 993–1001.

Frings S (2009). Chloride-based signal amplification in olfactory sensory neurons. In *Physiology and Pathology of Chloride Transporters and Channels in the Nervous System. From Molecules to Diseases*, ed. Alvarez-Leefmans FJ & Delpire E. Elsevier-Academic Press, San Diego, CA, USA.

Frings S, Reuter D & Kleene SJ (2000). Neuronal Ca^{2+}-activated Cl^- channels–homing in on an elusive channel species. *Prog Neurobiol* **60**, 247–289.

Galietta LJV (2009). The TMEM16 protein family: a new class of chloride channels? *Biophys J* **97**, 3047–3053.

Hartzell HC, Yu K, Xiao Q, Chien L & Qu Z (2009). Anoctamin/TMEM16 family members are Ca^{2+}-activated Cl^- channels. *J Physiol* **587**, 2127–2139.

Hengl T, Kaneko H, Dauner K, Vocke K, Frings S & Möhrlen F (2010). Molecular components of signal amplification in olfactory sensory cilia. *Proc Natl Acad Sci USA* **107**, 6052–6057.

Kaneko H, Nakamura T & Lindemann B (2001). Noninvasive measurement of chloride concentration in rat olfactory receptor cells with use of a fluorescent dye. *Am J Physiol Cell Physiol* **280**, C1387–C1393.

Kaneko H, Putzier I, Frings S, Kaupp UB & Gensch T (2004). Chloride accumulation in mammalian olfactory sensory neurons. *J Neurosci* **24**, 7931–7938.

Khakh BS & Lester HA (1999). Dynamic selectivity filters in ion channels. *Neuron* **23**, 653–658.

Kim S, Ma L & Yu CR (2011). Requirement of calcium-activated chloride channels in the activation of mouse vomeronasal neurons. *Nat Commun* **2**, 365.

Kleene SJ (1993). Origin of the chloride current in olfactory transduction. *Neuron* **11**, 123–132.

Kleene SJ (1997). High-gain, low-noise amplification in olfactory transduction. *Biophys J* **73**, 1110–1117.

Kleene SJ (1999). Both external and internal calcium reduce the sensitivity of the olfactory cyclic-nucleotide-gated channel to cAMP. *J Neurophysiol* **81**, 2675–2682.

Kleene SJ (2008). The electrochemical basis of odor transduction in vertebrate olfactory cilia. *Chem Senses* **33**, 839–859.

Kleene SJ (2009). Identifying olfaction's 'other channels'. *J Physiol* **587**, 4135–4136.

Kleene SJ & Gesteland (1981). Dissociation of frog olfactory epithelium with N-ethylmaleimide. *Brain Res* **229**, 536–540.

Kleene SJ & Gesteland RC (1991). Calcium-activated chloride conductance in frog olfactory cilia. *J Neurosci* **11**, 3624–3629.

Kunzelmann K, Tian Y, Martins JR, Faria D, Kongsuphol P, Ousingsawat J, Thevenod F, Roussa E, Rock J & Schreiber R (2011). Anoctamins. *Pflugers Arch* **462**, 195–208.

Kurahashi T & Yau KW (1993). Co-existence of cationic and chloride components in odorant-induced current of vertebrate olfactory receptor cells. *Nature* **363**, 71–74.

Lowe G & Gold GH (1993). Nonlinear amplification by calcium-dependent chloride channels in olfactory receptor cells. *Nature* **366**, 283–286.

Lynch JW & Barry PH (1989). Action potentials initiated by single channels opening in a small neuron (rat olfactory receptor). *Biophys J* **55**, 755–768.

Mayer U, Küller A, Daiber PC, Neudorf I, Warnken U, Schnölzer M, Frings S & Möhrlen F (2009). The proteome of rat olfactory sensory cilia. *Proteomics* **9**, 322–334.

Morrison EE & Costanzo RM (1990). Morphology of the human olfactory epithelium. *J Comp Neurol* **297**, 1–13.

Munger SD, Leinders-Zufall T & Zufall F (2009). Subsystem organization of the mammalian sense of smell. *Annu Rev Physiol* **71**, 115–140.

Nickell WT, Kleene NK, Gesteland RC & Kleene SJ (2006). Neuronal chloride accumulation in olfactory epithelium of mice lacking NKCC1. *J Neurophysiol* **95**, 2003–2006.

Pifferi S, Boccaccio A & Menini A (2006*a*). Cyclic nucleotide-gated ion channels in sensory transduction. *FEBS Lett* **580**, 2853–2859.

Pifferi S, Dibattista M & Menini A (2009*a*). TMEM16B induces chloride currents activated by calcium in mammalian cells. *Pflugers Arch* **458**, 1023–1038.

Pifferi S, Dibattista M, Sagheddu C, Boccaccio A, Al Qteishat A, Ghirardi F, Tirindelli R & Menini A (2009*b*). Calcium-activated chloride currents in olfactory sensory neurons from mice lacking bestrophin-2. *J Physiol* **587**, 4265–4279.

Pifferi S, Menini A & Kurahashi T (2009*c*). Signal Transduction in vertebrate olfactory cilia. In *The Neurobiology of Olfaction*, ed. Menini A, pp. 203–224. CRC Press, Taylor & Francis Group, Boca Raton, FL, USA.

Pifferi S, Pascarella G, Boccaccio A, Mazzatenta A, Gustincich S, Menini A & Zucchelli S (2006*b*). Bestrophin-2 is a candidate calcium-activated chloride channel involved in olfactory transduction. *Proc Natl Acad Sci USA* **103**, 12929–12934.

Pun RY & Kleene SJ (2004). An estimate of the resting membrane resistance of frog olfactory receptor neurones. *J Physiol* **559**, 535–542.

Rasche S, Toetter B, Adler J, Tschapek A, Doerner JF, Kurtenbach S, Hatt H, Meyer H, Warscheid B & Neuhaus EM (2010). Tmem16b is specifically expressed in the cilia of olfactory sensory neurons. *Chem Senses* **35**, 239–245.

Reisert J, Bauer PJ, Yau K & Frings S (2003). The Ca-activated Cl channel and its control in rat olfactory receptor neurons. *J Gen Physiol* **122**, 349–363.

Reisert J, Lai J, Yau K & Bradley J (2005). Mechanism of the excitatory Cl^- response in mouse olfactory receptor neurons. *Neuron* **45**, 553–561.

Reuter D, Zierold K, Schröder WH & Frings S (1998). A depolarizing chloride current contributes to chemoelectrical transduction in olfactory sensory neurons *in situ*. *J Neurosci* **18**, 6623–6630.

Sagheddu C, Boccaccio A, Dibattista M, Montani G, Tirindelli R & Menini A (2010). Calcium concentration jumps reveal dynamic ion selectivity of calcium-activated chloride currents in mouse olfactory sensory neurons and TMEM16b-transfected HEK 293T cells. *J Physiol* **588**, 4189–4204.

Schild D & Restrepo D (1998). Transduction mechanisms in vertebrate olfactory receptor cells. *Physiol Rev* **78**, 429–466.

Schroeder BC, Cheng T, Jan YN & Jan LY (2008). Expression cloning of TMEM16A as a calcium-activated chloride channel subunit. *Cell* **134**, 1019–1029.

Smith DW, Thach S, Marshall EL, Mendoza MG & Kleene SJ (2008). Mice lacking NKCC1 have normal olfactory sensitivity. *Physiol Behav* **93**, 44–49.

Stephan AB, Shum EY, Hirsh S, Cygnar KD, Reisert J & Zhao H (2009). ANO2 is the cilial calcium-activated chloride channel that may mediate olfactory amplification. *Proc Natl Acad Sci USA* **106**, 11776–11781.

Stöhr H, Heisig JB, Benz PM, Schöberl S, Milenkovic VM, Strauss O, Aartsen WM, Wijnholds J, Weber BHF & Schulz HL (2009). TMEM16B, a novel protein with calcium-dependent chloride channel activity, associates with a presynaptic protein complex in photoreceptor terminals. *J Neurosci* **29**, 6809–6818.

Tirindelli R, Dibattista M, Pifferi S & Menini A (2009). From pheromones to behavior. *Physiol Rev* **89**, 921–956.

Yang C & Delay RJ (2010). Calcium-activated chloride current amplifies the response to urine in mouse vomeronasal sensory neurons. *J Gen Physiol* **135**, 3–13.

Yang YD, Cho H, Koo JY, Tak MH, Cho Y, Shim W, Park SP, Lee J, Lee B, Kim B, Raouf R, Shin YK & Oh U (2008). TMEM16A confers receptor-activated calcium-dependent chloride conductance. *Nature* **455**, 1210–1215.

Yu T, McIntyre JC, Bose SC, Hardin D, Owen MC & McClintock TS (2005). Differentially expressed transcripts from phenotypically identified olfactory sensory neurons. *J Comp Neurol* **483**, 251–262.

Acknowledgements

We thank Michele Dibattista for comments on the manuscript. The research in our laboratory was supported by grants from the Italian Ministry of Education, University and Research (MIUR) and from the Italian Institute of Technology.

Author's present address

S. Pifferi: Max Delbrück Center for Molecular Medicine (MDC), Berlin-Buch, Germany.

Valentina Cenedese, Giulia Betto, Fulvio Celsi, O. Lijo Cherian, Simone Pifferi, and Anna Menini

The voltage-dependence of the TMEM16B/anoctamin2 calcium-activated chloride channel is modified by mutations in the first putative intracellular loop

J Gen Physiol. 2012 Mar 12. [Epub ahead of print]

Published March 12, 2012

Article

The voltage dependence of the TMEM16B/anoctamin2 calcium-activated chloride channel is modified by mutations in the first putative intracellular loop

Valentina Cenedese, Giulia Betto, Fulvio Celsi, O. Lijo Cherian, Simone Pifferi, and Anna Menini

Neurobiology Sector, International School for Advanced Studies, and Italian Institute of Technology, SISSA Unit, 34136 Trieste, Italy

Ca^{2+}-activated Cl^- channels (CaCCs) are involved in several physiological processes. Recently, TMEM16A/anoctamin1 and TMEM16B/anoctamin2 have been shown to function as CaCCs, but very little information is available on the structure–function relations of these channels. TMEM16B is expressed in the cilia of olfactory sensory neurons, in microvilli of vomeronasal sensory neurons, and in the synaptic terminals of retinal photoreceptors. Here, we have performed the first site-directed mutagenesis study on TMEM16B to understand the molecular mechanisms of voltage and Ca^{2+} dependence. We have mutated amino acids in the first putative intracellular loop and measured the properties of the wild-type and mutant TMEM16B channels expressed in HEK 293T cells using the whole cell voltage-clamp technique in the presence of various intracellular Ca^{2+} concentrations. We mutated E367 into glutamine or deleted the five consecutive glutamates $_{386}$EEEEE$_{390}$ and $_{399}$EYE$_{401}$. The EYE deletion did not significantly modify the apparent Ca^{2+} dependence nor the voltage dependence of channel activation. E367Q and deletion of the five glutamates did not greatly affect the apparent Ca^{2+} affinity but modified the voltage dependence, shifting the conductance–voltage relations toward more positive voltages. These findings indicate that glutamates E367 and $_{386}$EEEEE$_{390}$ in the first intracellular putative loop play an important role in the voltage dependence of TMEM16B, thus providing an initial structure–function study for this channel.

INTRODUCTION

Ca^{2+}-activated Cl^- channels (CaCCs) are expressed in many cell types, where they play various physiological roles. For example, CaCCs are involved in fast block of polyspermy in *Xenopus laevis* oocytes, in the regulation of smooth muscle contraction, in fluid secretion from exocrine glands, in the control of excitability in cardiac myocytes, as well as in olfactory, taste, and phototransduction (Frings et al., 2000; Hartzell et al., 2005; Leblanc et al., 2005; Petersen, 2005; Wray et al., 2005; Bers, 2008; Kleene, 2008; Lalonde et al., 2008; Petersen and Tepikin, 2008; Duran et al., 2010; Kunzelmann et al., 2011a).

Despite the fact that CaCCs are broadly present in several tissues, their molecular identity had remained elusive until 2008, when three independent studies reported that the expression of TMEM16A/anoctamin1 was associated with CaCCs (Caputo et al., 2008; Schroeder et al., 2008; Yang et al., 2008). The TMEM16 family comprises 10 members, and another member of the family, TMEM16B/anoctamin2, has also been shown to function as a CaCC when heterologously expressed in axolotl oocytes (Schroeder et al., 2008) or in HEK 293T cells (Pifferi et al., 2009; Stephan et al., 2009; Stöhr et al., 2009; Rasche et al., 2010; Sagheddu et al., 2010).

The study of knockout mice for TMEM16A (Rock and Harfe, 2008) and for TMEM16B (Billig et al., 2011) further confirmed that CaCC activity was reduced or abolished in several cells (Flores et al., 2009; Galietta, 2009; Hartzell et al., 2009; Kunzelmann et al., 2011b, 2012; Huang et al., 2012; Pifferi et al., 2012; Sanders et al., 2012; Scudieri et al., 2012).

Hydropathy analysis indicates that TMEM16 proteins have eight putative transmembrane domains with both N- and C-terminal domains located at the intracellular side of the membrane, and the predicted topology has been experimentally confirmed for TMEM16G/anoctamin7 (Das et al., 2008). At present, TMEM16A and TMEM16B have been shown to function as CaCCs, whereas it is unclear whether the other members of the family are CaCCs (Duran and Hartzell, 2011; Huang et al., 2012; Scudieri et al., 2012). Furthermore, splice variants have been identified both for TMEM16A (Caputo et al., 2008; Ferrera et al., 2009, 2011) and for TMEM16B

Correspondence to Anna Menini: menini@sissa.it

S. Pifferi's present address is Max Delbrück Center for Molecular Medicine, 13125 Berlin, Germany.

Abbreviations used in this paper: CaCC, Ca^{2+}-activated Cl^- channel; WT, wild type.

The Rockefeller University Press $30.00
J. Gen. Physiol.
www.jgp.org/cgi/doi/10.1085/jgp.201110764

Published March 12, 2012

(Stephan et al., 2009). However, although the functional properties of different isoforms have been extensively investigated for TMEM16A, only preliminary data have been presented for TMEM16B (Saidu, S.P., A.B. Stephan, S.M. Caraballo, H. Zhao, and J. Reisert. 2010. Association for Chemoreception Sciences Meeting. Abstr. P68).

At present, very little is known about the structure–function relations for these channels. The analysis of the sequence of TMEM16A and TMEM16B did not reveal any canonical voltage-sensing or Ca^{2+}-binding domains (Yang et al., 2008), but a comparison among the biophysical properties of the TMEM16A splice variants pointed to the functional relevance of the first putative intracellular loop (Caputo et al., 2008; Ferrera et al., 2009, 2011). Moreover, a recent study performed site-directed mutagenesis experiments on TMEM16A modifying some amino acids in the first putative intracellular loop and found that deletion of EAVK affected both the Ca^{2+} and voltage dependence of TMEM16A (Xiao et al., 2011).

Here, we aimed to perform a first site-directed mutagenesis investigation of TMEM16B to contribute to the understanding of the molecular mechanisms underlying the channel voltage and Ca^{2+} dependence. We identified some acidic amino acids in the first intracellular loop of TMEM16B ($_{367}$E, $_{386}$EEEEE$_{390}$, $_{399}$EYE$_{401}$), which are conserved in TMEM16A, where some of them have been studied (Xiao et al., 2011). We mutated or deleted the indicated glutamates and made a comparison between the electrophysiological properties measured in the whole cell configuration of the wild-type (WT) TMEM16B and its mutants. We have found that $_{367}$E and $_{386}$EEEEE$_{390}$ contribute to the voltage-dependent regulation of the TMEM16B channel.

MATERIALS AND METHODS

Site-directed mutagenesis of TMEM16B and heterologous expression

Full-length mouse TMEM16B cDNA in pCMV-Sport6 mammalian expression plasmid was obtained from RZPD (clone identification, IRAVp968H1167D; NCBI Protein database accession no. NP_705817.1). Mutations were made using a PCR-based site-directed mutagenesis kit (Gene Tailor; Invitrogen) and confirmed by DNA sequencing. HEK 293T cells (American Type Culture Collection) were transfected with 2 µg TMEM16B by using transfection reagent (FuGENE 6; Roche). Cells were co-transfected with 0.2 µg enhanced green fluorescent protein (eGFP; Takara Bio Inc.) for fluorescent identification of transfected cells. After 24 h, transfected cells were replated at a lower density and used for patch-clamp experiments between 48 and 72 h from transfection.

Electrophysiological recordings and ionic solutions

Current recordings from HEK 293T cells expressing TMEM16B or its mutants were performed in the whole cell voltage-clamp configuration, as described previously (Pifferi et al., 2006, 2009). Patch pipettes were made of borosilicate glass (World Precision Instruments, Inc.) and pulled with a PP-830 puller (Narishige). Patch pipettes filled with the intracellular solution had a resistance of ~3–5 MΩ when immersed in the bath solution. Currents were recorded with an Axopatch 1D or Axopatch 200B amplifier controlled by Clampex 9 or 10 via a Digidata 1332A or 1440 (Molecular Devices). Data were low-pass filtered at 5 kHz and sampled at 10 kHz. Experiments were performed at room temperature (20–25°C). As reported previously (Pifferi et al., 2006), control experiments in nontransfected and only eGFP-transfected cells did not show any significant Ca^{2+}-activated current.

The standard extracellular solution contained (in mM): 140 NaCl, 5 KCl, 2 $CaCl_2$, 1 $MgCl_2$, 10 glucose, and 10 HEPES, adjusted to pH 7.4 with NaOH. The intracellular solution filling the patch pipette contained (in mM): 140 CsCl, 10 HEPES, and 10 HEDTA, adjusted to pH 7.2 with CsOH, and no added Ca^{2+} for the nominally 0 Ca^{2+} solution, or various added Ca^{2+} concentrations, as calculated with the program WinMAXC (Patton et al., 2004), to obtain free Ca^{2+} in the range between 0.5 and 100 µM. The free Ca^{2+} concentrations were experimentally determined by Fura-4F (Invitrogen) measurements by using a luminescence spectrophotometer (LS-50B; PerkinElmer), as described previously (Pifferi et al., 2006). The total Cl^- concentration was 158 mM in the extracellular solution, whereas in the pipette solution it ranged from 140 mM in 0 Ca^{2+} to 160 mM in 100 µM Ca^{2+}, with a calculated

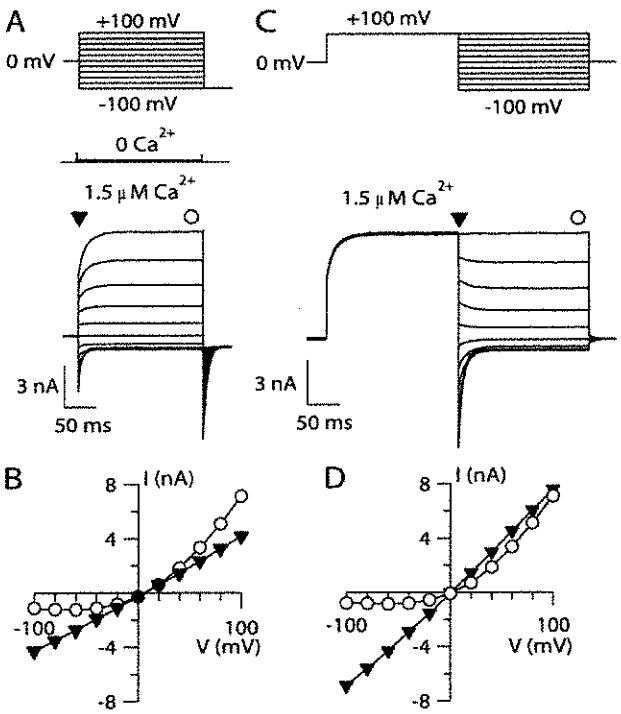

Figure 1. I-V relations of TMEM16B. (A) Representative whole cell voltage-clamp recordings obtained with an intracellular solution containing nominally 0 Ca^{2+} or 1.5 µM Ca^{2+}, as indicated. Voltage steps of 200-ms duration were given from a holding voltage of 0 mV to voltages between −100 and +100 mV in 20-mV steps, followed by a step to −100 mV, as indicated in the top part of the panel. (B) Steady-state I-V relation measured at the end of the voltage steps (circles) or instantaneous I-V measured at the beginning of each voltage step (inverted triangles) from the cell shown in B. (C) Representative recordings at 1.5 µM Ca^{2+} obtained with a voltage protocol consisting of a prepulse to +100 mV from a holding voltage of 0 mV, followed by voltage steps between −100 and +100 mV in 20-mV steps, as shown in the top part of the panel. (D) I-V relations measured from tail currents (inverted triangles) or at the steady state (circles).

Published March 12, 2012

equilibrium potential for Cl^- of −1.5 and +1.9 mV, respectively. All chemicals, unless otherwise stated, were purchased from Sigma-Aldrich.

In most experiments, we applied voltage steps of 200-ms duration from a holding potential of 0 mV ranging from −100 to +100 mV (or from −200 to +200 mV), followed by a step to −100 mV. A single-exponential function was fitted to tail currents to extrapolate the current value at the beginning of the step to −100 mV. In another set of experiments, channels were activated by a 200-ms pulse to +100 mV, and then rapidly closed by the application of hyperpolarizing steps. Single-exponential functions were fitted to tail currents at each voltage step.

Membrane capacitance and series resistance were compensated with the amplifier during the experiments. Membrane current density was calculated by dividing the current by the cell capacitance. The conductance, G, was calculated as $G = I/(V - V_{rev})$, where I is the tail current, V is the membrane voltage, and V_{rev} is the current reversal potential. Because in our experimental conditions the calculated equilibrium potential for Cl^- ranged between −1.5 and +1.9 mV and the measured V_{rev} was close to 0 mV, V_{rev} was set to 0 mV in all calculations.

Data analysis

Data are presented as mean ± SEM, with n indicating the number of cells. Statistical significance was determined using paired or unpaired t tests or ANOVA, as appropriate. When a statistically significant difference was determined with ANOVA, a post-hoc Tukey test was done to evaluate which data groups showed significant differences. P-values of <0.05 were considered significant. Data analysis and figures were made with Igor Pro software (WaveMetrics).

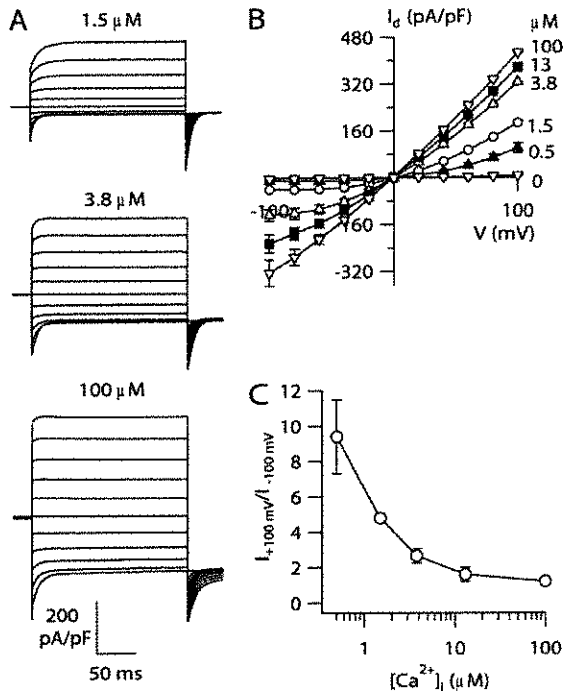

Figure 2. Ca^{2+}-dependent rectification of TMEM16B. (A) Whole cell currents activated by the indicated $[Ca^{2+}]_i$. Voltage protocol as in Fig. 1 A. (B) Average steady-state I-V relations from several cells (n = 3–6). (C) Average ratios between steady-state currents measured at +100 and −100 mV at various $[Ca^{2+}]_i$ (n = 3–6).

RESULTS

TMEM16B activation by Ca^{2+} and voltage

To study the activation of TMEM16B by $[Ca^{2+}]_i$ and voltage, we performed whole cell voltage-clamp recordings on HEK 293T cells transiently transfected with TMEM16B using intracellular solutions containing different free $[Ca^{2+}]_i$. Fig. 1 A shows that voltage steps between −100 and +100 mV from a holding voltage of 0 mV elicited very small currents with a nominally 0-Ca^{2+} pipette solution (8 ± 3 pA/pF at +100 mV; n = 8), whereas it induced large outward currents in the presence of 1.5 µM Ca^{2+}.

In the presence of Ca^{2+}, depolarizing voltage steps elicited an instantaneous outward current, indicating that channels were open at the holding potential of 0 mV, followed by a time-dependent outward relaxation (see also Fig. 5). Hyperpolarizing voltage steps induced instantaneous inward currents followed by a relaxation toward less negative values, in agreement with previous results (Pifferi et al., 2009; Stöhr et al., 2009; Rasche et al., 2010). The I-V relation measured at the steady state showed a pronounced outward rectification, whereas the instantaneous I-V curve measured at the beginning of each step was linear (Fig. 1 B). A similar result was obtained by activating TMEM16B with a different voltage protocol: channels were first activated by a 200-ms prepulse to +100 mV, and then tail currents were induced by voltage steps between −100 and +100 mV in 20-mV steps (Fig. 1 C). The I-V relation obtained by plotting the tail currents measured at the beginning of each step versus the step voltage was linear, whereas the steady-state I-V curve showed an outward rectification (Fig. 1 D), as in Fig. 1 B. These results clearly demonstrate that the I-V relation of the open channel is linear, and therefore the outward rectification is a result of a voltage-dependent mechanism that favors channel opening at

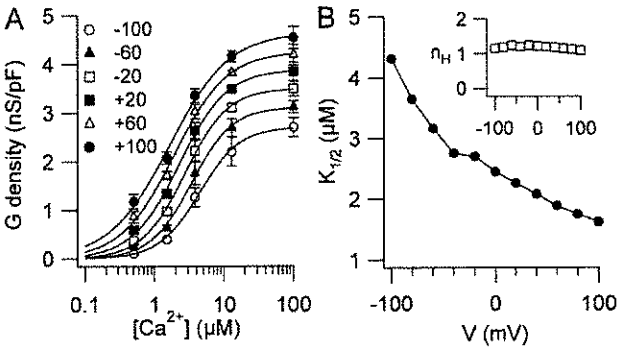

Figure 3. Ca^{2+} sensitivity of TMEM16B. (A) Conductance density calculated from tail currents measured at −100 mV after prepulses between −100 and +100 mV as indicated was plotted versus $[Ca^{2+}]_i$ (n = 3–6). Voltage protocol as in Fig. 1 A. Lines are the fit to the Hill equation (Eq. 1). (B) $K_{1/2}$ and n_H (inset) values plotted versus voltage.

Published March 12, 2012

depolarizing voltages. Thus, TMEM16B is activated by $[Ca^{2+}]_i$ and modulated by voltage at low $[Ca^{2+}]_i$.

To further examine the interplay between $[Ca^{2+}]_i$ and voltage in channel activation, we varied $[Ca^{2+}]_i$ (Fig. 2 A). Steady-state I-V relations measured at low $[Ca^{2+}]_i$ showed an outward rectification that became less pronounced as $[Ca^{2+}]_i$ increased (Fig. 2 B). We calculated a rectification index as the ratio between the steady-state current at +100 and −100 mV at each $[Ca^{2+}]_i$. The rectification index was 4.8 ± 0.2 at 1.5 µM Ca^{2+} and decreased to 1.4 ± 0.2 at 100 µM Ca^{2+}, showing that the I-V relation is Ca^{2+} dependent and becomes more linear as $[Ca^{2+}]_i$ increases (Fig. 2 C).

To analyze the Ca^{2+} dependence of TMEM16B activation at various voltages, we measured the dose–response relations. Tail currents at each $[Ca^{2+}]_i$ were measured at the beginning of the step to −100 mV after prepulses ranging from −100 to +100 mV. Fig. 3 A shows the average conductance densities plotted versus $[Ca^{2+}]_i$ and fit at each voltage by the Hill equation:

$$G = G_{max}\left[Ca^{2+}\right]_i^{nH} / \left(\left[Ca^{2+}\right]_i^{nH} + K_{1/2}{}^{nH}\right), \quad (1)$$

where G is the current density, G_{max} is the maximal current density, $K_{1/2}$ is the half-maximal $[Ca^{2+}]_i$, and n_H is the Hill coefficient.

The Hill coefficient was not voltage dependent with a value of 1.2 at −100 mV and 1.1 at +100 mV. The finding that the Hill coefficient was >1 indicates that the binding of more than one Ca^{2+} ion is necessary to open the channel. $K_{1/2}$ slightly decreased with membrane depolarization from 4.3 µM at −100 mV to 1.6 µM at +100 mV, as illustrated in Fig. 3 B. These data show that the Ca^{2+} sensitivity of TMEM16B is moderately voltage dependent, in agreement with previous results obtained with inside-out patches (Pifferi et al., 2009; Stephan et al., 2009).

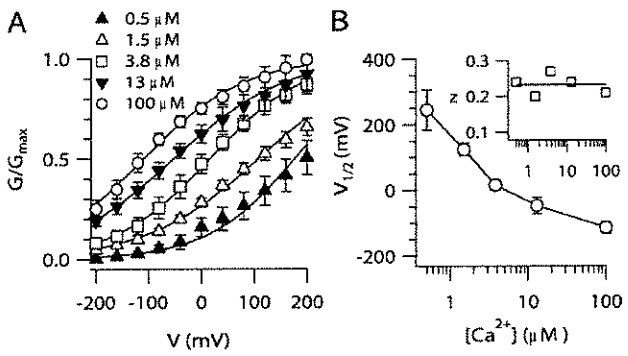

Figure 4. Voltage dependence of TMEM16B. (A) Normalized conductances at the indicated $[Ca^{2+}]_i$ calculated from tail currents at −100 mV after prepulses between −200 and +200 mV were plotted versus the prepulse voltage (n = 4–9). Lines are the fit to the Boltzmann equation (Eq. 2). (B) $V_{1/2}$ and z (inset) values plotted versus $[Ca^{2+}]_i$.

The voltage dependence of steady-state activation (G-V relation) was analyzed by measuring tail currents at the beginning of a step to −100 mV after prepulse voltages between −200 and +200 mV. The range of voltages was extended from the previous voltage protocols to obtain a better estimate of voltage dependence. Fig. 4 A shows the average conductance activated at a given $[Ca^{2+}]_i$ plotted versus membrane voltage and fit by the Boltzmann equation:

$$G / G_{max} = 1 / \left\{1 + \exp\left[z\left(V_{1/2} - V\right)F / RT\right]\right\}, \quad (2)$$

where G/G_{max} is the normalized conductance, z is the equivalent gating charge associated with voltage-dependent channel opening, V is the membrane potential, $V_{1/2}$ is the membrane potential producing half-maximal activation, F is the Faraday constant, R is the gas constant, and T is the absolute temperature.

The maximal conductance density G_{max} was determined by a global fit of G-V relations, and G at each $[Ca^{2+}]_i$ was then normalized to the same G_{max}. Because at the smaller $[Ca^{2+}]_i$ the prediction of G_{max} from the fit could be affected by a large error, we also estimated G_{max} at each $[Ca^{2+}]_i$. G_{max} at 0.5 µM Ca^{2+} was 4.1 ± 0.4 nS/pF, not significantly different from the value of 4.7 ± 0.4 nS/pF at 100 µM Ca^{2+}, indicating that the estimate of G_{max} was little affected by $[Ca^{2+}]_i$. Fig. 4 A shows that increasing

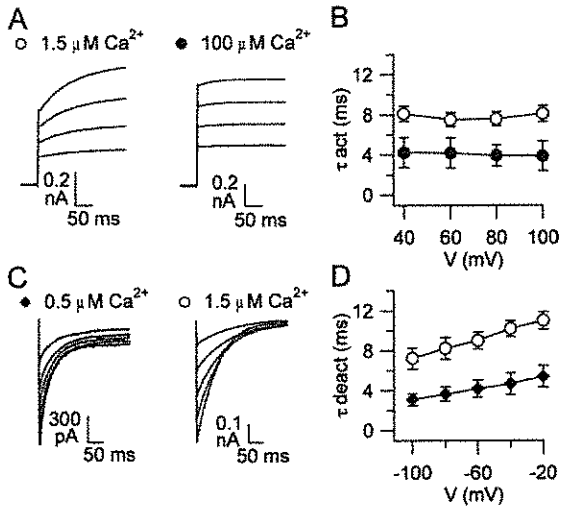

Figure 5. Activation and deactivation kinetics of TMEM16B. (A) Representative recordings at the indicated $[Ca^{2+}]_i$. Voltage protocol as in Fig. 1 A, with voltage steps from a holding voltage of 0 between +40 to +100 mV in 20-mV steps. Red dashed lines are the fit to a single-exponential function. (B) Average activation time constants (τ_{act}) plotted versus voltage (n = 6–8). (C) Representative recordings at the indicated $[Ca^{2+}]_i$. Voltage protocol as in Fig. 1 C, with a prepulse to +100 mV and tail currents induced by voltage steps between −100 and +100 mV in 20-mV steps. Only tail currents are illustrated. Red dashed lines are the fit to a single-exponential function. (D) Average deactivation time constants (τ_{deact}) plotted versus voltage (n = 4–9).

Published March 12, 2012

$[Ca^{2+}]_i$ produced a leftward shift in the G-V relation: $V_{1/2}$ was 124 ± 20 mV at 1.5 µM Ca^{2+} and became −115 ± 18 mV at 100 µM Ca^{2+}, whereas the equivalent gating charge was not largely modified (z = 0.23–0.30). Thus, $V_{1/2}$ decreased as $[Ca^{2+}]_i$ increased, indicating that more channels can be activated by depolarization in the presence of a high $[Ca^{2+}]_i$ (Fig. 4 B). At a given $[Ca^{2+}]_i$, the conductance increased with depolarization, showing that the conductance depends both on $[Ca^{2+}]_i$ and voltage.

Activation and deactivation kinetics are regulated by $[Ca^{2+}]_i$ and voltage

To characterize activation and deactivation kinetics, we analyzed the time-dependent components in response to voltage steps in the presence of a given $[Ca^{2+}]_i$. As shown in Figs. 2 A and 5 A, current activation in response to depolarizing voltage steps had two components: an instantaneous time-independent current, related to the fraction of channels open at the holding voltage of 0 mV, followed by an outward time-dependent relaxation, a

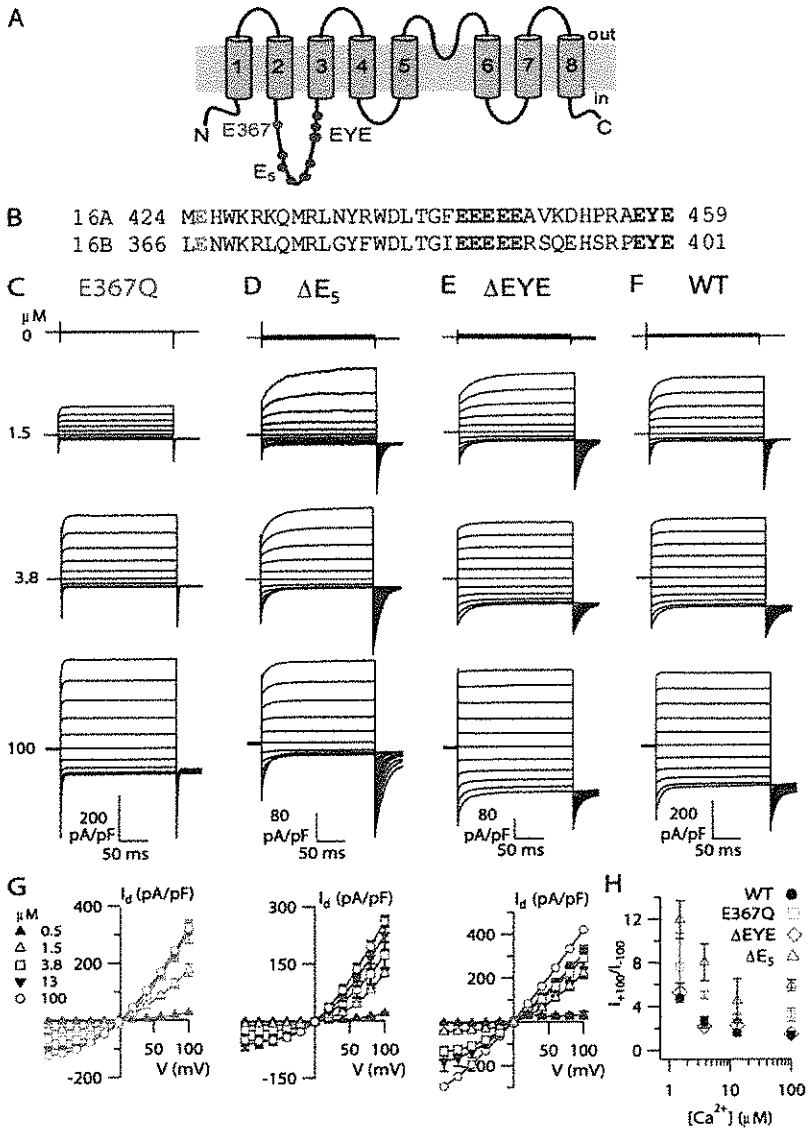

Figure 6. TMEM16B mutations. (A) Predicted topology of TMEM16A and TMEM16B from hydropathy analysis. (B) Alignment between mouse TMEM16A (*a,c*; available from GenBank/EMBL/DDBJ under accession no. NM_178642.4) and the retinal isoform of TMEM16B used in this study (NP_705817.1), with the mutations or deletions highlighted in color. (C–F) Representative recordings at the indicated $[Ca^{2+}]_i$ for E367Q (C), ΔE_5 (D), ΔEYE (E) mutants, and WT (F). Traces for WT are the same as in Fig. 2 A. Voltage protocol as in Fig. 1 A. (G) I-V steady-state relations (n = 3–8). (H) Average ratios between currents measured at +100 and −100 mV plotted versus $[Ca^{2+}]_i$ for each mutant (n = 3–8).

Published March 12, 2012

result of the increase in the fraction of channels opened by depolarization. The time-independent component became larger as voltage or $[Ca^{2+}]_i$ increased.

To examine the activation kinetics, we analyzed the time-dependent component of the current elicited by depolarizing voltage steps. Fig. 5 A shows that most of the time course of time-dependent relaxations was well fit by a single-exponential function. The time constant of current activation, τ_{act}, in the presence of 1.5 μM Ca^{2+} was 8.1 ± 0.8 ms at +100 mV and did not vary as a function of voltage at a given $[Ca^{2+}]_i$ (Fig. 5 B). At +100 mV, τ_{act} at 100 μM Ca^{2+} was 3.9 ± 1.4 ms, significantly smaller than the value of 8.1 ± 0.8 ms at 1.5 μM Ca^{2+}, showing that an increase in $[Ca^{2+}]_i$ accelerated activation.

The time constant of current deactivation (τ_{deact}) was calculated by fitting with a single-exponential function the tail currents obtained after a prepulse at +100 mV by voltage steps ranging between −100 and −20 mV (Fig. 5 C). In the presence of 0.5 μM Ca^{2+}, τ_{deact} was 3.0 ± 0.2 ms at −100 mV and 5.4 ± 0.5 ms at −20 mV, showing that less negative voltages slowed deactivation (Fig. 5 D). At −100 mV, τ_{deact} at 1.5 μM Ca^{2+} was 7.2 ± 0.8 ms, significantly different from the value of 3.0 ± 0.2 ms at 0.5 μM Ca^{2+}, showing that an increase in $[Ca^{2+}]_i$ slowed deactivation.

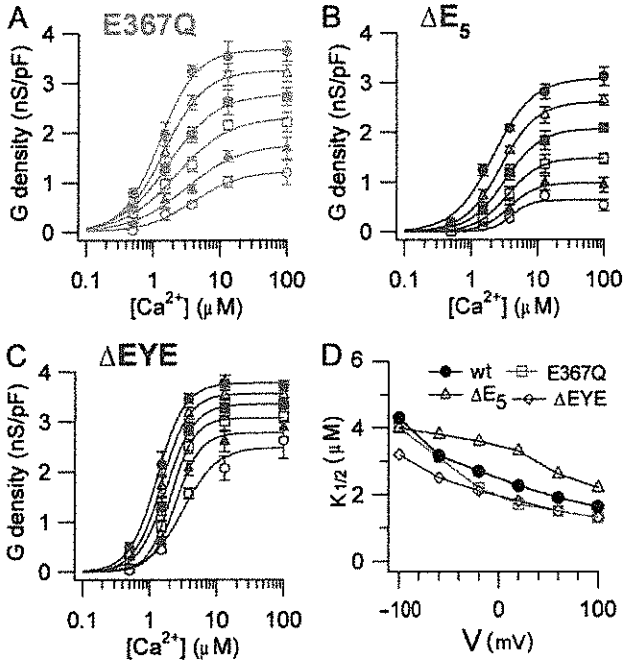

Figure 7. Ca^{2+} sensitivity of TMEM16B mutants. Conductance density calculated from tail currents measured at −100 mV after prepulses between −100 and +100 mV as indicated was plotted versus $[Ca^{2+}]_i$ for E367Q (A; n = 3–6), ΔE_5 (B; n = 3–5), and ΔEYE (C; n = 3–8) mutants. Lines are the fit to the Hill equation (Eq. 1). (D) $K_{1/2}$ values plotted versus voltage for each mutant.

In summary, the activation kinetics are voltage independent and become faster by increasing $[Ca^{2+}]_i$, whereas the deactivation kinetics are prolonged by depolarization and by increasing $[Ca^{2+}]_i$.

Functional characterization of mutations in the first putative intracellular loop

To investigate the molecular mechanisms responsible for channel activation by Ca^{2+} and by voltage, we performed a site-directed mutagenesis study. Hydropathy analysis indicates that each member of the TMEM16 family has eight transmembrane domains (Fig. 6 A). Analysis of the sequence of TMEM16B does not reveal the presence of any typical voltage sensor or Ca^{2+}-binding domain. However, some acidic amino acids are located in the first putative intracellular loop between transmembrane segment 2 and 3, and we hypothesized that some of them may be involved in Ca^{2+} and/or voltage activation of TMEM16B. As illustrated in Fig. 6 B, we mutated glutamate at position 367 into glutamine (E367Q), deleted the five consecutive glutamate residues $_{386}$EEEEE$_{390}$ (ΔE_5), or deleted $_{399}$EYE$_{401}$ (ΔEYE), and measured their biophysical properties.

Fig. 6 (C–F) illustrates recordings from each mutant channel in the presence of various $[Ca^{2+}]_i$. Similar to WT

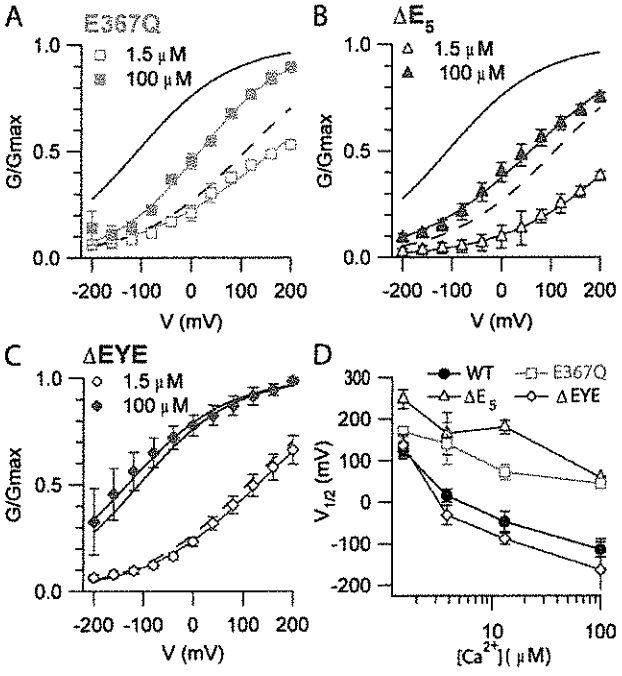

Figure 8. Voltage dependence of TMEM16B mutants. Normalized conductances at the indicated $[Ca^{2+}]_i$ calculated from tail currents at −100 mV after prepulses between −200 and +200 mV were plotted versus the prepulse voltage. Black lines are the fit to the Boltzmann equation (Eq. 2) for WT from Fig. 4 at 100 μM Ca^{2+} (solid line) or at 1.5 μM Ca^{2+} (dashed line). Colored lines are the fits to the Boltzmann equation for E367Q (A; n = 3–4), ΔE_5 (B; n = 3–5), and ΔEYE (C; n = 3–6) mutants. (D) Average $V_{1/2}$ values plotted versus $[Ca^{2+}]_i$.

Published March 12, 2012

(Fig. 2 A), the steady-state I-V relation for each mutant was Ca^{2+} dependent, showing an outward rectification at low $[Ca^{2+}]_i$ that became less pronounced as $[Ca^{2+}]_i$ increased (Fig. 6 G). However, although the overall Ca^{2+} dependence was similar, the rectification index, measured from the ratio between steady-state currents at +100 and −100 mV, was significantly higher at every $[Ca^{2+}]_i$ in E367Q and ΔE_5 mutants than in WT, whereas it remained similar in ΔEYE mutant channel (Fig. 6 H).

The dose–response relations for each mutant channel, evaluated from tail currents as described previously for the WT channel (Fig. 3), were fit by the Hill equation (Fig. 7, A–C). Fig. 7 D shows that $K_{1/2}$ at +100 mV (−100 mV) was 1.6 μM (4.3 μM) in WT, 1.3 μM (4.0 μM) in E367Q, 2.2 μM (4.0 μM) in ΔE_5, and 1.3 μM (3.2 μM) in ΔEYE. The Hill coefficient n_H at +100 mV (−100 mV) was 1.1 (1.2) in WT, 1.6 (1.2) in E367Q, 1.4 (2.9) in ΔE_5, and 2.0 (1.7) in ΔEYE. Thus, the mutations produced only some very small changes in $K_{1/2}$ or n_H, but overall no strong modifications in Ca^{2+} sensitivity were observed.

The G-V relations in mutant channels were measured at each $[Ca^{2+}]_i$ and compared with the corresponding relations in WT channels. Fig. 8 A shows that the E367Q mutation produced a rightward shift of the G-V relation at a given $[Ca^{2+}]_i$ with respect to WT; indeed, $V_{1/2}$ changed from 124 ± 20 mV in WT to 169 ± 6 mV in E367Q at 1.5 μM Ca^{2+}, and from −115 ± 18 mV in WT to 44 ± 8 mV in E367Q at 100 μM Ca^{2+} (Fig. 8 D). The deletion ΔE_5 also shifted the G-V relations to the right (Fig. 8, B and D): $V_{1/2}$ changed from 124 ± 20 mV in WT to 248 ± 39 mV in ΔE_5 at 1.5 μM Ca^{2+}, and from −115 ± 18 mV in WT to 58 ± 15 mV in ΔE_5 at 100 μM Ca^{2+}. Differently from the previous mutants, the ΔEYE deletion did not produce any significant change in the G-V relations (Fig. 8, C and D). The equivalent gating charge for each mutant varied between 0.15 and 0.32, values similar to those of the WT channel (z = 0.23–0.30). Thus, E367Q and the ΔE_5 deletion modified the voltage sensitivity: at a given $[Ca^{2+}]_i$, fewer channels can be open by depolarization compared with WT.

The kinetic properties of activation and deactivation of mutant channels also showed some interesting changes compared with WT channels. Upon depolarizing voltage steps, the activation of mutant channels was still characterized by two components: an instantaneous time-independent current, followed by an outward time-dependent relaxation (Fig. 6), which was well fit by a single-exponential function as in WT channels. In the presence of 1.5 μM Ca^{2+}, τ_{act} at +100 mV was 2.8 ± 0.3 ms in E367Q, faster than 7.5 ± 0.7 ms in the WT channel, whereas it became slower than WT in ΔE_5 (17.7 ± 3.0 ms) and in ΔEYE (25.5 ± 2.3 ms). These results indicate that each mutation altered the time course of activation. Indeed, the time necessary to respond to a depolarization decreased in E367Q, whereas it was progressively prolonged in ΔE_5 and in ΔEYE compared with WT. As in the WT channel, τ_{act} in each mutant was not significantly modified by voltage (Fig. 9 A).

Deactivation kinetics was also well fit by a single-exponential function and, similarly to WT, τ_{deact} showed an increase at less negative voltages for each mutant channel (Fig. 9 B). In the presence of 1.5 μM Ca^{2+}, τ_{deact} at −100 mV was 1.6 ± 0.3 ms in E367Q, smaller than 7.2 ± 0.8 ms in the WT channel, whereas it was not significantly different from WT in ΔE_5 (6.8 ± 0.3 ms) and became larger than WT in ΔEYE (12.3 ± 1.5 ms). The time necessary for channels to close upon repolarization decreased in E367Q but remained similar in ΔE_5, and it was prolonged in ΔEYE compared with WT. Thus, E367Q and ΔEYE mutants also showed a modified time course of deactivation.

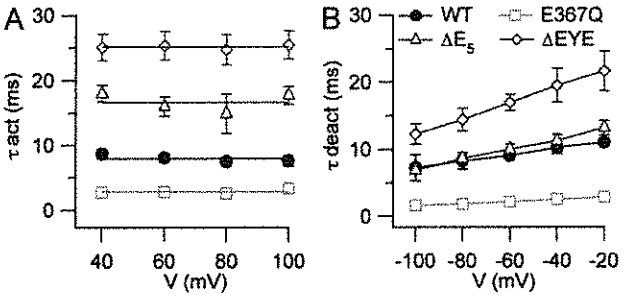

Figure 9. Activation and deactivation kinetics of TMEM16B mutants. Kinetics were measured as explained in Fig. 5. (A) Average activation time constants (τ_{act}) plotted versus voltage for E367Q (n = 5), ΔE_5 (n = 3), and ΔEYE (n = 6) mutants. (B) Average deactivation time constants (τ_{deact}) plotted versus voltage for E367Q (n = 4), ΔE_5 (n = 4), and ΔEYE (n = 5) mutants.

DISCUSSION

Here, we have provided the first site-directed mutagenesis study to investigate structure–function relations of the TMEM16B channel. Because previous studies have shown that TMEM16B in excised inside-out patches has a significant rundown (Pifferi et al., 2009, Fig. 5; Stephan et al., 2009, Fig. 3 A), whereas whole cell recordings are rather stable (Pifferi et al., 2009, Fig. 1 h), we decided to use the whole cell configuration.

We first characterized the WT TMEM16B channel and established one important difference between TMEM16A and TMEM16B activation properties in the absence of $[Ca^{2+}]_i$. Indeed, we found that TMEM16B cannot be activated by voltages up to +200 mV in the absence of Ca^{2+} (32 ± 10 pA/pF; n = 6; not depicted), whereas recent data from Hartzell's laboratory showed that TMEM16A was activated by strong depolarization in the absence of Ca^{2+} (~140 pA/pF at +200 mV; Fig. 5 A in Xiao et al., 2011). Thus, our data show that TMEM16B needs Ca^{2+} to be activated differently from TMEM16A, which can be activated by voltage also in the absence of Ca^{2+} (Xiao et al., 2011).

Published March 12, 2012

In the presence of Ca^{2+}, dose–response relations for TMEM16A and TMEM16B obtained by different laboratories reported variable values for $K_{1/2}$. For TMEM16A, from inside-out recordings, $K_{1/2}$ at +60 mV (−60 mV) was 0.3 µM (2.6 µM) (Yang et al., 2008), and at +100 mV (−100 mV) it was 0.4 µM (5.9 µM) (Xiao et al., 2011), whereas from whole cell recordings at +100 mV (−40 mV) it was 332 nM (~700 nM) (Ferrera et al., 2009). For TMEM16B, from previous work in inside-out patches, $K_{1/2}$ at +50 mV (−50 mV) was 3.3 µM (4.9 µM) (Pifferi et al., 2009), and at +40 mV (−40 mV) it was 1.2 µM (1.8 µM) (Stephan et al., 2009), whereas from whole cell recordings we found that $K_{1/2}$ at +40 mV (−40 mV) was 2.0 µM (2.7 µM), and at +100 mV (−100 mV) it was 1.6 µM (4.3 µM) (Fig. 3). Although there are some differences among studies reported from different laboratories, every report showed that the apparent affinity for Ca^{2+} is slightly voltage dependent, with higher apparent Ca^{2+} affinity at positive voltages, and the Hill coefficients are consistently higher than one, indicating that more than a Ca^{2+} ion is necessary to activate the channels. A comparison between TMEM16A and TMEM16B shows a fourfold difference between $K_{1/2}$ values at +100 mV: 0.4 µM (Xiao et al., 2011) for TMEM16A and 1.6 µM for TMEM16B (Fig. 3), indicating a lower apparent affinity for Ca^{2+} of TMEM16B compared with TMEM16A.

A critical question about the function of TMEM16A and TMEM16B is the following: what are the molecular mechanisms responsible for Ca^{2+} and voltage modulation of channel gating in each channel? Galietta's laboratory (Ferrera et al., 2009) has shown that human TMEM16A has various protein isoforms generated by alternative splicing, and it has labeled the four identified alternative segments as *a*, *b*, *c*, and *d*. A rare minimal version of TMEM16A lacking all alternative segments, TMEM16A (0), still shows CaCC properties, although the voltage dependence is reduced, (Caputo et al., 2008; Ferrera et al., 2009, 2011). Ferrera et al. (2009) showed that segment *b* modified the Ca^{2+} sensitivity by nearly fourfold, decreasing the apparent half-effective concentration at +80 mV from 350 to 90 nM, whereas segment *c* affected the voltage dependence but not the Ca^{2+} sensitivity of human TMEM16A (*abc*). Segment *c* is composed of the four amino acids EAVK, which have also been recently deleted from mouse TMEM16A (*ac*) in a study from Hartzell's laboratory (Xiao et al., 2011). Differently from Ferrera et al. (2009), Xiao et al. (2011) found that deletion of EAVK modified both Ca^{2+} and voltage dependence of TMEM16A. The discrepancy between the results can be a result of differences between human TMEM16A (*ab*) and mouse TMEM16A (*a*), and/or to the different techniques, whole cell versus inside-out recordings, used for the experiments in the different laboratories. Although the two studies reached some different conclusions, they both pointed to the relevance of the segment *c* in the regulation of the TMEM16A functional activity.

TMEM16B is expressed in the retina, at the synaptic terminal of photoreceptors (Stöhr et al., 2009; Billig et al., 2011), in the cilia of olfactory sensory neurons, and in the microvilli of vomeronasal sensory neurons (Stephan et al., 2009; Rasche et al., 2010; Sagheddu et al., 2010; Billig et al., 2011; Pifferi et al., 2012). Zhao's laboratory showed that the major TMEM16B olfactory isoform differs from the retinal isoform in the absence of the exon encoding the four amino acids ERSQ in the first putative intracellular loop (Stephan et al., 2009). It is worth pointing out here that segment *c* (EAVK) in TMEM16A is not present in TMEM16B, but that ERSQ residues are located in the corresponding positions in the retinal isoform of TMEM16B (Fig. 6). A comparison between the biophysical properties measured in inside-out patches from the retinal isoform (Pifferi et al., 2009) and from the olfactory isoform (missing ERSQ; Stephan et al., 2009) did not reveal any major difference in the rectification properties and in the dose–response relations between the two isoforms, although we cannot exclude that more detailed biophysical studies may reveal subtle differences. Indeed, the functional properties of additional isoforms for TMEM16B are under investigation (Saidu, S.P., A.B. Stephan, S.M. Caraballo, H. Zhao, and J. Reisert. 2010. Association for Chemoreception Sciences Meeting. Abstr. P68).

Although the amino acidic sequences of both TMEM16A and TMEM16B lack any classical voltage-sensor or Ca^{2+}-binding domain, a series of five consecutive glutamates located in the first putative intracellular loop has been identified as a good candidate to play a role in channel gating. Moreover, we have investigated if other glutamates in the same loop could also be involved in the activation of TMEM16B by Ca^{2+} and voltage. We found that deletion of the five glutamates, ΔE_5, did not greatly affect the apparent affinity for Ca^{2+} (Fig. 7), but it significantly shifted the activation curve to the right. Indeed, $V_{1/2}$ at 1.5 µM Ca^{2+} changed from 124 mV in WT to 248 mV, whereas the equivalent gating charge was not modified. In addition, the time necessary to respond to a depolarization was prolonged in ΔE_5, whereas the deactivation constant was not significantly affected (Fig. 9). Thus, the five consecutive glutamates are involved in the voltage dependence of the TMEM16B channel, whereas they do not seem to play a significant role in the apparent affinity for Ca^{2+}. These results are in agreement with a recent study in TMEM16A, showing that the substitution of the four correspondent glutamates into alanines ($_{444}$EEEE/AAAA$_{447}$) did not greatly affect the apparent affinity for Ca^{2+} but modified the voltage dependence, producing a shift of the activation curve to the right (Xiao et al., 2011).

In the TMEM16B mutant E367Q, both activation and deactivation kinetics were shortened; the dose–response relation for Ca^{2+} was not strongly modified, while the activation curve was shifted to the right. Finally, the deletion ΔEYE produced an increase in the time constants

Published March 12, 2012

for activation and deactivation, whereas it did not cause any large change in apparent affinity for Ca^{2+} or in voltage sensitivity.

Collectively, our results indicate that glutamates E367 and $_{386}$EEEEE$_{390}$ in the first putative intracellular loop play a relevant role in the modulation of the voltage dependence of TMEM16B.

Conclusions

In conclusion, we have found evidence that the five consecutive glutamates in the first putative intracellular loop are not involved in Ca^{2+} sensitivity in TMEM16B but have an important role in voltage dependence. Another glutamate in position 367 plays a similar role, further indicating that the first intracellular loop is involved in voltage-dependent activation of TMEM16B.

At present, the location of the Ca^{2+}-binding site in TMEM16A and TMEM16B remains unknown. It is possible that several residues in different regions contribute to bind Ca^{2+} ions, but it cannot be excluded that the Ca^{2+}-binding site is located in an accessory subunit expressed both in HEK 293T cells and in axolotl oocytes. Future work will have to shed light on the intricate mechanisms that couple Ca^{2+} gating and voltage dependence, including intriguing interactions between gating and permeation.

We thank Anna Boccaccio, Arin Marchesi, and Riccardo Scala for discussions; Federica Ferrero for help with cell cultures; and all members of the laboratory for discussions.

This study was supported by grants from the Italian Ministry of Education, University and Research, and from the Italian Institute of Technology.

Christopher Miller served as editor.

Submitted: 27 December 2011
Accepted: 17 February 2012

REFERENCES

Bers, D.M. 2008. Calcium cycling and signaling in cardiac myocytes. *Annu. Rev. Physiol.* 70:23–49. http://dx.doi.org/10.1146/annurev.physiol.70.113006.100455

Billig, G.M., B. Pál, P. Fidzinski, and T.J. Jentsch. 2011. Ca2+-activated Cl− currents are dispensable for olfaction. *Nat. Neurosci.* 14:763–769. http://dx.doi.org/10.1038/nn.2821

Caputo, A., E. Caci, L. Ferrera, N. Pedemonte, C. Barsanti, E. Sondo, U. Pfeffer, R. Ravazzolo, O. Zegarra-Moran, and L.J.V. Galietta. 2008. TMEM16A, a membrane protein associated with calcium-dependent chloride channel activity. *Science.* 322:590–594. http://dx.doi.org/10.1126/science.1163518

Das, S., Y. Hahn, D.A. Walker, S. Nagata, M.C. Willingham, D.M. Peehl, T.K. Bera, B. Lee, and I. Pastan. 2008. Topology of NGEP, a prostate-specific cell:cell junction protein widely expressed in many cancers of different grade level. *Cancer Res.* 68:6306–6312. http://dx.doi.org/10.1158/0008-5472.CAN-08-0870

Duran, C., and H.C. Hartzell. 2011. Physiological roles and diseases of tmem16/anoctamin proteins: are they all chloride channels? *Acta Pharmacol. Sin.* 32:685–692. http://dx.doi.org/10.1038/aps.2011.48

Duran, C., C.H. Thompson, Q. Xiao, and H.C. Hartzell. 2010. Chloride channels: often enigmatic, rarely predictable. *Annu. Rev. Physiol.* 72:95–121. http://dx.doi.org/10.1146/annurev-physiol-021909-135811

Ferrera, L., A. Caputo, I. Ubby, E. Bussani, O. Zegarra-Moran, R. Ravazzolo, F. Pagani, and L.J.V. Galietta. 2009. Regulation of TMEM16A chloride channel properties by alternative splicing. *J. Biol. Chem.* 284:33360–33368. http://dx.doi.org/10.1074/jbc.M109.046607

Ferrera, L., P. Scudieri, E. Sondo, A. Caputo, E. Caci, O. Zegarra-Moran, R. Ravazzolo, and L.J.V. Galietta. 2011. A minimal isoform of the TMEM16A protein associated with chloride channel activity. *Biochim. Biophys. Acta.* 1808:2214–2223. http://dx.doi.org/10.1016/j.bbamem.2011.05.017

Flores, C.A., L.P. Cid, F.V. Sepúlveda, and M.I. Niemeyer. 2009. TMEM16 proteins: the long awaited calcium-activated chloride channels? *Braz. J. Med. Biol. Res.* 42:993–1001. http://dx.doi.org/10.1590/S0100-879X2009005000028

Frings, S., D. Reuter, and S.J. Kleene. 2000. Neuronal Ca2+-activated Cl− channels—homing in on an elusive channel species. *Prog. Neurobiol.* 60:247–289. http://dx.doi.org/10.1016/S0301-0082(99)00027-1

Galietta, L.J.V. 2009. The TMEM16 protein family: a new class of chloride channels? *Biophys. J.* 97:3047–3053. http://dx.doi.org/10.1016/j.bpj.2009.09.024

Hartzell, C., I. Putzier, and J. Arreola. 2005. Calcium-activated chloride channels. *Annu. Rev. Physiol.* 67:719–758. http://dx.doi.org/10.1146/annurev.physiol.67.032003.154341

Hartzell, H.C., K. Yu, Q. Xiao, L.-T. Chien, and Z. Qu. 2009. Anoctamin/TMEM16 family members are Ca2+-activated Cl− channels. *J. Physiol.* 587:2127–2139. http://dx.doi.org/10.1113/jphysiol.2008.163709

Huang, F., X. Wong, and L.Y. Jan. 2012. International Union of Basic and Clinical Pharmacology. LXXXV: calcium-activated chloride channels. *Pharmacol. Rev.* 64:1–15. http://dx.doi.org/10.1124/pr.111.005009

Kleene, S.J. 2008. The electrochemical basis of odor transduction in vertebrate olfactory cilia. *Chem. Senses.* 33:839–859. http://dx.doi.org/10.1093/chemse/bjn048

Kunzelmann, K., P. Kongsuphol, K. Chootip, C. Toledo, J.R. Martins, J. Almaca, Y. Tian, R. Witzgall, J. Ousingsawat, and R. Schreiber. 2011a. Role of the Ca2+-activated Cl− channels bestrophin and anoctamin in epithelial cells. *Biol. Chem.* 392:125–134. http://dx.doi.org/10.1515/BC.2011.010

Kunzelmann, K., Y. Tian, J.R. Martins, D. Faria, P. Kongsuphol, J. Ousingsawat, F. Thevenod, E. Roussa, J. Rock, and R. Schreiber. 2011b. Anoctamins. *Pflugers Arch.* 462:195–208. http://dx.doi.org/10.1007/s00424-011-0975-9

Kunzelmann, K., R. Schreiber, A. Kmit, W. Jantarajit, J.R. Martins, D. Faria, P. Kongsuphol, J. Ousingsawat, and Y. Tian. 2012. Expression and function of epithelial anoctamins. *Exp. Physiol.* 97:184–192.

Lalonde, M.R., M.E. Kelly, and S. Barnes. 2008. Calcium-activated chloride channels in the retina. *Channels (Austin).* 2:252–260. http://dx.doi.org/10.4161/chan.2.4.6704

Leblanc, N., J. Ledoux, S. Saleh, A. Sanguinetti, J. Angermann, K. O'Driscoll, F. Britton, B.A. Perrino, and I.A. Greenwood. 2005. Regulation of calcium-activated chloride channels in smooth muscle cells: a complex picture is emerging. *Can. J. Physiol. Pharmacol.* 83:541–556. http://dx.doi.org/10.1139/y05-040

Patton, C., S. Thompson, and D. Epel. 2004. Some precautions in using chelators to buffer metals in biological solutions. *Cell Calcium.* 35:427–431. http://dx.doi.org/10.1016/j.ceca.2003.10.006

Petersen, O.H. 2005. Ca2+ signalling and Ca2+-activated ion channels in exocrine acinar cells. *Cell Calcium.* 38:171–200. http://dx.doi.org/10.1016/j.ceca.2005.06.024

Petersen, O.H., and A.V. Tepikin. 2008. Polarized calcium signaling in exocrine gland cells. *Annu. Rev. Physiol.* 70:273–299. http://dx.doi.org/10.1146/annurev.physiol.70.113006.100618

Published March 12, 2012

Pifferi, S., G. Pascarella, A. Boccaccio, A. Mazzatenta, S. Gustincich, A. Menini, and S. Zucchelli. 2006. Bestrophin-2 is a candidate calcium-activated chloride channel involved in olfactory transduction. *Proc. Natl. Acad. Sci. USA.* 103:12929–12934. http://dx.doi.org/10.1073/pnas.0604505103

Pifferi, S., M. Dibattista, and A. Menini. 2009. TMEM16B induces chloride currents activated by calcium in mammalian cells. *Pflugers Arch.* 458:1023–1038. http://dx.doi.org/10.1007/s00424-009-0684-9

Pifferi, S., V. Cenedese, and A. Menini. 2012. Anoctamin 2/TMEM16B: a calcium-activated chloride channel in olfactory transduction. *Exp. Physiol.* 97:193–199.

Rasche, S., B. Toetter, J. Adler, A. Tschapek, J.F. Doerner, S. Kurtenbach, H. Hatt, H. Meyer, B. Warscheid, and E.M. Neuhaus. 2010. Tmem16b is specifically expressed in the cilia of olfactory sensory neurons. *Chem. Senses.* 35:239–245. http://dx.doi.org/10.1093/chemse/bjq007

Rock, J.R., and B.D. Harfe. 2008. Expression of TMEM16 paralogs during murine embryogenesis. *Dev. Dyn.* 237:2566–2574. http://dx.doi.org/10.1002/dvdy.21676

Sagheddu, C., A. Boccaccio, M. Dibattista, G. Montani, R. Tirindelli, and A. Menini. 2010. Calcium concentration jumps reveal dynamic ion selectivity of calcium-activated chloride currents in mouse olfactory sensory neurons and TMEM16b-transfected HEK 293T cells. *J. Physiol.* 588:4189–4204. http://dx.doi.org/10.1113/jphysiol.2010.194407

Sanders, K.M., M.H. Zhu, F.C. Britton, S.D. Koh, and S.M. Ward. 2012. Anoctamins and gastrointestinal smooth muscle excitability. *Exp. Physiol.* 97:200–206.

Schroeder, B.C., T. Cheng, Y.N. Jan, and L.Y. Jan. 2008. Expression cloning of TMEM16A as a calcium-activated chloride channel subunit. *Cell.* 134:1019–1029. http://dx.doi.org/10.1016/j.cell.2008.09.003

Scudieri, P., E. Sondo, L. Ferrera, and L.J. Galietta. 2012. The anoctamin family: TMEM16A and TMEM16B as calcium-activated chloride channels. *Exp. Physiol.* 97:177–183. http://dx.doi.org/10.1113/expphysiol.2011.058198

Stephan, A.B., E.Y. Shum, S. Hirsh, K.D. Cygnar, J. Reisert, and H. Zhao. 2009. ANO2 is the cilial calcium-activated chloride channel that may mediate olfactory amplification. *Proc. Natl. Acad. Sci. USA.* 106:11776–11781. http://dx.doi.org/10.1073/pnas.0903304106

Stöhr, H., J.B. Heisig, P.M. Benz, S. Schöberl, V.M. Milenkovic, O. Strauss, W.M. Aartsen, J. Wijnholds, B.H.F. Weber, and H.L. Schulz. 2009. TMEM16B, a novel protein with calcium-dependent chloride channel activity, associates with a presynaptic protein complex in photoreceptor terminals. *J. Neurosci.* 29:6809–6818. http://dx.doi.org/10.1523/JNEUROSCI.5546-08.2009

Wray, S., T. Burdyga, and K. Noble. 2005. Calcium signalling in smooth muscle. *Cell Calcium.* 38:397–407. http://dx.doi.org/10.1016/j.ceca.2005.06.018

Xiao, Q., K. Yu, P. Perez-Cornejo, Y. Cui, J. Arreola, and H.C. Hartzell. 2011. Voltage- and calcium-dependent gating of TMEM16A/Ano1 chloride channels are physically coupled by the first intracellular loop. *Proc. Natl. Acad. Sci. USA.* 108:8891–8896. http://dx.doi.org/10.1073/pnas.1102147108

Yang, Y.D., H. Cho, J.Y. Koo, M.H. Tak, Y. Cho, W.-S. Shim, S.P. Park, J. Lee, B. Lee, B.-M. Kim, et al. 2008. TMEM16A confers receptor-activated calcium-dependent chloride conductance. *Nature.* 455:1210–1215. http://dx.doi.org/10.1038/nature07313

5 Discussion

One of the most common features of native CaCCs is a characteristic voltage - dependence that is modulated by intracellular Ca^{2+} (Caputo 2008, Bonigk 1999, Pifferi 2006, Reisert 2003), and this feature is well recapitulated by both TMEM16A and TMEM16B. However, the molecular mechanisms underlying Ca^{2+}- and voltage - gating are unknown.

The analysis of the amino acidic sequence reveals an absence of canonical voltage - sensing and Ca^{2+}- binding domains (Yang 2008). TMEM16A and TMEM16B channels share the 62% of amino acidic identity (Yang 2008). By an alignment between their sequences, we identified a series of acidic amino acids in the first intracellular loop ($_{367}$E, $_{386}$EEEEE$_{390}$ and $_{399}$EYE$_{401}$) which are highly conserved. It seems reasonable to hypothesize that these amino acids contribute to the gating of TMEM16B channel.

To investigate the role of these amino acids in the gating of the channel, we mutated or deleted those aminoacids and we made a comparison of the electrophysiological properties of TMEM16B WT and mutants in the whole-cell configuration.

We first characterized the WT TMEM16B and we found that it is not activated in the absence of Ca^{2+}, in contrast to what has been found for TMEM16A (Xiao *et al.*, 2011).

By comparing the dose-response relations of TMEM16A and TMEM16B, TMEM16A seems more sensitive to Ca^{2+} than TMEM16B. Indeed our results show a $K_{1/2}$ of 1.6 μM at +100 mV, and 2.7 μM at -40 mV, while Ferrera and colleagues found for TMEM16A 332 nM at +100 mV and 700 nM at -40 mV (Ferrera *et al.*, 2009). This behavior confirms previous works done in both channels in inside-out configuration (Yang *et al.*, 2008; Pifferi *et al.*, 2009*a*), indicating a lower apparent affinity for Ca^{2+} of TMEM16B compared to TMEM16A. The apparent affinity for Ca^{2+} is slightly voltage-dependent with higher values at positive voltages. Moreover the

Hill coefficients are consistently higher than one, indicating that more than one Ca^{2+} ion is necessary to activate the channels.

We found that deletion of the five glutamates, ΔE_5, did not greatly affect the apparent affinity for Ca^{2+}, but it significantly shifted the activation curve to higher potentials. Indeed, $V_{1/2}$ at 1.5 μM Ca^{2+} changed from 124 mV in WT to 248 mV, while the equivalent gating charge was not modified. Moreover, the activation kinetic was prolonged in ΔE_5, while the deactivation constant was not significantly affected. Thus, the five consecutive glutamates are involved in the voltage-dependence of the TMEM16B channel, while they do not seem to play a significant role in the apparent affinity for Ca^{2+}. These results confirm recent data obtained in TMEM16A showing that the substitution of the four correspondent glutamates into alanines ($_{444}$EEEE/AAAA$_{447}$) did not greatly affect the apparent affinity for Ca^{2+}, while modified the voltage-dependence producing a shift of the activation curve to the right (Xiao et al., 2011).

In the TMEM16B mutant E367Q, both activation and deactivation kinetics were shortened, the dose-response relation for Ca^{2+} was not strongly affected, whereas the activation curve was shifted to the right.

Finally, the deletion ΔEYE produced an increase in the time constants for activation and deactivation, while it did not cause any large change in apparent affinity for Ca^{2+} or in voltage sensitivity.

Overall, our results indicate that glutamates E367 and $_{386}$EEEEE$_{390}$ in the first putative intracellular loop plays a relevant role in the modulation of the voltage-dependence of TMEM16B.

CONCLUSIONS

TMEM16B sequence reveals the absence of canonical voltage - sensing and Ca^{2+}- binding domains, nevertheless our results indicate that the five consecutive glutamates in the first putative intracellular loop have an important role in voltage-dependence of TMEM16B, but are not involved in Ca^{2+} sensitivity. Also glutamate in position 367 plays a similar role, further indicating that the first intracellular loop is involved in voltage-dependent activation of TMEM16B.

At present, the location of the Ca^{2+} binding site in TMEM16A and TMEM16B remains unknown.

It is possible that several residues in different regions contribute to bind Ca^{2+} ions, but it cannot be excluded that the Ca^{2+} binding site is located in an accessory subunit expressed both in HEK 293T cells and in *Axolotl* oocytes.

Future work will have to shed light on the intricate mechanisms that couple Ca^{2+}-gating and voltage-dependence, including intriguing interactions between gating and permeation.

6 Bibliography

Allison AC (1954). The secondary olfactory areas in the human brain. *J Anat* **88,** 481–488.

Almaça J, Tian Y, Aldehni F, Ousingsawat J, Kongsuphol P, Rock JR, Harfe BD, Schreiber R & Kunzelmann K (2009). TMEM16 proteins produce volume-regulated chloride currents that are reduced in mice lacking TMEM16A. *J Biol Chem* **284,** 28571–28578.

Altschul SF, Gish W, Miller W, Myers EW & Lipman DJ (1990). Basic local alignment search tool. *J Mol Biol* **215,** 403–410.

Arreola J, Melvin JE & Begenisich T (1996). Activation of calcium-dependent chloride channels in rat parotid acinar cells. *J Gen Physiol* **108,** 35–47.

Bakalyar HA & Reed RR (1990). Identification of a specialized adenylyl cyclase that may mediate odorant detection. *Science* **250,** 1403–1406.

Barker JL & Ransom BR (1978). Amino acid pharmacology of mammalian central neurones grown in tissue culture. *J Physiol (Lond)* **280,** 331–354.

Barrett KE & Keely SJ (2000). Chloride secretion by the intestinal epithelium: molecular basis and regulatory aspects. *Annu Rev Physiol* **62,** 535–572.

Belluscio L, Gold GH, Nemes A & Axel R (1998). Mice deficient in G(olf) are anosmic. *Neuron* **20,** 69–81.

Bera TK, Das S, Maeda H, Beers R, Wolfgang CD, Kumar V, Hahn Y, Lee B & Pastan I (2004). NGEP, a gene encoding a membrane protein detected only in prostate cancer and normal prostate. *Proc Natl Acad Sci USA* **101,** 3059–3064.

Berschneider HM, Knowles MR, Azizkhan RG, Boucher RC, Tobey NA, Orlando RC & Powell DW (1988). Altered intestinal chloride transport in cystic fibrosis. *FASEB J* **2,** 2625–2629.

Billig GM, Pál B, Fidzinski P & Jentsch TJ (2011). Ca2+-activated Cl− currents are dispensable for olfaction. *Nat Neurosci* **14,** 763–769.

Bixby JL & Spitzer NC (1984). Early differentiation of vertebrate spinal neurons in the absence of voltage-dependent Ca2+ and Na+ influx. *Dev Biol* **106,** 89–96.

Boccaccio A & Menini A (2007). Temporal development of cyclic nucleotide-gated and Ca2+ -activated Cl- currents in isolated mouse olfactory sensory neurons. *J Neurophysiol* **98,** 153–160.

Breer H, Fleischer J & Strotmann J (2006). The sense of smell: multiple olfactory subsystems. *Cell Mol Life Sci* **63,** 1465–1475.

Buck L & Axel R (1991). A novel multigene family may encode odorant receptors: a molecular basis for odor recognition. *Cell* **65,** 175–187.

Buck LB (2000). The molecular architecture of odor and pheromone sensing in mammals. *Cell* **100,** 611–618.

Buck LB (2004). Olfactory receptors and odor coding in mammals. *Nutr Rev* **62,** S184–S188; discussion S224–S241.

Bönigk W, Bradley J, Müller F, Sesti F, Boekhoff I, Ronnett GV, Kaupp UB & Frings S (1999). The native rat olfactory cyclic nucleotide-gated channel is composed of three distinct subunits. *J Neurosci* **19,** 5332–5347.

Crain SM (1956). Resting and action potentials of cultured chick embryo spinal ganglion cells. *J Comp Neurol* **104,** 285–329.

Caggiano M, Kauer JS & Hunter DD (1994). Globose basal cells are neuronal progenitors in the olfactory epithelium: a lineage analysis using a replication-incompetent retrovirus. *Neuron* **13,** 339–352.

Caputo A, Caci E, Ferrera L, Pedemonte N, Barsanti C, Sondo E, Pfeffer U, Ravazzolo R, Zegarra-Moran O & Galietta LJV (2008). TMEM16A, a membrane protein associated with calcium-dependent chloride channel activity. *Science* **322,** 590–594.

Carles A, Millon R, Cromer A, Ganguli G, Lemaire F, Young J, Wasylyk C, Muller D, Schultz I, Rabouel Y, Dembélé D, Zhao C, Marchal P, Ducray C, Bracco L, Abecassis J, Poch O & Wasylyk B (2006). Head and neck squamous cell carcinoma transcriptome analysis by comprehensive validated differential display. *Oncogene* **25,** 1821–1831.

Carmichael ST, Clugnet MC & Price JL (1994). Central olfactory connections in the macaque monkey. *J Comp Neurol* **346,** 403–434.

De Castro F, Geijo-Barrientos E & Gallego R (1997). Calcium-activated chloride current in normal mouse sympathetic ganglion cells. *J Physiol (Lond)* **498 (Pt 2),** 397–408.

Chess A, Simon I, Cedar H & Axel R (1994). Allelic inactivation regulates olfactory receptor gene expression. *Cell* **78,** 823–834.

Chipperfield AR & Harper AA (2000). Chloride in smooth muscle. *Prog Biophys Mol Biol* **74,** 175–221.

Chung M-K, Güler AD & Caterina MJ (2008). TRPV1 shows dynamic ionic selectivity during agonist stimulation. *Nat Neurosci* **11,** 555–564.

Cunningham SA, Awayda MS, Bubien JK, Ismailov II, Arrate MP, Berdiev BK, Benos DJ & Fuller CM (1995). Cloning of an epithelial chloride channel from bovine trachea. *J Biol Chem* **270,** 31016–31026.

Currie KP, Wootton JF & Scott RH (1995). Activation of Ca(2+)-dependent Cl- currents in cultured rat sensory neurones by flash photolysis of DM-nitrophen. *J Physiol (Lond)* **482 (Pt 2),** 291–307.

Cuthbert AW (2011). New horizons in the treatment of cystic fibrosis. *Br J Pharmacol* **163,** 173–183.

Von Dannecker LEC, Mercadante AF & Malnic B (2005). Ric-8B, an olfactory putative GTP exchange factor, amplifies signal transduction through the olfactory-specific G-protein Galphaolf. *J Neurosci* **25,** 3793–3800.

Von Dannecker LEC, Mercadante AF & Malnic B (2006). Ric-8B promotes functional expression of odorant receptors. *Proc Natl Acad Sci USA* **103,** 9310–9314.

Davis AJ, Forrest AS, Jepps TA, Valencik ML, Wiwchar M, Singer CA, Sones WR, Greenwood IA & Leblanc N (2010). Expression profile and protein translation of TMEM16A in murine smooth muscle. *Am J Physiol, Cell Physiol* **299,** C948–C959.

Deschenes M, Feltz P & Lamour Y (1976). A model for an estimate in vivo of the ionic basis of presynaptic inhibition: an intracellular analysis of the GABA-induced depolarization in rat dorsal root ganglia. *Brain Res* **118,** 486–493.

Desper R & Gascuel O (2004). Theoretical Foundation of the Balanced Minimum Evolution Method of Phylogenetic Inference and Its Relationship to Weighted Least-Squares Tree Fitting. *Molecular Biology and Evolution* **21,** 587–598.

Dhallan RS, Yau KW, Schrader KA & Reed RR (1990). Primary structure and functional expression of a cyclic nucleotide-activated channel from olfactory neurons. *Nature* **347,** 184–187.

Dho S, Stewart K & Foskett JK (1992). Purinergic receptor activation of Cl- secretion in T84 cells. *Am J Physiol* **262,** C67–C74.

Duchen MR, Valdeolmillos M, O'Neill SC & Eisner DA (1990). Effects of metabolic blockade on the regulation of intracellular calcium in dissociated mouse sensory neurones. *J Physiol (Lond)* **424,** 411–426.

Duran C & Hartzell HC (2011). Physiological roles and diseases of Tmem16/Anoctamin proteins: are they all chloride channels? *Acta Pharmacol Sin* **32,** 685–692.

Espinosa I, Lee C-H, Kim MK, Rouse B-T, Subramanian S, Montgomery K, Varma S, Corless CL, Heinrich MC, Smith KS, Wang Z, Rubin B,

Nielsen TO, Seitz RS, Ross DT, West RB, Cleary ML & van de Rijn M (2008). A novel monoclonal antibody against DOG1 is a sensitive and specific marker for gastrointestinal stromal tumors. *Am J Surg Pathol* **32,** 210–218.

Evans MG & Marty A (1986). Calcium-dependent chloride currents in isolated cells from rat lacrimal glands. *J Physiol (Lond)* **378,** 437–460.

Fallah G, Römer T, Detro-Dassen S, Braam U, Markwardt F & Schmalzing G (2011). TMEM16A(a)/anoctamin-1 shares a homodimeric architecture with CLC chloride channels. *Mol Cell Proteomics* **10,** M110.004697.

Ferrera L, Caputo A & Galietta LJV (2010). TMEM16A protein: a new identity for Ca(2+)-dependent Cl^- channels. *Physiology (Bethesda)* **25,** 357–363.

Ferrera L, Caputo A, Ubby I, Bussani E, Zegarra-Moran O, Ravazzolo R, Pagani F & Galietta LJV (2009). Regulation of TMEM16A chloride channel properties by alternative splicing. *J Biol Chem* **284,** 33360–33368.

Ferrera L, Scudieri P, Sondo E, Caputo A, Caci E, Zegarra-Moran O, Ravazzolo R & Galietta LJV (2011). A minimal isoform of the TMEM16A protein associated with chloride channel activity. *Biochim Biophys Acta* **1808,** 2214–2223.

Fesenko EE, Kolesnikov SS & Lyubarsky AL (1985). Induction by cyclic GMP of cationic conductance in plasma membrane of retinal rod outer segment. *Nature* **313,** 310–313.

Firestein S & Shepherd GM (1991). A kinetic model of the odor response in single olfactory receptor neurons. *J Steroid Biochem Mol Biol* **39,** 615–620.

Firestein S & Werblin FS (1987). Gated currents in isolated olfactory receptor neurons of the larval tiger salamander. *Proc Natl Acad Sci USA* **84,** 6292–6296.

Firestein S, Picco C & Menini A (1993). The relation between stimulus and response in olfactory receptor cells of the tiger salamander. *J Physiol (Lond)* **468,** 1–10.

Firestein S, Shepherd GM & Werblin FS (1990). Time course of the membrane current underlying sensory transduction in salamander olfactory receptor neurones. *J Physiol (Lond)* **430,** 135–158.

Flores CA, Cid LP, Sepúlveda FV & Niemeyer MI (2009). TMEM16 proteins: the long awaited calcium-activated chloride channels? *Braz J Med Biol Res* **42,** 993–1001.

Frings S, Lynch JW & Lindemann B (1992). Properties of cyclic nucleotide-gated channels mediating olfactory transduction. Activation, selectivity, and blockage. *J Gen Physiol* **100,** 45–67.

Frings S, Reuter D & Kleene SJ (2000). Neuronal Ca2+ -activated Cl- channels--homing in on an elusive channel species. *Prog Neurobiol* **60,** 247–289.

Frings S, Seifert R, Godde M & Kaupp UB (1995). Profoundly different calcium permeation and blockage determine the specific function of distinct cyclic nucleotide-gated channels. *Neuron* **15,** 169–179.

Galietta LJV (2009). The TMEM16 protein family: a new class of chloride channels? *Biophys J* **97,** 3047–3053.

Galindo BE & Vacquier VD (2005). Phylogeny of the TMEM16 protein family: some members are overexpressed in cancer. *Int J Mol Med* **16,** 919–924.

Giovannucci DR, Bruce JIE, Straub SV, Arreola J, Sneyd J, Shuttleworth TJ & Yule DI (2002). Cytosolic Ca(2+) and Ca(2+)-activated Cl(-) current dynamics: insights from two functionally distinct mouse exocrine cells. *J Physiol (Lond)* **540,** 469–484.

Godfrey PA, Malnic B & Buck LB (2004). The mouse olfactory receptor gene family. *Proc Natl Acad Sci USA* **101,** 2156–2161.

Graziadei PP, Levine RR & Graziadei GA (1978). Regeneration of olfactory axons and synapse formation in the forebrain after bulbectomy in neonatal mice. *Proc Natl Acad Sci USA* **75,** 5230–5234.

Greenwood IA & Large WA (1999). Modulation of the decay of Ca2+-activated Cl- currents in rabbit portal vein smooth muscle cells by external anions. *J Physiol (Lond)* **516 (Pt 2),** 365–376.

Greenwood IA, Ledoux J & Leblanc N (2001). Differential regulation of Ca(2+)-activated Cl(-) currents in rabbit arterial and portal vein smooth muscle cells by Ca(2+)-calmodulin-dependent kinase. *J Physiol (Lond)* **534,** 395–408.

Grishin NV (1995). Estimation of the number of amino acid substitutions per site when the substitution rate varies among sites. *J Mol Evol* **41,** 675–679.

Grosmaitre X, Vassalli A, Mombaerts P, Shepherd GM & Ma M (2006). Odorant responses of olfactory sensory neurons expressing the odorant receptor MOR23: a patch clamp analysis in gene-targeted mice. *Proc Natl Acad Sci USA* **103,** 1970–1975.

Grubb BR & Boucher RC (1999). Pathophysiology of gene-targeted mouse models for cystic fibrosis. *Physiol Rev* **79,** S193–S214.

Guggino WB (2001). Cystic fibrosis salt/fluid controversy: in the thick of it. *Nat Med* **7,** 888–889.

Hartzell C, Putzier I & Arreola J (2005). Calcium-activated chloride channels. *Annu Rev Physiol* **67,** 719–758.

Hartzell HC, Qu Z, Yu K, Xiao Q & Chien L-T (2008). Molecular physiology of bestrophins: multifunctional membrane proteins linked to best disease and other retinopathies. *Physiol Rev* **88,** 639–672.

Hartzell HC, Yu K, Xiao Q, Chien L-T & Qu Z (2009). Anoctamin/TMEM16 family members are Ca2+-activated Cl- channels. *J Physiol (Lond)* **587,** 2127–2139.

Haynes L & Yau KW (1985). Cyclic GMP-sensitive conductance in outer segment membrane of catfish cones. *Nature* **317,** 61–64.

Hengl T, Kaneko H, Dauner K, Vocke K, Frings S & Möhrlen F (2010). Molecular components of signal amplification in olfactory sensory cilia. *Proc Natl Acad Sci USA* **107,** 6052–6057.

Hiraoka M & Kawano S (1989). Calcium-sensitive and insensitive transient outward current in rabbit ventricular myocytes. *J Physiol (Lond)* **410,** 187–212.

Huang F, Rock JR, Harfe BD, Cheng T, Huang X, Jan YN & Jan LY (2009). Studies on expression and function of the TMEM16A calcium-activated chloride channel. *Proc Natl Acad Sci USA* **106,** 21413–21418.

Huang F, Wong X & Jan LY (2012). International Union of Basic and Clinical Pharmacology. LXXXV: Calcium-Activated Chloride Channels. *Pharmacol Rev* **64,** 1–15.

Huang P, Liu J, Di A, Robinson NC, Musch MW, Kaetzel MA & Nelson DJ (2001). Regulation of human CLC-3 channels by multifunctional Ca2+/calmodulin-dependent protein kinase. *J Biol Chem* **276,** 20093–20100.

Huang X, Godfrey TE, Gooding WE, McCarty KS Jr & Gollin SM (2006). Comprehensive genome and transcriptome analysis of the 11q13 amplicon in human oral cancer and synteny to the 7F5 amplicon in murine oral carcinoma. *Genes Chromosomes Cancer* **45,** 1058–1069.

Jentsch TJ (2002). Chloride channels are different. *Nature* **415,** 276–277.

Johnson LG, Boyles SE, Wilson J & Boucher RC (1995). Normalization of raised sodium absorption and raised calcium-mediated chloride secretion by adenovirus-mediated expression of cystic fibrosis transmembrane conductance regulator in primary human cystic fibrosis airway epithelial cells. *J Clin Invest* **95,** 1377–1382.

Kachintorn U, Vajanaphanich M, Traynor-Kaplan AE, Dharmsathaphorn K & Barrett KE (1993). Activation by calcium alone of chloride secretion in T84 epithelial cells. *Br J Pharmacol* **109,** 510–517.

Kalay E, Caylan R, Kiroglu AF, Yasar T, Collin RWJ, Heister JGAM, Oostrik J, Cremers CWRJ, Brunner HG, Karaguzel A & Kremer H (2007). A novel locus for autosomal recessive nonsyndromic hearing impairment, DFNB63, maps to chromosome 11q13.2-q13.4. *J Mol Med* **85,** 397–404.

Kaneko H, Nakamura T & Lindemann B (2001). Noninvasive measurement of chloride concentration in rat olfactory receptor cells with use of a fluorescent dye. *Am J Physiol, Cell Physiol* **280,** C1387–C1393.

Kaneko H, Putzier I, Frings S, Kaupp UB & Gensch T (2004). Chloride accumulation in mammalian olfactory sensory neurons. *J Neurosci* **24,** 7931–7938.

Kashyap MK, Marimuthu A, Kishore CJH, Peri S, Keerthikumar S, Prasad TSK, Mahmood R, Rao S, Ranganathan P, Sanjeeviah RC, Vijayakumar M, Kumar KVV, Montgomery EA, Kumar RV & Pandey A (2009). Genomewide mRNA profiling of esophageal squamous cell carcinoma for identification of cancer biomarkers. *Cancer Biol Ther* **8,** 36–46.

Katoh M & Katoh M (2003). FLJ10261 gene, located within the CCND1-EMS1 locus on human chromosome 11q13, encodes the eight-transmembrane protein homologous to C12orf3, C11orf25 and FLJ34272 gene products. *Int J Oncol* **22,** 1375–1381.

Katoh M & Katoh M (2005). Identification and characterization of TMEM16H gene in silico. *Int J Mol Med* **15,** 353–358.

Kaupp UB (2010). Olfactory signalling in vertebrates and insects: differences and commonalities. *Nat Rev Neurosci* **11,** 188–200.

Kaupp UB & Seifert R (2002). Cyclic nucleotide-gated ion channels. *Physiol Rev* **82,** 769–824.

Kaupp UB, Niidome T, Tanabe T, Terada S, Bönigk W, Stühmer W, Cook NJ, Kangawa K, Matsuo H & Hirose T (1989). Primary structure and functional expression from complementary DNA of the rod photoreceptor cyclic GMP-gated channel. *Nature* **342,** 762–766.

Khakh BS & Lester HA (1999). Dynamic selectivity filters in ion channels. *Neuron* **23,** 653–658.

Kidd JF & Thorn P (2000). Intracellular Ca2+ and Cl- channel activation in secretory cells. *Annu Rev Physiol* **62,** 493–513.

Kleene SJ (1993). Origin of the chloride current in olfactory transduction. *Neuron* **11,** 123–132.

Kleene SJ (1994). Inhibition of olfactory cyclic nucleotide-activated current by calmodulin antagonists. *Br J Pharmacol* **111,** 469–472.

Kleene SJ (1995). Block by external calcium and magnesium of the cyclic-nucleotide-activated current in olfactory cilia. *Neuroscience* **66,** 1001–1008.

Kleene SJ (1997). High-gain, low-noise amplification in olfactory transduction. *Biophys J* **73,** 1110–1117.

Kleene SJ (1999). Both external and internal calcium reduce the sensitivity of the olfactory cyclic-nucleotide-gated channel to CAMP. *J Neurophysiol* **81,** 2675–2682.

Kleene SJ (2008). The electrochemical basis of odor transduction in vertebrate olfactory cilia. *Chem Senses* **33,** 839–859.

Kleene SJ & Gesteland RC (1981). Dissociation of frog olfactory epithelium with N-ethylmaleimide. *Brain Res* **229,** 536–540.

Kleene SJ & Gesteland RC (1991). Calcium-activated chloride conductance in frog olfactory cilia. *J Neurosci* **11,** 3624–3629.

Korn SJ, Bolden A & Horn R (1991). Control of action potentials and Ca2+ influx by the Ca(2+)-dependent chloride current in mouse pituitary cells. *J Physiol (Lond)* **439,** 423–437.

Kunzelmann K, Kongsuphol P, Aldehni F, Tian Y, Ousingsawat J, Warth R & Schreiber R (2009). Bestrophin and TMEM16-Ca(2+) activated Cl(-) channels with different functions. *Cell Calcium* **46,** 233–241.

Kunzelmann K, Mall M, Briel M, Hipper A, Nitschke R, Ricken S & Greger R (1997). The cystic fibrosis transmembrane conductance regulator attenuates the endogenous Ca2+ activated Cl- conductance of Xenopus oocytes. *Pflugers Arch* **435,** 178–181.

Kurahashi T (1989). Activation by odorants of cation-selective conductance in the olfactory receptor cell isolated from the newt. *J Physiol (Lond)* **419,** 177–192.

Kurahashi T (1990). The response induced by intracellular cyclic AMP in isolated olfactory receptor cells of the newt. *J Physiol (Lond)* **430,** 355–371.

Kurahashi T & Kaneko A (1991). High density cAMP-gated channels at the ciliary membrane in the olfactory receptor cell. *Neuroreport* **2,** 5–8.

Kurahashi T & Kaneko A (1993). Gating properties of the cAMP-gated channel in toad olfactory receptor cells. *J Physiol (Lond)* **466,** 287–302.

Kurahashi T & Yau KW (1993). Co-existence of cationic and chloride components in odorant-induced current of vertebrate olfactory receptor cells. *Nature* **363,** 71–74.

Kurahashi T & Yau KW (1994). Olfactory transduction. Tale of an unusual chloride current. *Curr Biol* **4,** 256–258.

Kuruma A & Hartzell HC (1999). Dynamics of calcium regulation of chloride currents in Xenopus oocytes. *Am J Physiol* **276,** C161–C175.

Kuruma A & Hartzell HC (2000). Bimodal control of a Ca(2+)-activated Cl(-) channel by different Ca(2+) signals. *J Gen Physiol* **115,** 59–80.

Large WA & Wang Q (1996). Characteristics and physiological role of the Ca(2+)-activated Cl- conductance in smooth muscle. *Am J Physiol* **271,** C435–C454.

Larsson HP, Kleene SJ & Lecar H (1997). Noise analysis of ion channels in non-space-clamped cables: estimates of channel parameters in olfactory cilia. *Biophys J* **72,** 1193–1203.

Leinders-Zufall T, Rand MN, Shepherd GM, Greer CA & Zufall F (1997). Calcium entry through cyclic nucleotide-gated channels in individual cilia of olfactory receptor cells: spatiotemporal dynamics. *J Neurosci* **17,** 4136–4148.

Liman ER & Buck LB (1994). A second subunit of the olfactory cyclic nucleotide-gated channel confers high sensitivity to cAMP. *Neuron* **13,** 611–621.

Loewen ME & Forsyth GW (2005). Structure and function of CLCA proteins. *Physiol Rev* **85,** 1061–1092.

Lowe G (2003). Electrical signaling in the olfactory bulb. *Curr Opin Neurobiol* **13,** 476–481.

Lowe G & Gold GH (1991). The spatial distributions of odorant sensitivity and odorant-induced currents in salamander olfactory receptor cells. *J Physiol (Lond)* **442,** 147–168.

Lowe G & Gold GH (1993*a*). Nonlinear amplification by calcium-dependent chloride channels in olfactory receptor cells. *Nature* **366,** 283–286.

Lowe G & Gold GH (1993*b*). Contribution of the ciliary cyclic nucleotide-gated conductance to olfactory transduction in the salamander. *J Physiol (Lond)* **462,** 175–196.

Lowe G, Nakamura T & Gold GH (1989). Adenylate cyclase mediates olfactory transduction for a wide variety of odorants. *Proc Natl Acad Sci USA* **86,** 5641–5645.

Ludwig J, Margalit T, Eismann E, Lancet D & Kaupp UB (1990). Primary structure of cAMP-gated channel from bovine olfactory epithelium. *FEBS Lett* **270,** 24–29.

Ma M, Chen WR & Shepherd GM (1999). Electrophysiological characterization of rat and mouse olfactory receptor neurons from an intact epithelial preparation. *J Neurosci Methods* **92,** 31–40.

Malnic B, Hirono J, Sato T & Buck LB (1999). Combinatorial receptor codes for odors. *Cell* **96,** 713–723.

Manoury B, Tamuleviciute A & Tammaro P (2010). TMEM16A/anoctamin 1 protein mediates calcium-activated chloride currents in pulmonary arterial smooth muscle cells. *J Physiol (Lond)* **588,** 2305–2314.

Marmorstein AD, Marmorstein LY, Rayborn M, Wang X, Hollyfield JG & Petrukhin K (2000). Bestrophin, the product of the Best vitelliform macular dystrophy gene (VMD2), localizes to the basolateral plasma membrane of the retinal pigment epithelium. *Proc Natl Acad Sci USA* **97,** 12758–12763.

Matchkov VV, Larsen P, Bouzinova EV, Rojek A, Boedtkjer DMB, Golubinskaya V, Pedersen FS, Aalkjaer C & Nilsson H (2008). Bestrophin-3 (vitelliform macular dystrophy 2-like 3 protein) is essential for the cGMP-dependent calcium-activated chloride conductance in vascular smooth muscle cells. *Circ Res* **103,** 864–872.

Mayer ML (1985). A calcium-activated chloride current generates the after-depolarization of rat sensory neurones in culture. *J Physiol (Lond)* **364,** 217–239.

Mayer U, Küller A, Daiber PC, Neudorf I, Warnken U, Schnölzer M, Frings S & Möhrlen F (2009). The proteome of rat olfactory sensory cilia. *Proteomics* **9,** 322–334.

Menco BP, Bruch RC, Dau B & Danho W (1992). Ultrastructural localization of olfactory transduction components: the G protein subunit Golf alpha and type III adenylyl cyclase. *Neuron* **8,** 441–453.

Menco M (1980). Qualitative and quantitative freeze-fracture studies on olfactory and respiratory epithelial surfaces of frog, ox, rat, and dog. IV. Ciliogenesis and ciliary necklaces (including high-voltage observations). *Cell Tissue Res* **212,** 1–16.

Menini A, Lagostena L & Boccaccio A (2004). Olfaction: from odorant molecules to the olfactory cortex. *News Physiol Sci* **19,** 101–104.

Mercer AJ, Rabl K, Riccardi GE, Brecha NC, Stella SL Jr & Thoreson WB (2011). Location of release sites and calcium-activated chloride channels relative to calcium channels at the photoreceptor ribbon synapse. *J Neurophysiol* **105,** 321–335.

Michalakis S, Reisert J, Geiger H, Wetzel C, Zong X, Bradley J, Spehr M, Hüttl S, Gerstner A, Pfeifer A, Hatt H, Yau K-W & Biel M (2006). Loss of CNGB1 protein leads to olfactory dysfunction and subciliary cyclic nucleotide-gated channel trapping. *J Biol Chem* **281,** 35156–35166.

Milenkovic VM, Langmann T, Schreiber R, Kunzelmann K & Weber BHF (2008). Molecular evolution and functional divergence of the bestrophin protein family. *BMC Evol Biol* **8,** 72.

Mombaerts P (1999). Seven-transmembrane proteins as odorant and chemosensory receptors. *Science* **286,** 707–711.

Mombaerts P (2004). Odorant receptor gene choice in olfactory sensory neurons: the one receptor-one neuron hypothesis revisited. *Curr Opin Neurobiol* **14,** 31–36.

Mombaerts P, Wang F, Dulac C, Chao SK, Nemes A, Mendelsohn M, Edmondson J & Axel R (1996). Visualizing an olfactory sensory map. *Cell* **87,** 675–686.

Morrison EE & Costanzo RM (1990). Morphology of the human olfactory epithelium. *J Comp Neurol* **297,** 1–13.

Munger SD, Lane AP, Zhong H, Leinders-Zufall T, Yau KW, Zufall F & Reed RR (2001). Central role of the CNGA4 channel subunit in Ca2+-calmodulin-dependent odor adaptation. *Science* **294,** 2172–2175.

Munger SD, Leinders-Zufall T & Zufall F (2009). Subsystem organization of the mammalian sense of smell. *Annu Rev Physiol* **71,** 115–140.

Nakamura T & Gold GH (1987). A cyclic nucleotide-gated conductance in olfactory receptor cilia. *Nature* **325,** 442–444.

Nakamura T, Kaneko H & Nishida N (1997). Direct measurement of the chloride concentration in newt olfactory receptors with the fluorescent probe. *Neurosci Lett* **237,** 5–8.

Namkung W, Thiagarajah JR, Phuan P-W & Verkman AS (2010). Inhibition of Ca2+-activated Cl- channels by gallotannins as a possible molecular basis for health benefits of red wine and green tea. *FASEB J* **24,** 4178–4186.

Nickell WT, Kleene NK & Kleene SJ (2007). Mechanisms of neuronal chloride accumulation in intact mouse olfactory epithelium. *J Physiol (Lond)* **583,** 1005–1020.

Nickell WT, Kleene NK, Gesteland RC & Kleene SJ (2006). Neuronal chloride accumulation in olfactory epithelium of mice lacking NKCC1. *J Neurophysiol* **95,** 2003–2006.

Nilius B & Droogmans G (2001). Ion channels and their functional role in vascular endothelium. *Physiol Rev* **81,** 1415–1459.

Nilius B, Gerke V, Prenen J, Szücs G, Heinke S, Weber K & Droogmans G (1996). Annexin II modulates volume-activated chloride currents in vascular endothelial cells. *J Biol Chem* **271,** 30631–30636.

Nilius B, Prenen J, Voets T, Van den Bremt K, Eggermont J & Droogmans G (1997). Kinetic and pharmacological properties of the calcium-activated chloride-current in macrovascular endothelial cells. *Cell Calcium* **22,** 53–63.

Otowa T, Yoshida E, Sugaya N, Yasuda S, Nishimura Y, Inoue K, Tochigi M, Umekage T, Miyagawa T, Nishida N, Tokunaga K, Tanii H, Sasaki T, Kaiya H & Okazaki Y (2009). Genome-wide association study of panic disorder in the Japanese population. *J Hum Genet* **54,** 122–126.

Owen DG, Segal M & Barker JL (1984). A Ca-dependent Cl- conductance in cultured mouse spinal neurones. *Nature* **311,** 567–570.

Owen DG, Segal M & Barker JL (1986). Voltage-clamp analysis of a Ca2+- and voltage-dependent chloride conductance in cultured mouse spinal neurons. *J Neurophysiol* **55,** 1115–1135.

Papp Z, Sipido KR, Callewaert G & Carmeliet E (1995). Two components of [Ca2+]i-activated Cl- current during large [Ca2+]i transients in single rabbit heart Purkinje cells. *J Physiol (Lond)* **483 (Pt 2),** 319–330.

Park MK, Lomax RB, Tepikin AV & Petersen OH (2001). Local uncaging of caged Ca(2+) reveals distribution of Ca(2+)-activated Cl(-) channels in pancreatic acinar cells. *Proc Natl Acad Sci USA* **98,** 10948–10953.

Park SH, Chung HK, Kim DJ, Han MR, Park MS, Oh U, Kim HJ & Han BW (2011). Overexpression, crystallization and preliminary X-ray crystallographic analysis of the C-terminal cytosolic domain of mouse anoctamin 1. *Acta Crystallogr Sect F Struct Biol Cryst Commun* **67,** 1250–1252.

Pawłowski K, Lepistö M, Meinander N, Sivars U, Varga M & Wieslander E (2006). Novel conserved hydrolase domain in the CLCA family of alleged calcium-activated chloride channels. *Proteins* **63,** 424–439.

Perez-Cornejo P & Arreola J (2004). Regulation of Ca(2+)-activated chloride channels by cAMP and CFTR in parotid acinar cells. *Biochem Biophys Res Commun* **316,** 612–617.

Petrukhin K, Koisti MJ, Bakall B, Li W, Xie G, Marknell T, Sandgren O, Forsman K, Holmgren G, Andreasson S, Vujic M, Bergen AA, McGarty-Dugan V, Figueroa D, Austin CP, Metzker ML, Caskey CT & Wadelius C (1998). Identification of the gene responsible for Best macular dystrophy. *Nat Genet* **19,** 241–247.

Pifferi S, Boccaccio A & Menini A (2006*a*). Cyclic nucleotide-gated ion channels in sensory transduction. *FEBS Lett* **580,** 2853–2859.

Pifferi S, Cenedese V & Menini A (2011). Anoctamin2/TMEM16B: a calcium-activated chloride channel in olfactorytransduction. *Exp. Physiol*. 97:193-199.

Pifferi S, Dibattista M & Menini A (2009*a*). TMEM16B induces chloride currents activated by calcium in mammalian cells. *Pflugers Arch* **458,** 1023–1038.

Pifferi S, Dibattista M, Sagheddu C, Boccaccio A, Al Qteishat A, Ghirardi F, Tirindelli R & Menini A (2009*b*). Calcium-activated chloride currents in olfactory sensory neurons from mice lacking bestrophin-2. *J Physiol (Lond)* **587,** 4265–4279.

Pifferi S, Pascarella G, Boccaccio A, Mazzatenta A, Gustincich S, Menini A & Zucchelli S (2006*b*). Bestrophin-2 is a candidate calcium-activated chloride channel involved in olfactory transduction. *Proc Natl Acad Sci USA* **103,** 12929–12934.

Piper AS & Large WA (2003). Multiple conductance states of single Ca2+-activated Cl- channels in rabbit pulmonary artery smooth muscle cells. *J Physiol (Lond)* **547,** 181–196.

Qu Z & Hartzell C (2004). Determinants of anion permeation in the second transmembrane domain of the mouse bestrophin-2 chloride channel. *J Gen Physiol* **124,** 371–382.

Qu Z & Hartzell HC (2000). Anion permeation in Ca(2+)-activated Cl(-) channels. *J Gen Physiol* **116,** 825–844.

Qu Z & Hartzell HC (2001). Functional geometry of the permeation pathway of Ca2+-activated Cl-channels inferred from analysis of voltage-dependent block. *J Biol Chem* **276,** 18423–18429.

Qu Z, Fischmeister R & Hartzell C (2004). Mouse bestrophin-2 is a bona fide Cl(-) channel: identification of a residue important in anion binding and conduction. *J Gen Physiol* **123,** 327–340.

Rasche S, Toetter B, Adler J, Tschapek A, Doerner JF, Kurtenbach S, Hatt H, Meyer H, Warscheid B & Neuhaus EM (2010). Tmem16b is specifically expressed in the cilia of olfactory sensory neurons. *Chem Senses* **35,** 239–245.

Ratcliff R, Evans MJ, Cuthbert AW, MacVinish LJ, Foster D, Anderson JR & Colledge WH (1993). Production of a severe cystic fibrosis mutation in mice by gene targeting. *Nat Genet* **4,** 35–41.

Reisert J & Bradley J (2005). Activation of olfactory cyclic-nucleotide gated channels revisited. *J Physiol (Lond)* **569,** 4–5.

Reisert J & Matthews HR (2001). Response properties of isolated mouse olfactory receptor cells. *J Physiol (Lond)* **530,** 113–122.

Reisert J, Bauer PJ, Yau K-W & Frings S (2003). The Ca-activated Cl channel and its control in rat olfactory receptor neurons. *J Gen Physiol* **122,** 349–363.

Reisert J, Lai J, Yau K-W & Bradley J (2005). Mechanism of the excitatory Cl- response in mouse olfactory receptor neurons. *Neuron* **45,** 553–561.

Ressler KJ, Sullivan SL & Buck LB (1993). A zonal organization of odorant receptor gene expression in the olfactory epithelium. *Cell* **73,** 597–609.

Restrepo D, Miyamoto T, Bryant BP & Teeter JH (1990). Odor stimuli trigger influx of calcium into olfactory neurons of the channel catfish. *Science* **249,** 1166–1168.

Rock JR & Harfe BD (2008). Expression of TMEM16 paralogs during murine embryogenesis. *Dev Dyn* **237,** 2566–2574.

Romanenko VG, Catalán MA, Brown DA, Putzier I, Hartzell HC, Marmorstein AD, Gonzalez-Begne M, Rock JR, Harfe BD & Melvin JE (2010). Tmem16A encodes the Ca2+-activated Cl- channel in mouse submandibular salivary gland acinar cells. *J Biol Chem* **285,** 12990–13001.

Sagheddu C, Boccaccio A, Dibattista M, Montani G, Tirindelli R & Menini A (2010). Calcium concentration jumps reveal dynamic ion selectivity of calcium-activated chloride currents in mouse olfactory sensory neurons and TMEM16b-transfected HEK 293T cells. *J Physiol (Lond)* **588,** 4189–4204.

Saito H, Kubota M, Roberts RW, Chi Q & Matsunami H (2004). RTP family members induce functional expression of mammalian odorant receptors. *Cell* **119,** 679–691.

Schild D & Restrepo D (1998). Transduction mechanisms in vertebrate olfactory receptor cells. *Physiol Rev* **78,** 429–466.

Schneppenheim R, Castaman G, Federici AB, Kreuz W, Marschalek R, Oldenburg J, Oyen F & Budde U (2007). A common 253-kb deletion involving VWF and TMEM16B in German and Italian patients with severe von Willebrand disease type 3. *J Thromb Haemost* **5,** 722–728.

Schoppa NE & Urban NN (2003). Dendritic processing within olfactory bulb circuits. *Trends Neurosci* **26,** 501–506.

Schreiber M & Salkoff L (1997). A novel calcium-sensing domain in the BK channel. *Biophys J* **73,** 1355–1363.

Schreiber R, Uliyakina I, Kongsuphol P, Warth R, Mirza M, Martins JR & Kunzelmann K (2010). Expression and function of epithelial anoctamins. *J Biol Chem* **285,** 7838–7845.

Schroeder BC, Cheng T, Jan YN & Jan LY (2008). Expression cloning of TMEM16A as a calcium-activated chloride channel subunit. *Cell* **134,** 1019–1029.

Scott RH, McGuirk SM & Dolphin AC (1988). Modulation of divalent cation-activated chloride ion currents. *Br J Pharmacol* **94,** 653–662.

Scudieri P, Sondo E, Ferrera L & Galietta LJ (2011). The anoctamin family: TMEM16A and TMEM16B as calcium-activated chloride channels. *Exp. Physiol.* 97:177-183.

Seifert R, Eismann E, Ludwig J, Baumann A & Kaupp UB (1999). Molecular determinants of a Ca2+-binding site in the pore of cyclic nucleotide-gated channels: S5/S6 segments control affinity of intrapore glutamates. *EMBO J* **18,** 119–130.

Serizawa S, Miyamichi K, Nakatani H, Suzuki M, Saito M, Yoshihara Y & Sakano H (2003). Negative feedback regulation ensures the one receptor-one olfactory neuron rule in mouse. *Science* **302,** 2088–2094.

Sheridan JT, Worthington EN, Yu K, Gabriel SE, Hartzell HC & Tarran R (2011). Characterization of the oligomeric structure of the Ca(2+)-activated Cl- channel Ano1/TMEM16A. *J Biol Chem* **286,** 1381–1388.

Shykind BM (2005). Regulation of odorant receptors: one allele at a time. *Hum Mol Genet* **14 Spec No 1,** R33–R39.

Sipido KR, Callewaert G & Carmeliet E (1993). [Ca2+]i transients and [Ca2+]i-dependent chloride current in single Purkinje cells from rabbit heart. *J Physiol (Lond)* **468,** 641–667.

Smith DW, Thach S, Marshall EL, Mendoza M-G & Kleene SJ (2008). Mice lacking NKCC1 have normal olfactory sensitivity. *Physiol Behav* **93,** 44–49.

Snouwaert JN, Brigman KK, Latour AM, Malouf NN, Boucher RC, Smithies O & Koller BH (1992). An animal model for cystic fibrosis made by gene targeting. *Science* **257,** 1083–1088.

Stapleton SR, Scott RH & Bell BA (1994). Effects of metabolic blockers on Ca(2+)-dependent currents in cultured sensory neurones from neonatal rats. *Br J Pharmacol* **111,** 57–64.

Stephan AB, Shum EY, Hirsh S, Cygnar KD, Reisert J & Zhao H (2009). ANO2 is the cilial calcium-activated chloride channel that may mediate olfactory amplification. *Proc Natl Acad Sci USA* **106,** 11776–11781.

Stöhr H, Heisig JB, Benz PM, Schöberl S, Milenkovic VM, Strauss O, Aartsen WM, Wijnholds J, Weber BHF & Schulz HL (2009). TMEM16B, a novel protein with calcium-dependent chloride channel activity, associates with a presynaptic protein complex in photoreceptor terminals. *J Neurosci* **29,** 6809–6818.

Sullivan SL, Ressler KJ & Buck LB (1994). Odorant receptor diversity and patterned gene expression in the mammalian olfactory epithelium. *Prog Clin Biol Res* **390,** 75–84.

Sun H, Tsunenari T, Yau K-W & Nathans J (2002). The vitelliform macular dystrophy protein defines a new family of chloride channels. *Proc Natl Acad Sci USA* **99,** 4008–4013.

Suzuki J, Umeda M, Sims PJ & Nagata S (2010). Calcium-dependent phospholipid scrambling by TMEM16F. *Nature* **468,** 834–838.

Takeuchi H, Imanaka Y, Hirono J & Kurahashi T (2003). Cross-adaptation between olfactory responses induced by two subgroups of odorant molecules. *J Gen Physiol* **122,** 255–264.

Tian Y, Kongsuphol P, Hug M, Ousingsawat J, Witzgall R, Schreiber R & Kunzelmann K (2011). Calmodulin-dependent activation of the epithelial calcium-dependent chloride channel TMEM16A. *FASEB J* **25,** 1058–1068.

Tsunenari T, Nathans J & Yau K-W (2006). Ca2+-activated Cl- current from human bestrophin-4 in excised membrane patches. *J Gen Physiol* **127,** 749–754.

Tsunenari T, Sun H, Williams J, Cahill H, Smallwood P, Yau K-W & Nathans J (2003). Structure-function analysis of the bestrophin family of anion channels. *J Biol Chem* **278,** 41114–41125.

Vassar MJ & Holcroft JW (1994). The case against using the APACHE system to predict intensive care unit outcome in trauma patients. *Crit Care Clin* **10,** 117–126; discussion 127–134.

Verkman AS & Galietta LJV (2009). Chloride channels as drug targets. *Nat Rev Drug Discov* **8,** 153–171.

Wei L, Vankeerberghen A, Cuppens H, Cassiman JJ, Droogmans G & Nilius B (2001). The C-terminal part of the R-domain, but not the PDZ binding motif, of CFTR is involved in interaction with Ca(2+)-activated Cl- channels. *Pflugers Arch* **442,** 280–285.

West RB, Corless CL, Chen X, Rubin BP, Subramanian S, Montgomery K, Zhu S, Ball CA, Nielsen TO, Patel R, Goldblum JR, Brown PO,

Heinrich MC & van de Rijn M (2004). The novel marker, DOG1, is expressed ubiquitously in gastrointestinal stromal tumors irrespective of KIT or PDGFRA mutation status. *Am J Pathol* **165,** 107–113.

White MM & Aylwin M (1990). Niflumic and flufenamic acids are potent reversible blockers of Ca2(+)-activated Cl- channels in Xenopus oocytes. *Mol Pharmacol* **37,** 720–724.

Wong ST, Trinh K, Hacker B, Chan GC, Lowe G, Gaggar A, Xia Z, Gold GH & Storm DR (2000). Disruption of the type III adenylyl cyclase gene leads to peripheral and behavioral anosmia in transgenic mice. *Neuron* **27,** 487–497.

Xiao Q, Yu K, Perez-Cornejo P, Cui Y, Arreola J & Hartzell HC (2011). Voltage- and calcium-dependent gating of TMEM16A/Ano1 chloride channels are physically coupled by the first intracellular loop. *Proc Natl Acad Sci USA* **108,** 8891–8896.

Yang YD, Cho H, Koo JY, Tak MH, Cho Y, Shim W-S, Park SP, Lee J, Lee B, Kim B-M, Raouf R, Shin YK & Oh U (2008). TMEM16A confers receptor-activated calcium-dependent chloride conductance. *Nature* **455,** 1210–1215.

Young JM & Trask BJ (2002). The sense of smell: genomics of vertebrate odorant receptors. *Hum Mol Genet* **11,** 1153–1160.

Young JM, Shykind BM, Lane RP, Tonnes-Priddy L, Ross JA, Walker M, Williams EM & Trask BJ (2003). Odorant receptor expressed sequence tags demonstrate olfactory expression of over 400 genes, extensive alternate splicing and unequal expression levels. *Genome Biol* **4,** R71.

Yu T-T, McIntyre JC, Bose SC, Hardin D, Owen MC & McClintock TS (2005). Differentially expressed transcripts from phenotypically identified olfactory sensory neurons. *J Comp Neurol* **483,** 251–262.

Zhainazarov AB & Ache BW (1995). Odor-induced currents in Xenopus olfactory receptor cells measured with perforated-patch recording. *J Neurophysiol* **74,** 479–483.

Zhang X & Firestein S (2002). The olfactory receptor gene superfamily of the mouse. *Nat Neurosci* **5,** 124–133.

Zhang Y, Stanton JB, Wu J, Yu K, Hartzell HC, Peachey NS, Marmorstein LY & Marmorstein AD (2010). Suppression of Ca2+ signaling in a mouse model of Best disease. *Hum Mol Genet* **19,** 1108–1118.

Zhao H & Firestein S (1999). Vertebrate odorant receptors. *Cell Mol Life Sci* **56,** 647–659.

Zheng J & Zagotta WN (2004). Stoichiometry and assembly of olfactory cyclic nucleotide-gated channels. *Neuron* **42,** 411–421.

Zhuang H & Matsunami H (2007). Synergism of accessory factors in functional expression of mammalian odorant receptors. *J Biol Chem* **282,** 15284–15293.

Zufall F & Firestein S (1993). Divalent cations block the cyclic nucleotide-gated channel of olfactory receptor neurons. *J Neurophysiol* **69,** 1758–1768.

Zygmunt AC (1994). Intracellular calcium activates a chloride current in canine ventricular myocytes. *Am J Physiol* **267,** H1984–H1995.

Zygmunt AC, Robitelle DC & Eddlestone GT (1997). Ito1 dictates behavior of ICl(Ca) during early repolarization of canine ventricle. *Am J Physiol* **273,** H1096–H1106.

Acknowledgments

I owe my deepest gratitude to my supervisor Anna Menini. With her enthusiasm, her inspiration and her great effort to explain things clear and simple, she provided me a constant smiling guide and she enriched my growth as student. She brought me closer to the reality of what doing research means, enabling me to grasp its rich complexity and she taught me the state of mind of trying to find always a solution to a problem. During the period of my PhD, she provided encouragement, sound advice, good teaching, good company and an example of what "woman-in-science" means. Her ability to combine work with an immediate empathy will always inspire me.

I'm also indebted to Simone Pifferi. His advices and productive comments on my data were very precious and represented a great challenge for me to improve my knowledge. I thank Simone also for his friendship, for discussions about art, philosophy and life in general.

I would like to thank Anna Boccaccio. Anna is one of the kindest person I have ever met. She is authoritative, she communicate knowledge with every word without any kind of pressure. She has always created a peaceful environment around her and this let us to be very productive. I would like to become a scientist like her.

Thanks to Claudia Sagheddu. Our friendship grew up sharing the whole day in the lab, side by side. She represented the first big example of a person whose ideas were very different from mine, different points of view, and different approach to life. By knowing her, I learned and developed a lot of new aspects of myself. For this reason I will be grateful to her, more than she can imagine.

Thanks also to Giulia Betto for her collaboration and for her sincere friendship.

Fulvio Celsi has always given good advices both for scientific and personal issues. Sharing the same office was very nice. Thank you.

I would like to acknowledge all the other members of Lab Menini, past and present: Asma, Devendra, Lijo, Cristian, Gianluca, Anna, Michele, Ahmed and Juray. Thank you guys for sharing our different experiences and for let my days in the lab being so nice.

Thanks to all the Neurobiology technical staff for the help they gave every time I needed.

Thanks Marta. Your wisdom and strength in facing life will always let me consider you as an inspiring guide.

Thanks Maya for your breeziness and your will to constantly discover new things. Your presence in my life let me feel many difficult moments much lighter.

Thanks to all the friends known at Sissa: Stefano, Sara, Elena, Alessia, Rocco, Marilena, Alessio, Riccardo, Antonio, Leila, Pietro, Daniele, Gianluca e Claudia. Sharing my joy with you made it double.

Thanks to my parents for their constant support on my choices. They gave me the strength to face difficult moments not forcing me to be strong, but letting me feel strong.

At last but not least, I would like to thank Paolo for being always there for me and for bringing a ray of sunshine in my life.